NOTICE

AVIS

The quality of this microform is heavily dependent upon the quality of the original thesis submitted for microfilming. Every effort has been made to ensure the highest quality of reproduction possible.

La qualité de cette microforme dépend grandement de la qualité de la thèse soumise au microfilmage. Nous avons tout fait pour assurer une qualité supérieure de reproduction.

If pages are missing, contact the university which granted the degree.

S'il manque des pages, veuillez communiquer avec l'université qui a conféré le grade.

Some pages may have indistinct print especially if the original pages were typed with a poor typewriter ribbon or if the university sent us an inferior photocopy.

La qualité d'impression de certaines pages peut laisser à désirer, surtout si les pages originales ont été dactylographiées à l'aide d'un ruban usé ou si l'université nous a fait parvenir une photocopie de qualité inférieure.

Reproduction in full or in part of this microform is governed by the Canadian Copyright Act, R.S.C. 1970, c. C-30, and subsequent amendments.

La reproduction, même partielle, de cette microforme est soumise à la Loi canadienne sur le droit d'auteur, SRC 1970, c. C-30, et ses amendements subséquents.

Canada

THE UNIVERSITY OF ALBERTA

LAY-UP AND RATE EFFECTS ON FIBREGLASS/EPOXY
LAMINATES AND TUBULARS

BY

© Malachy CARROLL

A THESIS
SUBMITTED TO THE FACULTY OF GRADUATE STUDIES AND RESEARCH
IN PARTIAL FULFILMENT OF THE REQUIREMENTS FOR THE DEGREE
OF MASTER OF SCIENCE

DEPARTMENT OF MECHANICAL ENGINEERING

EDMONTON, ALBERTA

SPRING 1994

ISBN 0-612-11171-7

Canada

UNIVERSITY OF ALBERTA

RELEASE FORM

NAME OF AUTHOR: Malachy Carroll
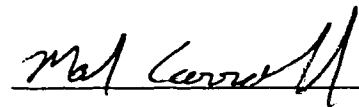
TITLE OF THESIS: Lay-up and Rate Effects on Fibreglass/Epoxy
Laminates and Tubulars

DEGREE: Master of Science

YEAR THIS DEGREE GRANTED: 1994

Permission is hereby granted to the University of Alberta Library to reproduce single copies of this thesis and to lend or sell such copies for private, scholarly or scientific research purposes only.

The author reserves all other publication and other rights in association with the copyright in the thesis, and except as hereinbefore provided neither the thesis nor any substantial portion thereof may be printed or otherwise reproduced in any material form whatever without the author's prior written permission.

76 Fairway Dr.
Edmonton, Alberta
Canada, T6J 2C4

April 22, 1994
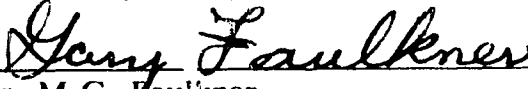
UNIVERSITY OF ALBERTA

FACULTY OF GRADUATE STUDIES AND RESEARCH

The undersigned certify that they have read, and recommend to the Faculty of Graduate

Studies and Research for acceptance, a thesis entitled LAY-UP AND RATE EFFECTS

IN FIBREGLASS/EPOXY LAMINATES AND TUBULARS submitted by MALACHY

CARROLL in partial fulfilment of the requirements for the degree of MASTER OF

SCIENCE.

Dr. F. Ellyin (Supervisor)

Dr. M.G. Faulkner

Mr. Allen Chiu

Dr. R. Eadie (External Examiner)

April 13 1994

ABSTRACT

In this study, a better understanding of the behaviour of glass fibre reinforced epoxy composite materials with respect to long and short term material properties, angle ply interaction and effect of multiaxial loading on the material behaviour is developed. These phenomena are investigated using multidirectional laminates and filament wound tubes tested under uniaxial and biaxial loading respectively.

Coupon specimens, representative of multidirectional laminates, were tested under tensile monotonic and cyclic loading conditions. The analysis of the experimental results demonstrate that the monotonic and fatigue strength varies with lay-up sequence. In addition, an understanding of the failure mechanisms has been developed with the aid of finite element analysis. The free edge effect and the constraint effect of $0°$ plies is discussed.

The free edge effect is eliminated with the testing of filament wound tubes. Two types of commercial tubes, bidirectional $\pm55°$ and multidirectional, were subjected to biaxi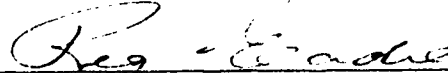al monotonic loading at various stress ratios of axial stress to hoop stress, σ_A/σ_H, and stress rates with the use of a biaxial testing machine. The $\pm55°$ filament wound tubes and the multidirectional tubes were tested with three rates and one rate of loading respectively. The stress-strain curves are analyzed and biaxial failure envelopes in terms of stress and strain are constructed with the results which demonstrate the complexity of the behaviour of the tubes. It is shown that the rate and ratio of biaxial loading effects the monotonic failure strength, damage accumulation and the mode of failure. In addition, these results are discussed based on macro and micro observations of damage and failure modes.

ACKNOWLEDGEMENTS

TABLE OF CONTENTS

LIST OF FIGURES

CHAPTER 1

INTRODUCTION

A composite is defined as a material that is made up of separate parts or components: combined or compounded. Some examples of composites are: fibres, which can be short or long, whiskers and particles combined with plastics, ceramics or metals. This generalized definition cannot fully describe the advanced polymeric composite materials used in this investigation. Therefore, for the purpose of this study, composite materials are formed by aligning extremely strong and stiff continuous fibres in a polymeric resin matrix.

The development of the composite materials used in this investigation dates back to the early 1940's where interest in advanced materials for the aerospace industry originated. Applications such as rocket casings, aircraft wing skins and even rotor blades for helicopters were being developed for composite materials in order to take advantage of their superior mechanical properties. The advantageous characteristics of composite materials are high strength and stiffness, light weight, chemical resistance, toughness, good fatigue strength and non-magnetic properties. Billions of dollars have been spent in past years to develop advanced composite materials. This is because for many of the applications desired, the premium for weight reduction was very high. Because material costs have dropped and manufacturing processes have been refined, the use of advanced composite materials for applications other than in the high priced aerospace industry has become practical.

In general, composite materials are designed to take advantage of the specific material properties of their constituents. Fibres, used as the reinforcement, are very strong and stiff in the axial direction but they are easily damaged if unprotected and they are only useful if load can be transferred to them. The fibres provide virtually all of the load carrying characteristics of the composite. The use of many fibres in composite materials provides sufficient redundancy so that if one fibre is flawed and breaks the material properties as a whole will not be affected because the load will be redistributed among the remaining fibres. Fibres are produced from glass, boron, carbon and graphite. E-glass type fibres are used in this investigation because of the moderate cost and good material properties they exhibit. They are a calcium aluminoborosilicate glass with typical stiffness and strength levels of 72.4 GPa and 3450 MPa respectively.

The other component in these types of composite materials, the matrix or binder material, is low in strength, low in weight, can plastically deform and exhibits time dependent properties such as creep. The matrix is considered the "weak link" in the composite because appropriate resins do not exist that will allow the exploitation of the full capabilities of fibre properties. In addition, the matrix determines the temperature and environmental limitations of the composite.

When these materials are combined the matrix binds the fibres together, provides a medium for load transfer to the fibres, all the interlaminar shear strength, resistance to cracking, and protects the fibres from the environment. The result is a material that has better combinations of mechanical properties than their individual components.

Glass fibre reinforced epoxies come in various forms which produce various

material properties and behaviour. The unidirectional fibre reinforced epoxy is a material that has all the fibres orientated in one direction. This type of composite material is said to have material properties of the same order as the fibres in the direction of the fibres and material properties less than the matrix perpendicular to the fibre direction. Unidirectional laminates are very stiff and strong in the fibre direction but have poor physical properties in any other direction. It has been shown in experimental studies that they tend to exhibit almost linear stress-strain behaviour until failure when loaded on the fibre axis.

A bidirectional fibre reinforced epoxy involves the combination of two fibre directions in the same plane either interwoven or arranged in discrete layers. Generally, these layers can be described by a stacking sequence of $(+\theta,-\theta)_N$ where N is the number of layers present. The properties of these composites are more complex and can be modified depending on the fibre orientation and loading conditions. Typically, they exhibit a significant nonlinear stress-strain behaviour because the matrix is capable of plastic deformation.

An expansion of the bidirectional composite is the multidirectional fibre reinforced epoxy. This composite material involves the use of many different orientations of fibres again either interwoven or in separate layers. The stacking sequence of these composite can be described by $(\theta_1,\theta_2,....,\theta_N)_{T\ or\ S}$ where T is the total lay-up and S indicates a symmetry. These composites also exhibit complex material properties and nonlinear stress-strain behaviour.

Figure 1.1 illustrates the difference in material stress-strain behaviour that typical

laminated composite materials exhibit.

The behaviour of fibre reinforced composite materials is complicated by the fact that they are not only anisotropic but on the micro scale they are inhomogeneous. These properties cause a variety of failure mechanisms associated with fibre reinforced composite materials. For example, when a composite material is under load, the matrix can develop cracks, plies may delaminate or fibres can debond from the matrix. This damage leads to a localized or global failure of the composite material involving one or more of many failure modes possible. For example, a unidirectional composite material loaded on the fibre axis may fail by breakage of fibres, characterized by a clear cut fracture surface perpendicular to the loading direction or cracks in the matrix parallel to the fibres may be joined. For bidirectional and a multidirectional fibre reinforced materials under complex loading, failure may occur in the form of extensive matrix cracking causing the binding properties to fail or interlaminar delamination where individual layers separate. These failure mechanisms can happen slowly or instantaneously depending on loading conditions and fibre orientations. The investigation of the failure modes and damage propagation is an integral part of the characterization of composite materials.

In general, fibre reinforced epoxy composites, in any configuration, exhibit strength, stiffness, failure modes and overall behaviour that is dependent on fibre direction and sequence of layers. It is important to investigate the material properties of fibre reinforced composite materials with respect to these variables and multiaxial loading conditions. The stress-strain behaviour is studied and correlated with damage

4

mechanisms in a fibre reinforced epoxy. In addition, the strength, which is ultimately related to failure level, is investigated with respect to failure modes. Therefore, in this study a relationship between fibre orientation, layer stacking sequence and loading conditions and material performance, is developed with respect to strength, stiffness, damage accumulation and failure mode. Specifically, two forms of composite structures are investigated: the laminate and the filament wound tube. The advantage and disadvantage of each form is discussed and each is physically tested and analyzed computationally, analytically or phenomenologically. An understanding of the material behaviour is developed in order to predict the performance of these types of materials in specific applications.

Most engineering applications for these types of glass/epoxy composites are concerned with long term performance. This study demonstrates the complexity of the behaviour, short and long term, of laminated and tubular composite materials. Chapter 2 gives the background information on the material behaviour of multidirectional laminates and the filament wound tubes. The effect of ply stacking sequence on monotonic strength and fatigue life is reported in chapter 3. The short and long term monotonic strengths and behaviour for bidirectional filament wound tubes under biaxial loading is studied in chapter 5. The monotonic strength of multidirectional filament wound tubes is examined in chapter 6. The outcome of these investigations provide insight into the short and long term behaviour of glass/epoxy composites.

5
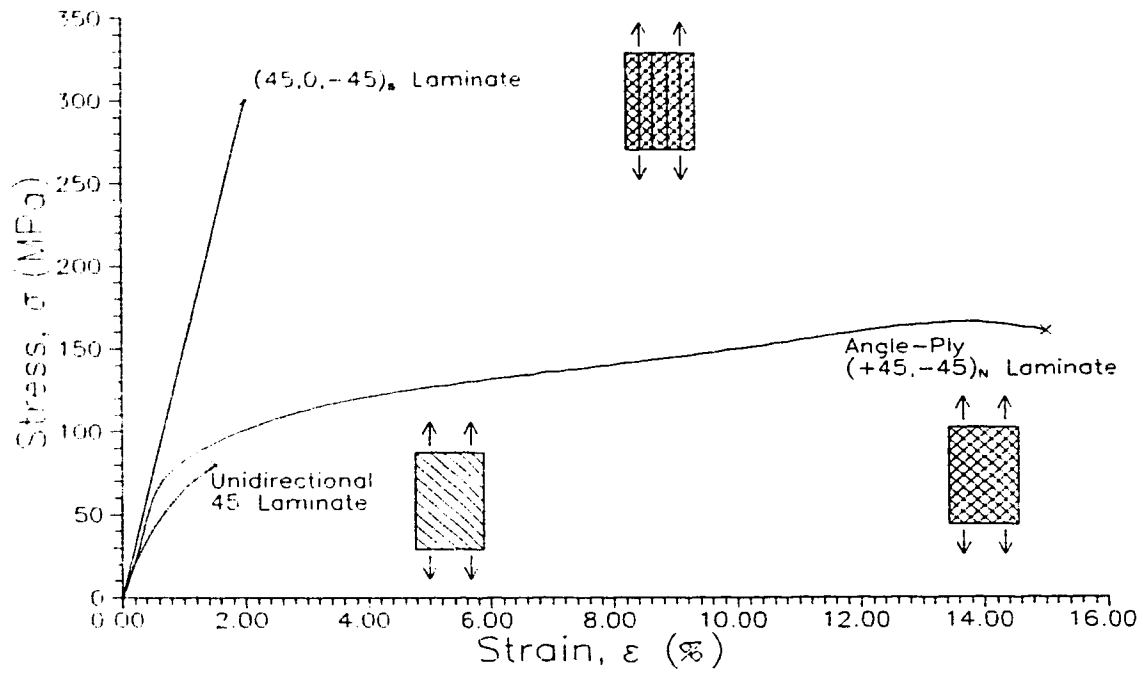
Figure 1.1 Stress-Strain Behaviour of Unidirectional 45°, Angle-Ply ±45° and [45°,0°,-45°]ₛ Fibreglass/Epoxy Laminates

6

CHAPTER 2

BACKGROUND INFORMATION

2.1   Introduction

The classical approach to describe the fatigue life of most metals is to determine a relationship between stress and number of loading cycles to failure. This is ascertained through the performance of cyclic loading tests with a predetermined ratio of maximum stress to minimum stress and varying stress levels. Figure 2.1 shows a log-log plot of the failure stress, σ, with respect to number cycles to failure, N_t, which is used to characterize the fatigue life of metals. Three parameters to extract from this graph are: σ_f, is the intercept of the S-N curve with the y axis; α, the slope of the S-N curve, and σ_n, the point were the S-N curve changes slope. The σ_t parameter may be approximated to the monotonic strength, α is the change in the number failure cycles with respect to stress level and the fatigue limit or endurance limit, σ_n, marks the point where any additional decrease in stress level does not produce a failure or indicates a change in fatigue behaviour. These parameters are constant and rate independent for metals at room temperature.

The fatigue life of fibre reinforced epoxy materials is more complex than for metals. The anisotropy and the inhomogeneity of these materials causes the fatigue parameters to vary under different conditions. This thesis will demonstrate that the monotonic tensile strength and the α parameter vary with fibre orientation, stacking

7

sequence of angle plies and loading rate. In addition, it is known that the fatigue limit for composites materials does not exist.

2.2   Composite Material

The composite materials considered in this study are glass fibre reinforced epoxy matrix laminates and glass filament wound epoxy tubes. They have a very high strength to weight ratio, a high modulus, excellent corrosion and chemical resistance. In addition, the investigated forms are relatively economical to produce. In general, this experimental investigation will concentrate on the mechanical properties of these composites considering various types of loading, rates of loading, and orientation of fibres.

The study will look at two forms of glass fibre reinforced epoxy: the flat laminate and the filament wound tube. The coupon specimen will be representative of the flat laminate and will be tested with respect to varying sequence of laminae and different types of uniaxial loading: i.e. monotonic and cyclic loading. Two types of tubular specimens, ±55° and multidirectional, will be tested considering monotonic biaxial loading at varying stress rates.

The composites of interest will be investigated with respect to these parameters and will be analyzed with the aid of analytical and computational analysis of data and macro and micro observation of failures and damage development. The observations and analysis will be used to draw conclusions on the material properties of these composite

materials.

Different types of loading were used in order to help characterize the composites. Uniaxial loading will be used in the investigation of the sequence effect of multidirectional laminates (Fig. 2.2.c). This uniaxial loading will provide insight into the behaviour of multidirectional laminates and can be used to predict properties and behaviour in laminates under biaxial loading conditions. Experiments were performed using uniaxial tension on coupon specimens with varying laminae lay-ups.

Most laminates and filament wound products experience multiaxial states of stress; therefore, biaxial loading (Fig. 2.2.b & 2.2.d) will be used to investigate the filament wound tubular specimens. Experiments are carried out on these tubes using axial tension and compression and internal pressure. In addition to the biaxial loading conditions, tubular specimens with two different fibre orientation schemes are investigated.

2.3   Coupon Specimens

A laminate, by definition, is a material which is made of or arranged in thin sheets. With respect to this investigation a laminate is a structure composed of layers of fibre reinforced epoxy sheets with varying orientations of fibres. The direction of these fibres within a layer and the position of the layer within the laminate has an effect on the material properties of the laminate with respect to monotonic strength, stress and strain distribution, fatigue life and time dependence. These properties will be investigated and discussed based on physical testing and analytical and computational

9

analysis.

It is well recognized that the excellent monotonic and fatigue properties of fibre-reinforced plastics are usually observed in unidirectional laminates when loaded in the reinforcement direction (Fig. 2.2.a). However, these observations are of limited value when attempts are made to characterize the behaviour of multidirectional laminates which are used in engineering applications. This is because the inherent anisotropy and multiple modes of failure of these composites, severely limits our understanding of the true nature of the failure process, the location, mode and extent of damage (Dew-Hignes and Way, 1973, Goetchius, 1987, Hahn, 1979, Highsmith and Reifsnider, 1982, O'Brien, 1985, Stinchomb and Reifsnider, 1979, among others).

The strength of symmetric composite laminates containing identical ply orientations can be significantly dependent on the stacking sequence of the plies contained in the laminated composites (e.g. see Foye and Baker, 1970, Spain, 1967, Halpin and Wu, 1971, Daniel, 1974). The theoretical explanation of the above phenomenon is beyond the scope of the Classical Laminate Theory, since in this formulation, the predicted stresses in symmetric composites under in-plane loading are independent of stacking arrangement. Pagano and Pipes (1971) were the first to attribute the ply stacking sequence effect to the interlaminar stresses induced in the free-edge of a flat coupon. They showed that the interlaminar normal stress, as well as the interlaminar shear stress is instrumental in predicting delamination and the subsequent decrease in strength.

Over the past two decades, a number of solutions (eg. Kassapoglu and Lagace,

1986. Pipes and Pigano. Soni and Pagano. 1982. 1970 Wang and Crossman. 1977. Wang and Choi, 1982 a., Wang and Choi, 1982 b., Whitney and Browning. 1972. and others) have been presented for interlaminar stresses. The existence of free edge effects, among other phenomena, initiated a number of experimental investigations devoted to such delamination and stacking sequence of laminated composites (e.g. Bakis and Stinchcomb, 1986. Lagace. 1986, Ramani and Williams. 1977, Stinchomb and Reifsnider, 1979, Sun and Zhou, 1988). The results indicate that the stacking sequence effect on the tensile strength of notched coupons may not be the same as for unnotched coupons (Lagace, 1986). Additionally, considering interlaminar stresses, the constraint effect from the nearest plies may contribute to the development of different damage modes. To better understand the lay-up sequence effect in the fibre-reinforced plastic composites, both experimental and computational data are required.

The monotonic and fatigue behaviour of symmetric fibreglass-epoxy laminates is summarized in chapter 3 using three different ply angle orientations: $45''$, $-45''$ and $0''$ which were interchanged in three configurations: $[45_2,-45_2,0_2]_s$, $[45_2,0_2,-45_2]_s$, and $[0_2,45_2,-45_2]_s$. The experimental results form the basis for numerical calculations which involves the use of three dimensional finite element analysis. The sequence effect in the monotonic and fatigue loading is discussed based on numerical analysis of interlaminar stresses and damage mechanisms observed. The present work utilizes the same material as in Ellyin, Kujawski and Chiu (1993) but concentrates on lay-up sequence effect in multidirectional laminates. Both of these investigations reveal a complicated but consistent behaviour in tensile monotonic and fatigue loading. They indicate that there

11

is an appreciable difference in strength and stiffness for each lay up. Following the monotonic tests, cyclic loading is applied to the laminates of interest. It is observed that the trend in the fatigue tests is not the same as the monotonic ones. The effect of frequency of cyclic loading is also investigated for these laminates.

2.4   Filament Wound Tubes

An extension of the laminated coupon specimen is the filament wound tubular specimen. The advantages of testing tubular specimens are that the tube does not have edge effects that modify the performance of the composite, a multiaxial state of stress can be achieved and damage is more easily detected because of fluid leakage. On the other hand, tubular specimens need more elaborate testing facilities including complicated gripping systems, an axial load frame and a high pressure system (see chapter 4). In addition, the manufacturing processes is complicated but consistent specimens are still possible. This study reported in chapter 5, involves the examination of similar parameters as the coupon specimen, i.e. monotonic strength, time dependence and effect of orientation of fibres, except that they are investigated under biaxial states of stress.

2.4.1   Filament Winding

Reinforcements on tubes and pressure vessels have been used for centuries to improve burst strength. For example, wire wrappings have been used to reinforce

cannon barrels and to hold wooden kegs together. However, the use of filament winding to manufacture high strength and low weight structures is relatively recent. Filament winding is a process that is used to reinforce plastic parts with, for example, high strength and stiffness continuous fibres, yarn, or tape. This process involves the winding of the reinforcement on a form or mandrel whose shape corresponds to the inner structure of the part being fabricated. Automated machines are used to carry out this process to a high degree of accuracy where precise control of the winding pattern and direction of reinforcements can be controlled. The reinforcements are either wetted with resin as it is wound or preinpregnated with resin before it is wound and therefore, curing of the resin material can take place during or after the winding process.

2.4.2 Experimental Investigation of Filament Wound Tubes

Filament wound composite tubes have been the subject of numerous experimental investigations as demonstrated in the literature (Soden, Kitching, Tse, Tsavalas and Hinton, 1993, Soden, Kitching and Tse, 1989, Highton, Adeoye and Soden, 1985, Hull, Legg and Spencer, 1978, Rosenow, 1984, Soden, Leadbetter, Griggs and Eckold, 1978 a., Al-Salehi, Al-Hassani and Hinton, 1989, Spencer and Hull, 1978, Soden, Leadbetter, Griggs and Eckold, 1978 b.). Biaxial testing has evolved from the three basic tests on tubes of pure axial load, pure internal pressure and pressure vessel type loading where hoop stress to axial stress is 2 to 1, to any ratio of internal pressure to axial load at any rate of loading with the development of advanced biaxial testing apparatus. Most studies

are directed towards failure envelopes for thin walled cylinders with only a few wound layers.

Most filament wound tubes consist of an axisymmetric shell with fibres wound in helices at angles of $+\theta$ and $-\theta$ to the axis of symmetry. Since the wind angle is a major variable in determining the tubes mechanical performance many studies concentrate on this aspect. It has been determined that the optimum winding angle for filament wound tubes is dependent on the loading conditions the tube will experience. The most relevant and recent experimental investigations, performed by Soden et al. (1993, 1989, 1985), look at the failure stress envelopes and deformation of filament wound tubes with wind angles of $\pm45^\circ$, $\pm55^\circ$ and $\pm75^\circ$ under various biaxial and uniaxial loading conditions. Fibreglass reinforced epoxy resin tubes, similar in material to this investigation, were used with wall thicknesses ranging from 1 to 3 mm. The thick specimens were used for axial compression testing but the experiments and analysis was performed under the assumption of membrane stress states. Soden et al. (1993) observed that the tubes tested under various biaxial loading conditions failed with greatly varying strengths subsequently producing asymmetric biaxial failure envelopes. A biaxial failure envelope is a graph of the axi al failure strength versus the circumferential failure strength. In addition, they noted a large difference in the failure envelopes for the three different tubular winding angles.

Soden et al.'s (1985), first experimental program in this series was the investigation of the $\pm75^\circ$ tubes. Biaxial and uniaxial loading was applied to the specimens through a complicated test rig. A rough failure envelope was developed for

14

the tubes even though it was difficult to control the stress ratios, the loading path was not always linear, rate of loading was not rigorously controlled, there was a relatively large variation in tube wall thickness, shell buckling occurred in some specimens under compression and some failures occurred outside the test section. They concluded that the axial tensile strength is improved with pressure while the axial compressive strength is not. This information helps the prediction of the shape of failure envelopes for different fibre orientations.

The second study in the series investigated the behaviour of $\pm 55°$ filament wound tubes again with respect to uniaxial and biaxial loading. This experimental program is of particular interest because not only does it have similar material but identical fibre orientations as our investigation. It involved similar problems as the first study although the testing procedure was refined somewhat. A biaxial failure envelope was produced that demonstrated that the maximum axial strength occurs at a stress ratio of 2 hoop to 1 axial and is 4 times the axial stress under uniaxial tension, confirming the conclusion arrived at in the first study. The maximum hoop strength occurred at a ratio of approximately 3 hoop to 1 axial.

Soden et al.'s (1993) final study reviewed the previous two and added experimental data for $\pm 45°$ tubes determined in a similar manner. This paper also discussed the strain behaviour of these tubes and will be further discussed in relation to our results. The stress-strain curves produced from the test results demonstrated that the linear elastic behaviour was exhibited only to about 0.2% strain and they became nonlinear well below failure stress levels. All these results convinced Soden et al. that

15

failure envelopes and stress-strain data should be used in the design and evaluation of filament wound tubes.

Winding angles of $\pm 55°$ are common because it is near the "optimum" design for pressure vessel type loading (hoop/axial = 2:1). Cylindrical pressure vessels always experience a similar stress conditions with internal pressure. The internal pressure not only induces hoop stress but the force created on the end caps induces an axial stress of 1/2 the hoop stress for the thin-walled configuration. This stress condition will give the highest principal stress at 55° off axis and therefore, the fibres are orientated in the direction of maximum stress.

Netting analysis is a simplistic method to predict the stress ratio or fibre direction where the fibres are the predominant load carrying component. The fibre direction is determined assuming the matrix does not carry any load and the failure stress can only be calculated if both the fibre volume and the strength of the fibres are known. Since the winding angle is known, $\pm 55°$, the optimum stress ratio can be derived as follows:

$$f = \frac{pr}{t\sin^2\theta}$$
$$f_1 = f\sin^2\theta, \quad f_2 = f\cos^2\theta$$
$$\frac{f_1}{f_2} = \frac{f\sin^2\theta}{f\cos^2\theta}$$
$$\frac{f_1}{f_2} = \tan^2\theta \quad \theta = 55°$$
$$\frac{f_1}{f_2} \approx 2 \quad \rightarrow \quad 2H:1A$$

Where f is the stress in the wall in the winding direction, f_1 is equal to the hoop stress, f_2 is the axial stress, r is the mean radius of the tubes, t is the wall thickness, p is the internal pressure at failure and θ is the winding angle of the filament wound tubes. This

analysis was used as a guide in this experimental program in order to develop an efficient testing program.

Considering previous experimental investigations, and the fact that only a limited number of specimens were available, carefully chosen stress ratios were used to investigate the mechanical behaviour of the tubulars. Five stress ratios were chosen and the filament wound tubes were loaded monotonically at predetermined rates, keeping these ratios constant, until failure occurred. These stress ratios where chosen in order to define the failure envelopes and characterize the stress-strain behaviour of the tubular specimens. Therefore, in addition to the stress ratio determined by the netting analysis, four other ratios were chosen considering a few experimental criteria. Since the material properties needed to be determined, i.e. the elastic modulus and Poisson's ratio in the hoop and axial directions, the pure axial and hoop loading needed to be performed and a few other points to help determine the shape of the envelope. Details are presented in chapter 4.

There has been limited research performed on multidirectional filament wound tubes but the material property advantages are obvious. As discussed previously, the $\pm 55°$ tubes are strongest when loaded under specific loading conditions; therefore, if variable loading conditions are present, it would be advantageous to have multiple angles within the tube. These tubes were designed to take particular advantage of the properties of each layer under there designed loading condition. The $0°$ fibres will give the tube higher strength along its longitudinal axis and therefore providing higher strength and modulus when loaded axially. In addition, the $0°$ may prevent the tube from exhibiting

17

any time dependent properties when loaded axially because glass fibres exhibit little time dependence. The $\pm 45^{\circ}$ layers will give the tube high strength and stiffness under a stress ratio of 1 hoop to 1 axial as determined by netting analysis and demonstrated by Soden et al.(1993). The $\pm 70^{\circ}$ fibres will give a minimum radial displacement (Givens, 1994) and very high failure stress under pure internal pressure (Soden et al., 1985). These three fibre directions combined in one tube may reveal that this type of lay-up may have excellent material properties. However, the fact that only limited numbers of each layer is present in the tube may contribute to an overall weaker tube. Additionally, interaction between these layers will affect the behaviour of the tubes, in particular, interlaminar shear may be high between layers with high angle differences. These material properties and behaviour are determined using a similar loading scheme as the $\pm 55^{\circ}$. in order to determine the shape of the failure envelope (see chapter 6). A comparison of this overall envelope with the envelopes of the individual layers may reveal that only advantageous properties are adopted by the hybrid tubes. On the other hand, the interaction of these different layers may be detrimental to the overall strength of the tubes.

2.4.3 Time Dependent Behaviour

It is well recognized that fibre-reinforced plastics loaded in the reinforcement direction have excellent fatigue and static properties. Ideally, when designing a composite material the specific loading direction is known and therefore unidirectional

18

laminates can be used and oriented in the direction of the load. This enables the composite to take advantage of the high stiffness and strength of the fibre and the binding and load transferring properties of the matrix. The resulting laminate shown in Fig. 2.2.a takes advantage of the useful properties of the fibres and the matrix. This unidirectional laminate is very strong and stiff and exhibits very little viscous or time dependent effects if loaded in the fibre direction.

On the other hand, if the loading condition is multiaxial, difficulty arises in designing the optimum composite laminate. Figure 2.2.b illustrates this problem assuming biaxial loading conditions on a bidirectional laminate analogous to the $\pm 55^\circ$ filament wound tubes used in this investigation. Under biaxial loading conditions the principal direction of the stresses changes with the ratio of axial stress to transverse load. In the case of a tube with axial load and internal pressure, the axial to hoop stress ratio will vary. Considering a known constant biaxial loading condition the laminate can be designed so the fibres are in the direction of loading. This ideal condition will give the laminate similar properties to the unidirectional uniaxially loaded laminate. There are many methods for determining the angle of the fibres in the laminate in order to meet this condition, the simplest being netting analysis previously discussed.

If the loading condition is variable, it is safe to assume that the orientation of the principal stress direction will not always be in the fibre direction. This will considerably weaken the composite because the matrix will take a portion of the load applied to the composite and will present other complicating phenomena such as time dependent behaviour. This viscous behaviour reveals itself in different ways including: creep under

constant loading, stress relaxation under constant strain and dependence of stress on strain ra or on stress rate. These effects are very important to consider in fibre-reinforced composite structures because stresses and deformations determined on the basis of elastic analysis may change considerably with time. Figure 2.3(a) shows creep, Fig. 2.3(b) illustrates stress relaxation and Fig. 2.3(c) shows typical stress-strain relationship for varying stress rates.

There have been many studies done on different types of laminated composites all of which suggest the material behaviour depends on loading rate (eg. Dillard, 1991, Krokosky, 1967, Macek and Hackett, 1992, Shapery, 1974). Different types of failure are suggested by Suvorova (1985) in relation to loading rates. At low loading rates approaching static fatigue, failure occurs when a critical level of damage is achieved. Increasing the loading rate will increase the strength of the composite because there is not sufficient time for damage initiation and subsequent accumulation. At moderate loading rates, cracks propagate from initial defects until there is a failure. Contrary to the slow loading rate, increasing the loading rate will decrease the strength of the matrix because the matrix will act more brittle like and the stresses induced by loading may not have time to distribute uniformly. Under very high loading rates, damage may not have time to occur and the composite will fail instantly through the weakest element of the composite. Therefore, increasing the loading rate will increase the strength because there is less time for the failure mechanisms to fully develop. The filament wound tubular specimen of interest in this study will be loaded using slow rates and therefore the first scenario applies.

Most of the research directed towards time-dependent behaviour in filament wound tubes has been performed under pure internal pressure or pressure vessel loading conditions at high rates of strain. A study by Al-Salehi et al. (1989) investigates the strength of angle ply glass reinforced tubes under high rates of loading. Even though these tests were mainly burst tests using very high rates of strain some important conclusions were drawn. The tube burst strength increases significantly with the increased strain rate for all tube winding angles which included the $\pm 55°$ wind angle. In addition, strain to failure also increased with increased strain rate in a similar fashion to tube strength. Al-Salehi et al.'s (1989) study illustrated the fact that time dependence is an important property and needs to be investigated in order to predict the life of FRP tubes.

Creep in filament-wound glass-reinforced epoxy pipes subjected to internal pressurization was investigated by Mieras (1973). He determined that above certain deformation levels irreversible creep phenomena occurred which contributed to premature failure in the form of resin cracking and consequently weepage of liquid from pipes. This type of time dependent behaviour depends on how much load the matrix is carrying which depends on the direction of the principal stresses as discussed previously. It was determined in Mieras (1973) investigation that again the stress at which this failure occurs increases with decreasing time under load.

Mieras' investigation determined that the irreversible creep causes damage accumulation leading to crack development in the matrix resin of the composite material. Damage accumulation can develop in many forms such as the propagation of a single

crack transversely or longitudinally, delamination between layers of filament wound fibres, or local development of cracks in the composite. In addition, instant failure of the material due to the breakage of the weakest element is also common (Savorova, 1985). These types of failure do have a direct relation with time but are not necessarily a result of the time dependent or viscous properties of the composite materials. Failure modes and mechanics of fibre-reinforced epoxy tubes under biaxial loading conditions will be discussed later on.

There has been limited research performed on the time dependent behaviour of filament wound tubes subjected to multiaxial loading with low strain rates similar to the rates used in the present investigation. A paper by Soden et al. (1989) reports on the $\pm 55°$ filament wound tubes under various biaxial loading conditions. Different stress ratios were used to developed a biaxial failure envelope; in addition, different strain rates were used for some stress ratios, i.e., stress ratio of 2.5 hoop stress to 1 axial stress and 5.5 hoop stress to 1 axial stress respectively. This portion of the study involved the observation of strain rate on the ultimate strength of the specimens. Although limited data is available, the slower strain rate produced lower failure stresses, indicating the presence of time dependent properties. It was determined that these different failure strengths could only be observed with strain rates differing by an order of magnitude or greater.

Another approach to describing the time-dependent behaviour of filament wound tubes is the observation of changing linear elastic range under different strain rates and creep stress levels. In an investigation by Bax (1970) it was observed that under long

term static loading conditions, the linear elastic range can differ between the short term tests. This suggests time-dependent properties are present in the elastic range and may affect the elastic properties of the tubes under long periods of loading even at stress levels well with in the linear elastic range. In addition to static creep tests, load path to static load used for the creep tests was investigated and determined to have an effect on the final failure. Therefore, it was concluded that static creep tests can not describe the time-dependent behaviour of the tubes because load path has an effect on the creep behaviour.

There are some advantages to the viscoelastic properties of composite materials. Viscoelasticity plays a major role in the redistribution of residual stresses induced during curing. Additionally, under loading, the viscoelastic properties tend to shift the load from the time-dependent matrix material to the fibre which is more capable of carrying the load. Without this property composite materials may develop matrix cracking and accumulate damage more easily.

It is concluded that the study of the time-dependent properties in composite materials, specifically filament wound tubes, is important in the material characterization. If the tubes are to be used in conditions involving high loads, long duration loading or cyclic loading, the time-dependent properties should be investigated. In the present study three relatively slow rates of biaxial monotonic loading will be used to test ±55° glass filament wound tubular specimens until failure. These results demonstrate significant time dependence and the long term performance of the tubes is predicted.

23

2.5   Summary of Investigation

The purpose of this investigation is to develop some insight into the behaviour of glass fibre reinforced epoxy composite materials with respect to long and short term material properties, angle ply interaction and effect of multiaxial loading on the material behaviour. These phenomena are investigated using multidirectional laminates and filament wound tubes tested under uniaxial and biaxial loading.

The multidirectional laminates were tested under monotonic and cyclic loading conditions. The analysis of the experimental results demonstrate that the monotonic strength and the slope of the S-N curve, α, varies with respect to lay-up sequence. In addition, an understanding of the failure mechanisms has been developed with the aid of finite element analysis.

The filament wound tubes were subjected to biaxial monotonic loading at various stress ratios and stress rates. These tests demonstrate the complexity of the stress-strain behaviour of the tubes. It is shown that the rate and ratio of biaxial loading affects the monotonic failure strength, damage accumulation and the mode of failure. A methodology is proposed for the application of these composite materials in industry.
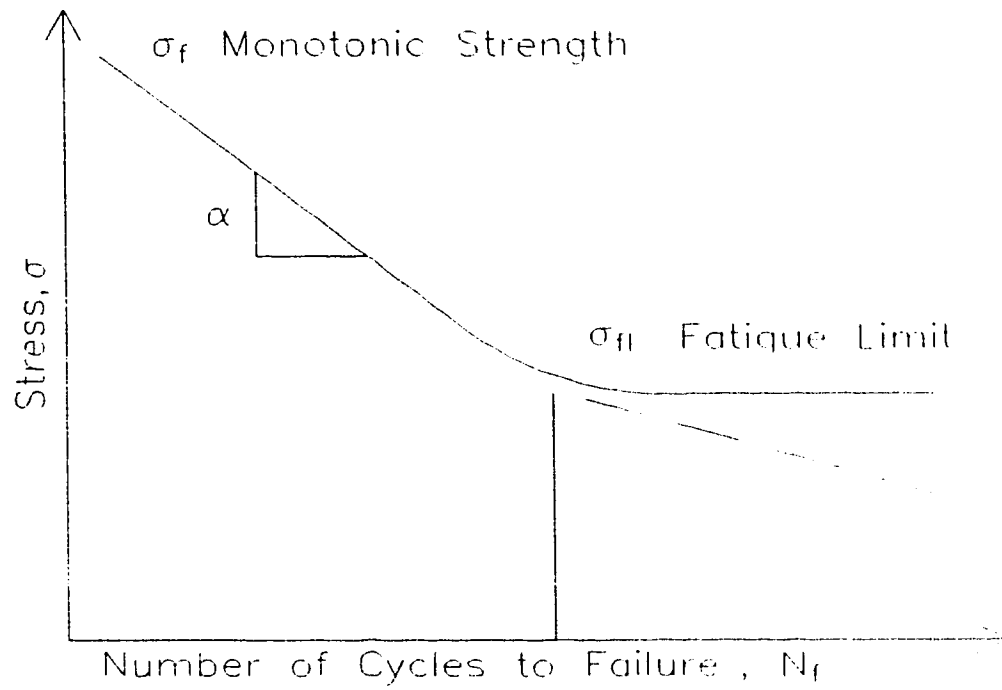
Figure 2.1 Typical S-N Curve for Metal

25

a. Unidirectional Laminate
Uniaxial Loading

b. Bidirectional Laminate
Biaxial Loading

c. Multidirectional Laminate
Uniaxial Loading

d. Multidirectional Laminate
Biaxial Loading
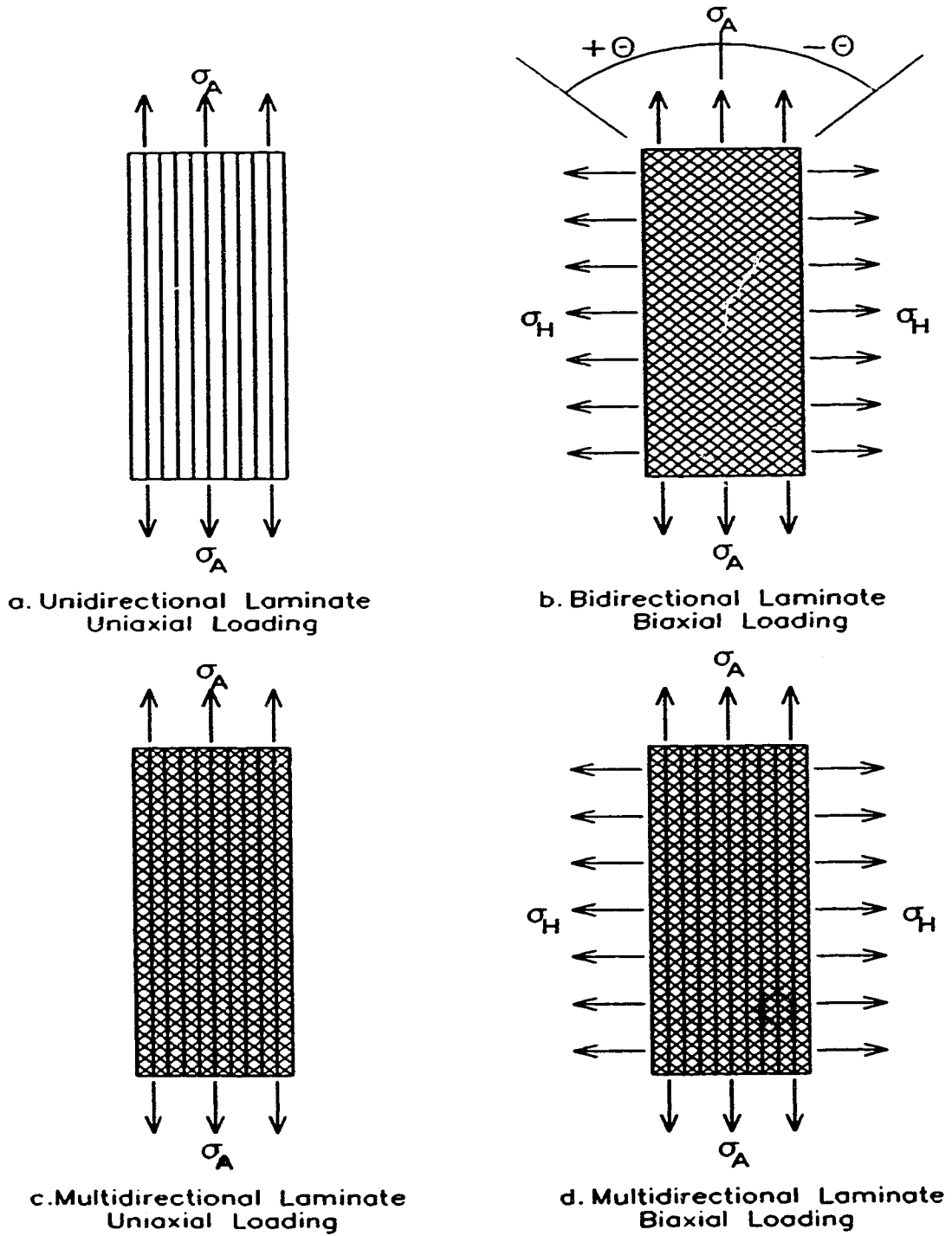
Figure 2.2   Laminates

26
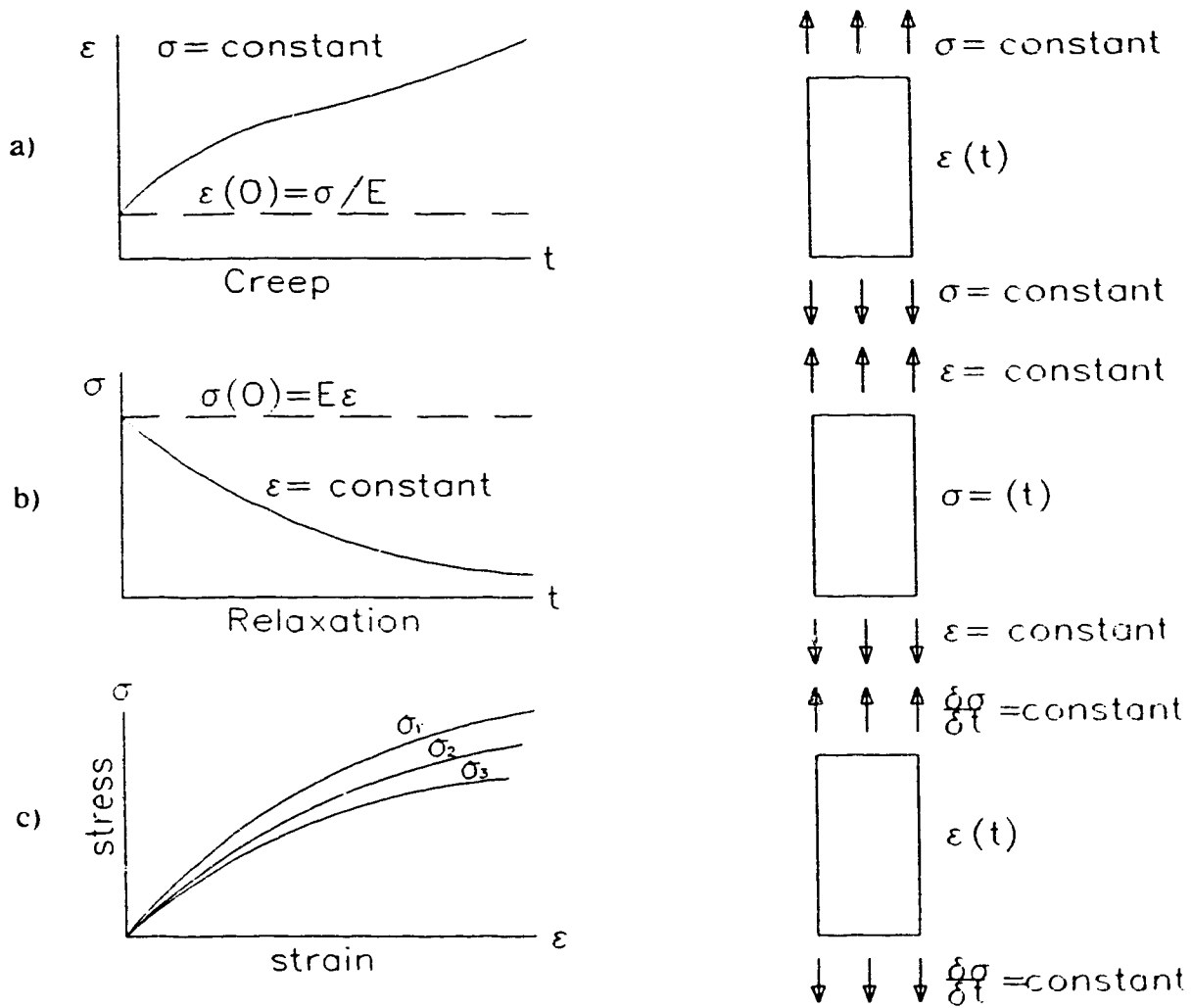
Figure 2.3 Time Dependent Properties

CHAPTER 3

LAY-UP SEQUENCE EFFECT IN LAMINATES

3.1   Introduction

The sequence effect in multidirectional laminates is investigated in order to explore the overall behaviour of composite laminates. The only type of modification to the composite is the order of the angle plies in the laminate. In this study $\pm 45°$ and $0°$ layers were interchanged in three different configurations: $[45_2,-45_2,0_2]_s$, $[45_2,0_2,-45_2]_s$ and $[0_2,45_2,-45_2]_s$. The monotonic and fatigue performances are investigated experimentally and the results discussed based on a numerical analysis.

3.2   Material and Specimen

The material used in this investigation was 3M "Scotchply" type 1003 unidirectional prepreg tape which contained continuous filament "E" type glass fibres imbedded in $36\% \pm 3\%$ (by weight) epoxy resin. The manufacturer determined the material properties using ASTM D-638 for the tensile strength and modulus. These values were used as constants in the finite element calculations.

The $[45_2,-45_2,0_2]_s$, $[45_2,0_2,-45_2]_s$ and $[0_2,45_2,-45_2]_s$ laminates were manufactured with this prepreg material using a specially developed procedure which minimized voids and defects in the lay-up. The multidirectional specimens consist of a total of 12 layers

28

(each layer .0254mm thick) with two layers of prepreg for each direction. Coupons (Fig. 3.1) with a length of 200mm, width of 12.85mm and thickness of 3mm were assembled in a steel mold. Once the laminate lay-up was completed, it was placed in a vacuum of < 1.3 Pa for 18 hours to undergo a "vacuum stripping" which removed most of the air between each laminae. The mold and the laminate were then placed in an oven preheated to 230°C for curing. When the gel point (160°C) of the epoxy resin was reached, a pressure of 690 KPa was applied to the lay-up. After one hour of curing at 160° C, the mold and laminates were allowed to cool to room temperature. The laminate specimens were then removed from the mold and tapered aluminum tabs where glued to the ends with 3M type DP-110 Grey Flexible Epoxy Adhesive to facilitate gripping. The resulting test section had a length of 63.5mm, Fig. 3.1.

3.3 Monotonic Tests

3.3.1 Experimental Procedure

Three tension monotonic load tests were performed on each lay-up at room temperature. A constant positive strain rate of .4%/min was applied by an Instron mechanical-hydraulic servo-controlled tension-compression testing machine. The corresponding load was monitored and recorded on an X-Y plotter.

3.3.2 Results

Three tests for each lay-up were deemed sufficient because of the small amount of scatter observed in the results. The failure loads of the monotonic tests are presented in Fig. 3.2.

For all tests the dominant damage was an edge delamination in the form of layers separating from one another. This delamination leads to a reduction in stiffness and a gradual increase in the amount of load that the $0°$ fibres support. In localized areas, $0°$ fibre breakage occurs followed quickly by the complete failure of the specimen.

In terms of the average values of failure strength, it is observed that the $[45_2, -45_2, 0_2]_s$ lay-up, with an average failure strength of 351MPa, is 7% stronger than the $[45_2, 0_2, -45_2]_s$ failure strength of 327MPa, and 11% stronger than the $[0_2, 45_2, -45_2]_s$ laminate, failure strength of 317MPa. The above then demonstrates the presence of a sequence effect. These results are similar to a trend observed in Daniel's (1986) experimental study which investigated a comparable lay-up effect in graphite/epoxy laminates. In addition, the stiffness of the lay-ups differed among the three types of laminates, following a similar trend as the strength: $[45_2, -45_2, 0_2]_s$ laminates with an average stiffness $\approx$ '.0 GPa is 3% stiffer than the $[45_2, 0_2, -45_2]_s$ laminates with an average stiffness of 17.5 GPa, and 6% stiffer than the $[0_2, 45_2, -45_2]_s$ laminates whose average stiffness is 17.0 GPa. Finite element analysis performed on this problem presents some explanations for the difference in strength and stiffness and will be discussed further in section 3.5.

3.4   Cyclic Tests

3.4.1   Procedure

To shorten the time involved in the tests, only two of the three laminates were tested under fatigue loading conditions. The strongest and stiffest lay-up, according to the monotonic tests, and the weakest and least stiff lay-ups were tested, i.e. $[45_2,-45_2,0_2]_s$ and $[0_2,45_2,-45_2]_s$ respectively. The coupon specimens were prepared in the same manner as the monotonic test specimens. Tension-tension cyclic loads with a load ratio $R = P_{min}/P_{max} = .05$ were applied to the coupon specimens using a MTS electro-hydraulic servo-controlled testing machine. The cyclic loads were applied at two frequencies: one fast, 3.33Hz, and the other slow .417Hz. An IBM PC was used to provide the sinusoidal load signal and to record cycles to failure and stress-strain response at selected cycles. An extensometer with a gauge length of 25.4mm was mounted on the edge of the coupon to facilitate the accurate recording of the longitudinal strain. For each specific test, the maximum load was predetermined by selecting a percentage of the monotonic failure strength.

3.4.2   Results

Fatigue test results for both types of laminates investigated, are summarized in Table 1 in appendix A. Figure 3.3 illustrates a typical change in stiffness over the life

of a specimen for the two laminates of interest: $[45_2,-45_2,0_2]_s$ and $[0_2,45_2,-45_2]_s$. These curves again display the fact that the $[45_2,-45_2,0_2]_s$ lay-up is stiffer which may consequently contribute to its poorer fatigue behaviour and shorter life. The curve for the $[45_2,-45_2,0_2]_s$ laminate is not complete because the extensometer, mounted on the edge of the specimen, slips when significant damage develops. A general trend is observed which indicates loss of specimen stiffness with increasing life ratio. The stiffness drops quickly as the initial damage develops and then decreases gradually towards an apparent steady value as transverse cracks saturate the off axis plies ($\pm 45°$). This saturation is similar for both laminates, but the number of cycles it takes to reach this state is significantly different. In addition, the change in stiffness with increasing life ratio follows similar trends for all other stress levels tested.

The fatigue life curves for the two laminates are presented in Fig. 3.4. There is quite a bit of scatter at high stress levels because the static failure mode observed in our monotonic tests is dominant. As the stress levels decrease the scatter becomes smaller. A best fit curve appears to well represent each set of data. It is noted that the best fit fatigue life lines, corresponding to the two sets of laminates, cross-over. The significant influence of the sequence effect on fatigue life is evident from examining Fig. 3.4.

It was observed that there is no frequency effect in the laminates tested. This is because the overall stress-strain response is essentially rate (frequency) independent due to the dominant role of the $0°$ layers contained in each laminate which restrain the development of cyclic creep in each laminate. In the case of angle-ply $\pm 45°$ symmetric laminates of the same material, a significant frequency effect was observed due to cyclic

creep which depends on the applied stress level and frequency (Kujawski and Ellyin, 1993).

3.5   Finite Element Analysis

Finite element analysis was performed on the configurations of interest using the computer code ANSYS, version 4.4A1. In order to effectively model the specimen and achieve reasonable results, the symmetry of the configuration was used to advantage. The stress distributions determined gives an insight into the behaviour of the laminates.

The dominant mechanism of failure in these specimens under uniaxial tension is interlaminar delamination originating from the free edge, therefore, the analysis is directed towards the interlaminar stresses close to the free edge of each specimen. These interlaminar stresses are large enough to cause free edge delamination to occur and initiate failure in these specimens. The analysis to be described below indicates which specific laminate specimen will be the most prone to interlaminar delamination under uniaxial tension. The stresses close to the free edge were investigated for two lay-up sequences: $[45_2,-45_2,0_2]_s$ and $[0_2,45_2,-45_2]_s$ which are the strongest and weakest lay-up respectively, according to monotonic test results. Additionally, the monotonic stress-strain curves indicate an almost elastic response until failure, Fig. 3.5, therefore, a linear elastic model is utilized.

3.5.1 Numerical Approach

The composite specimens consist of transversely isotropic material, for which the y-z plane is isotropic (Fig. 3.6). It is assumed the lay-up is sufficiently long in the x direction and that the transverse laminate cross section is the only plane of interest. The extent of this finite element analysis is an investigation of the elastic stress field and the analysis is formulated on the basis of a quasi-three-dimensional state where a uniform strain of ϵ_x is applied to the laminate. Excluding the effects from the ends, the general solution for the displacements, u,v and w, of the laminate will have the following form:

$$
\begin{aligned}
u(x,y,z) &= U_o(x) + U(y,z) \\
v(x,y,z) &= V(y,z) \\
w(x,y,z) &= W(y,z)
\end{aligned}
\qquad (3.1)
$$

Because the laminate has two apparent planes of symmetry, the x-y plane and the x-z plane (Fig. 3.6), the model can be reduced to one quadrant of the cross section. The use of the Classical Laminate Theory further reduces the model with the definition of the z' axis. The corresponding dimensions with respect to width and thickness of the laminate are shown in Fig. 3.6. The resulting boundary conditions are as follows:

$$
\begin{aligned}
U(0,z') &= 0 \\
V(0,z') &= 0 \\
W(y,0) &= 0
\end{aligned}
\qquad (3.2)
$$

These boundary conditions are applied to a finite element mesh pictured in Fig. 3.7. The stress strain relationship, eqn. 3.3, is for a transversely isotropic symmetry with the y-z plane being the plane of isotropy and there are five independent material constants.

34

$$
\begin{Bmatrix} \epsilon_{11} \\ \epsilon_{22} \\ \epsilon_{33} \\ \epsilon_{23} \\ \epsilon_{13} \\ \epsilon_{12} \end{Bmatrix} =
\begin{bmatrix}
\dfrac{1}{E_1} & -\dfrac{\nu_{12}}{E_2} & -\dfrac{\nu_{12}}{E_1} & 0 & 0 & 0 \\[2ex]
-\dfrac{\nu_{12}}{E_1} & \dfrac{1}{E_2} & -\dfrac{\nu_{23}}{E_2} & 0 & 0 & 0 \\[2ex]
-\dfrac{\nu_{12}}{E_1} & -\dfrac{\nu_{23}}{E_2} & \dfrac{1}{E_2} & 0 & 0 & 0 \\[2ex]
0 & 0 & 0 & \dfrac{2(1+\nu_{23})}{E_2} & 0 & 0 \\[2ex]
0 & 0 & 0 & 0 & \dfrac{1}{G_{12}} & 0 \\[2ex]
0 & 0 & 0 & 0 & 0 & \dfrac{1}{G_{12}}
\end{bmatrix}
\begin{Bmatrix} \sigma_{11} \\ \sigma_{22} \\ \sigma_{33} \\ \sigma_{23} \\ \sigma_{13} \\ \sigma_{12} \end{Bmatrix}
\qquad (3.3)
$$

This stress-strain formulation is consistent with the quasi-three-dimensional model used in this analysis which assumes for transverse isotropy the following engineering elastic constants:

$$
\begin{aligned}
&E_1 && E_2 = E_3 \\
&\nu_{23} && \nu_{12} = \nu_{13} \\
&G_{12} = G_{13} \\
&G_{23} = \dfrac{E_2}{2(1+\nu_{23})}
\end{aligned}
\qquad (3.4)
$$

Where $E_1 = E_L$ is the longitudinal elastic modulus, $E_2 = E_T$ is the transverse modulus, and $E_3 = E_T$ is perpendicular to the LT plane. The following constants were specified by the manufacturer of the prepreg material used for the construction of the laminate specimens in the reported tests:

$$
\begin{aligned}
E_1 &= 39 \ GPa \\
E_2 &= 10 \ GPa \\
\nu_{12} &= .275 \\
\nu_{23} &= .275 \\
G_{12} &= 4.0 \ GPa
\end{aligned}
\qquad (3.5)
$$

35

Because the elastic stress field contains high gradients, the finite elements are placed to maximise accuracy of the computed results. The finite element mesh, consisting of 900, eight node three dimensional elements, is finer in areas of these high gradients (Fig. 3.7). Smaller elements are employed close to the ply interfaces, because there are stress concentrations within 1/20th of the layer thickness at the interface, and close to the free edge because the free edge effects extend only a few ply thicknesses into the interior.

The specific element used is rectangular and has three degrees of freedom at each node. It is formulated with a 2x2x2 lattice of integration points utilizing the Gaussian integration procedure. This element features a variable element coordinate system making it possible to orient material properties in any in-plane direction. Essentially, the model has the same material properties for all elements except for the fact that they are oriented at 45° and -45° in the off-axis layers.

3.5.2 Results

Consider the two six layer laminates of interest, $[45_2,-45_2,0_2]_s$ and $[0_2,45_2,-45_2]_s$, under uniaxial strain, ϵ_x as shown in Fig. 3.6. In the case of an infinite width laminate, the Classical Lamination Theory predicts a uniform state of plane stress in each layer. The Classical Laminate Theory stress components, σ_x and τ_{xy}, vary from layer to layer but are constant within each layer. Since the effects of the free edge of the laminate are being considered and consequently the in-plane shear stresses are required to vanish along

the free edge, the Classical Laminate Theory does not apply to our model, it is only used as a boundary condition.

The finite element analysis predicts that each laminate has different stress distribution near the free edge. Therefore, these stresses will have an effect on the monotonic and fatigue performance of the laminate. The results are presented in Figs. 3.8-3.12 which show the normal and shear stress distributions between each ply in the laminates from close to the free edge until they converge to a steady state value approximately five times the thickness of a single layer. The distance from the free edge is normalized with respect to the thickness of a single layer in the laminate, (y-b)/t, and the corresponding stresses with respect to the average stress in the axial direction, i.e. σ_z/σ_x.

Figure 3.8 presents the results for the interlaminar normal stress, σ_z, in the $[0_2,45_2,-45_2]_s$ laminate. The normal stress is of interest because it contributes to interlaminar delamination if it is tensile. It can be observed that close to the free edge there is a significant increase in the normal stress especially between the $45°$ and $0°$ layers. This normal stress is in tension and therefore indicates the inducement of premature delamination within these layers starting at the edge of the laminate. It is important to note that the normal stresses in a perfectly elastic model approach infinity at the free edge.

Figure 3.9 presents similar results for the $[45_2,-45_2,0_2]_s$ laminate. It can be observed that there is a small normal stress between - $45°$ and $0°$ layers but a significantly higher normal stress between $45°$ and $-45°$ layers. This high normal stress

37

is in compression and therefore does not induce premature delamination.

Figures 3.10 and 3.11 present the variations in interlaminar shear stresses, σ_{yz}, for the two laminates investigated. It can be observed that the shear stresses are relatively high close to the free edge, however, the overall magnitude of shear stress is smaller for the $[45_2,-45_2,0_2]_s$ laminate in comparison to that of $[0_2,45_2,-45_2]_s$. These shear stresses will also contribute to delamination close to the free edge. As discussed previously, the shear stress is required to be zero along the free edge of the laminate which can be observed in the trend of the stresses in the figures.

Figure 3.12 presents the normal stress distribution across the laminate thickness along the free edge. The magnitude of normal stress is presented two nodes in from the free edge from the surface to the centre line of the laminate. It can be observe that the $[45_2,-45_2,0_2]_s$ laminate has normal stresses along this line predominately in compression. In contrast, the $[0_2,45_2,-45_2]_s$ laminate has normal stresses that are in tension and therefore indicating that the free edge effects on this lay up may induce premature delamination.

3.6   Discussion

Monotonic tensile and fatigue behaviour of symmetric fibreglass-epoxy laminates were studied with respect to failure strength, stiffness, fatigue life and damage mechanisms considering three different ply sequences: $[45_2,-45_2,0_2]_s$, $[45_2,0_2,-45_2]_s$ and $[0_2,45_2,-45_2]_s$. All three lay-ups were tested under monotonic tensile loading and only

the first and last of the above lay-ups were tested under fatigue loading. In addition, the first and last of the above lay-ups were analyzed by 3D finite element discretization.

Monotonic tensile tests were performed on coupon specimens with the three stacking sequences of interest utilizing a constant strain rate. Without changing the laminate material or specimen dimensions, a 10% increase in the strength and a 7% increase in the stiffness was observed between the weakest laminate, $[0_2,45_2,-45_2]_s$, and the strongest laminate, $[45_2,-45_2,0_2]_s$. Interlaminar stresses close to the free edge affect the monotonic strength of these laminates. The $[45_2,-45_2,0_2]_s$ is the strongest because the interlaminar normal stresses are always compressive, unlike the other laminates, and consequently no premature delamination develops (compare Figs. 3.8, 3.9 & 3.12). The sequence of the layers in the laminate is simple to change and produces significantly different global behaviour. Strength and elastic modulus are effected by lay-up sequence.

The trend observed in the cyclic tests at low stress levels is opposite to the one in the monotonic loads. Under lower stress levels the $[0_2,45_2,-45_2]_s$ laminate has a longer fatigue life. This phenomena can be attributed to the constraint effect of the $0°$ plies on the $45°$ plies. The $0°$ plies retard the growth of transverse cracks in the internal plies. In addition, the internal plies constrain the $0°$ plies from developing longitudinal cracks because the resulting transverse stress on the $0°$ plies is compressive. This compressive transverse stress, σ_y, is a result of the different Poisson ratios in the plies as depicted in Fig. 3.13. The Poisson's ratio for the $0°$ ply is 0.27, supplied by the manufacturer, and the $\pm45°$ is 0.78, from the literature. The resulting transverse stress is approximately 23% the axial stress in the $0°$ plies and about 11% for the $45°$ plies in each laminate,

39

respectively. These values were obtained from the finite element analysis. The later constraint effect is also present in the $[45_2,-45_2,0_2]_s$ laminate but the $45°$ plies have an exposed surface with no constraints thus: it is free to develop transverse cracks and therefore approach the saturation state faster than the other laminate. The fatigue failure of these lay-ups is dominated by delamination at high stress levels and transverse cracking at lower stress levels.

Unlike the case of $[\pm45]_{5s}$ laminates (Kujawski and Ellyin, 1993) this investigation indicates that the applied loading frequency did not appear to have a significant influence on the fatigue life because the $0°$ plies restrain the development of cyclic creep.

The finite element analysis was completed assuming linear elastic and therefore only predicts the stresses under these conditions. It gives us an insight into the interlaminar stress distribution in these laminates. Additionally, the change of lay up sequence appears to significantly change the distribution of stresses close to the free edge of the laminate. It was observed that there are high tensile normal stresses close to the free edge in the $[0_2,45_2,-45_2]_s$ laminate and therefore one can predict that in monotonic tests this laminate will fail before the other lay-ups because of premature delamination originating from the free edge.

The fa·· that the monotonic results are similar to the high stress short fatigue life tests and differ from the lower stress longer life tests, demonstrates the need for both types of testing in order to properly characterize these types of laminates.

3.7 Conclusions

The results of experimental and numerical investigations reported here lead to the following conclusions:

I   Strength and stiffness are affected by lay-up sequence and edge effect.

II   Low stress level fatigue tests indicate ply constraint effects.

III   There is no apparent frequency effect.

IV   Finite element analysis can be used to predict lay-up sequence effects, and interlaminar stresses.
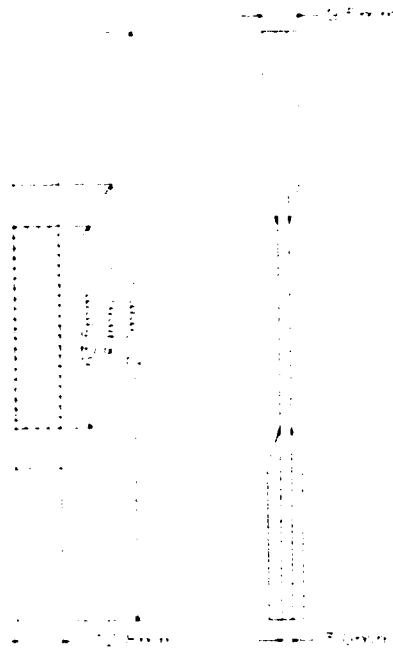
Figure 3.1 Coupon Specimen Schematic
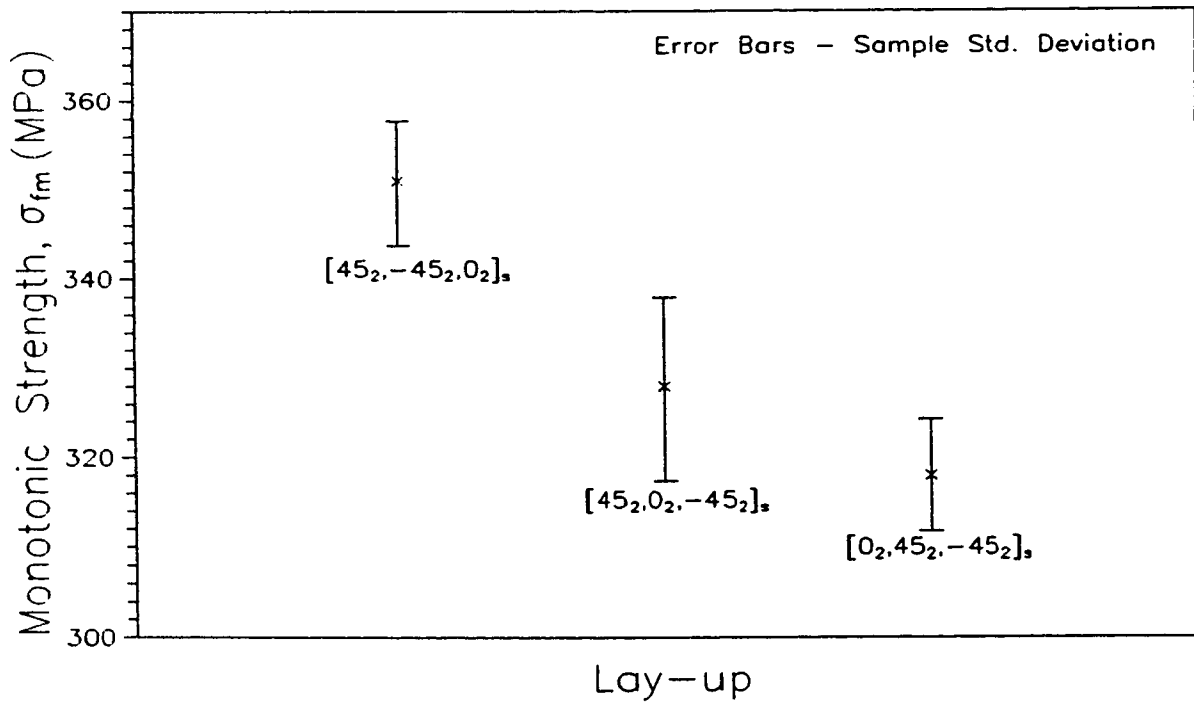
Figure 3.2 Monotonic Failure Strengths
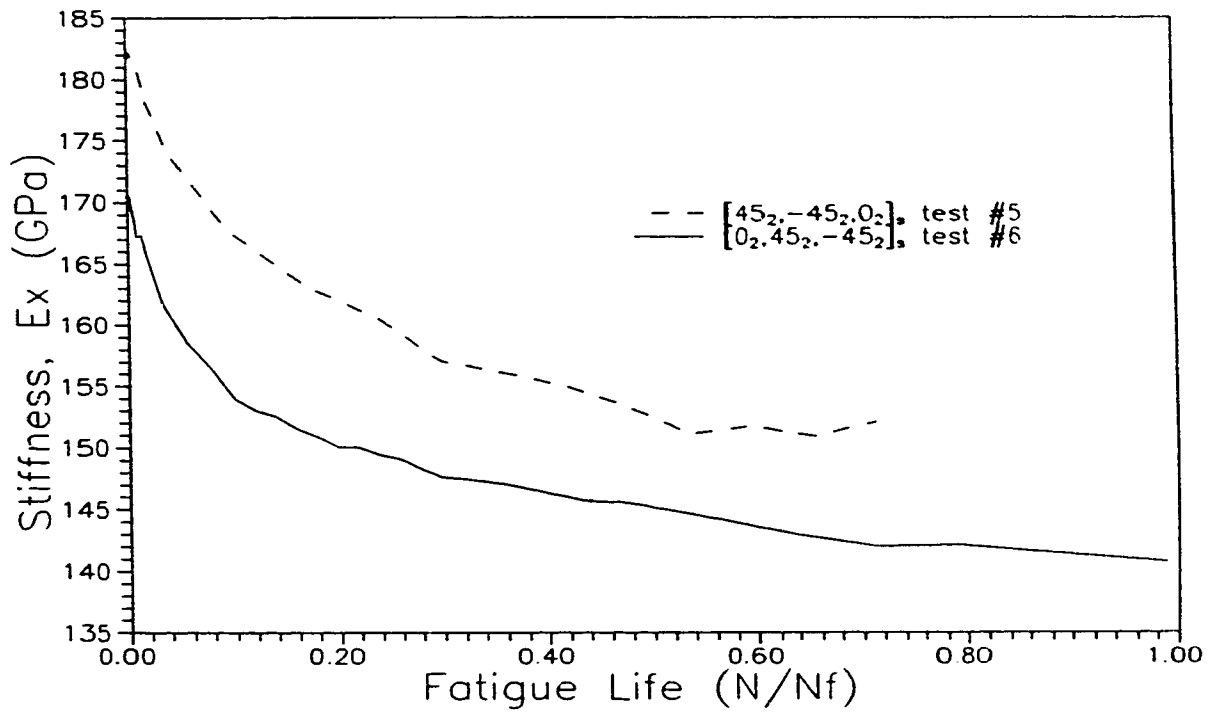
Figure 3.3 Typical Change in Stiffness Over Fatigue Life
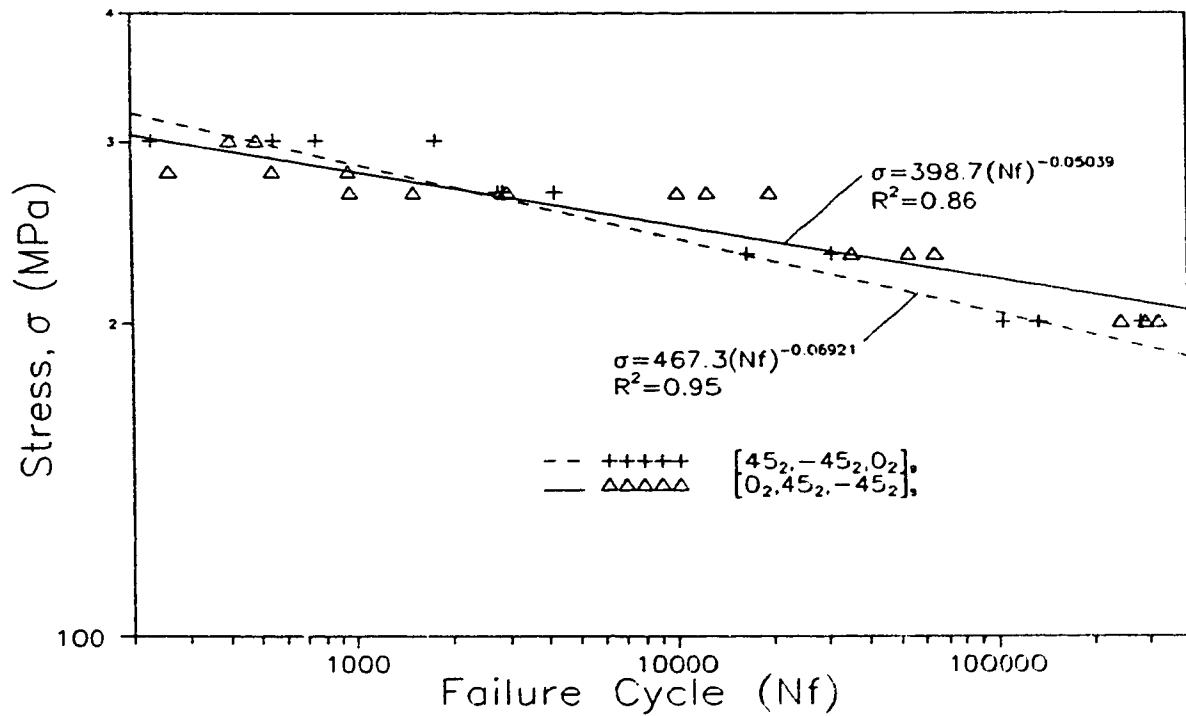
Figure 3.4 Fatigue Life vs. Stress Level

43
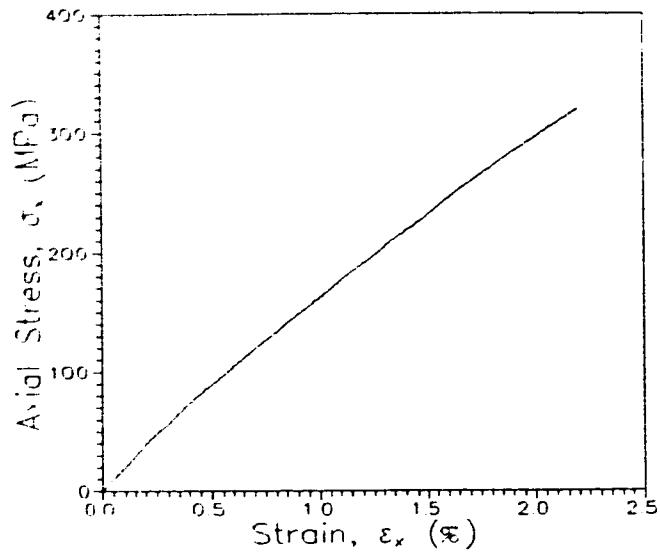
Figure 3.5 Typical Monotonic Stress-Strain Curve - $[45_2, -45_2, 0_2]_s$
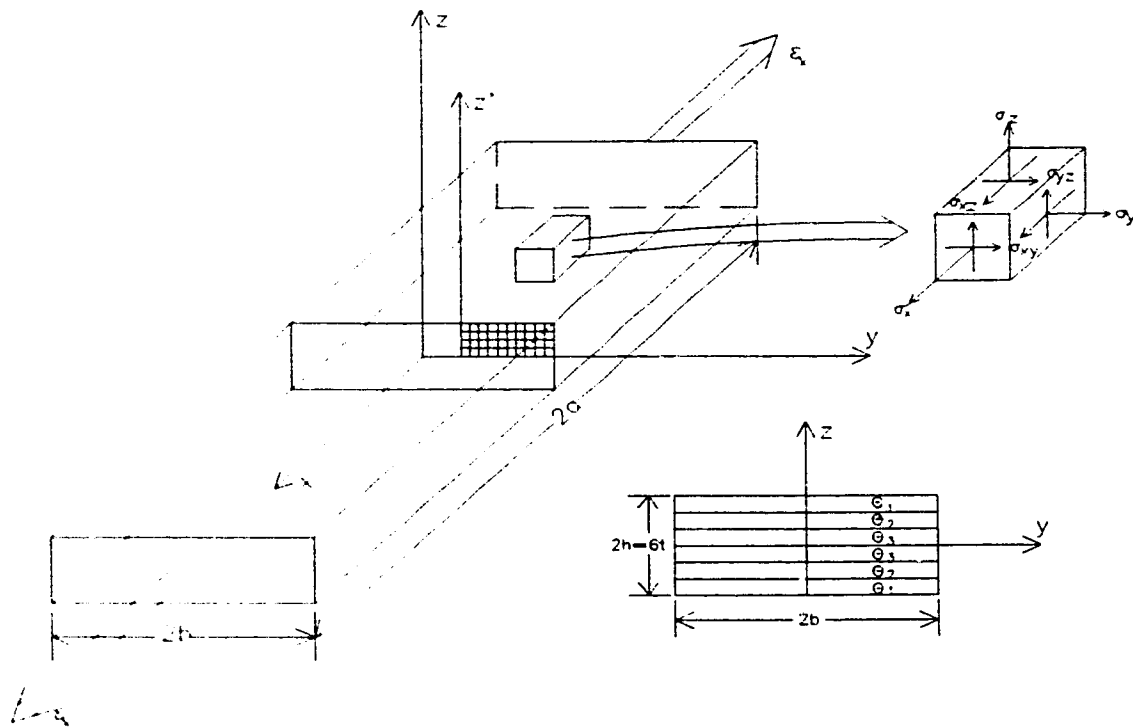
Figure 3.6 Geometry of Laminated Coupon Specimen Under Uniaxial Tension

44
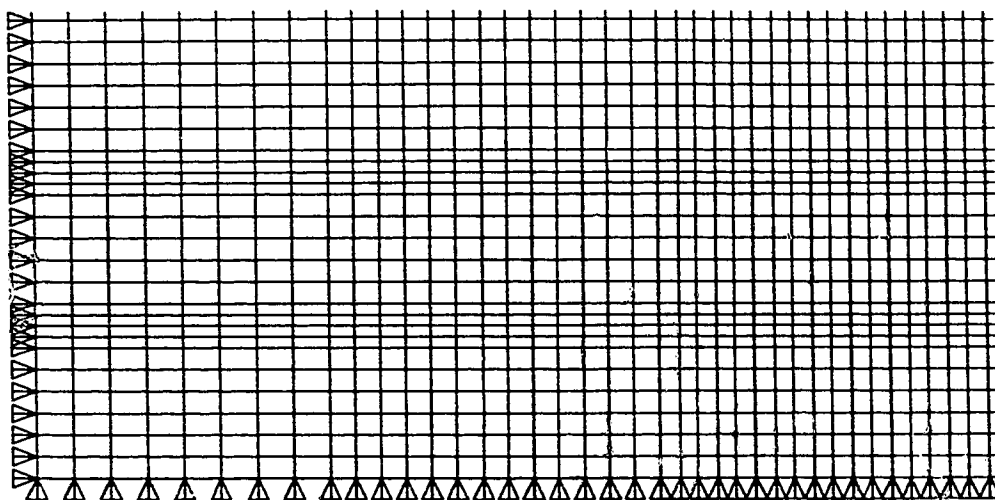
Figure 3.7 Finite Element Mesh
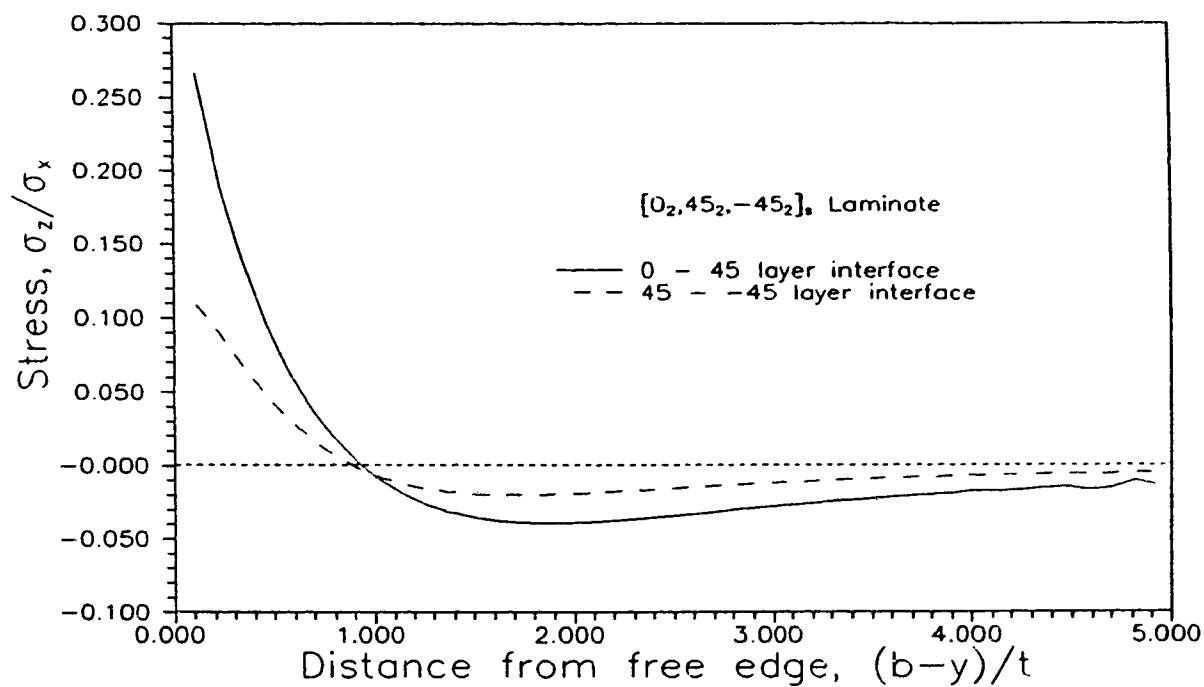
Figure 3.8 Normalized Interlaminar Normal Stress, σ_z/σ_x, Verses Distance From Free Edge, (b-y)/t, of a $[0_2,45_2,-45_2]_s$ Laminate

45
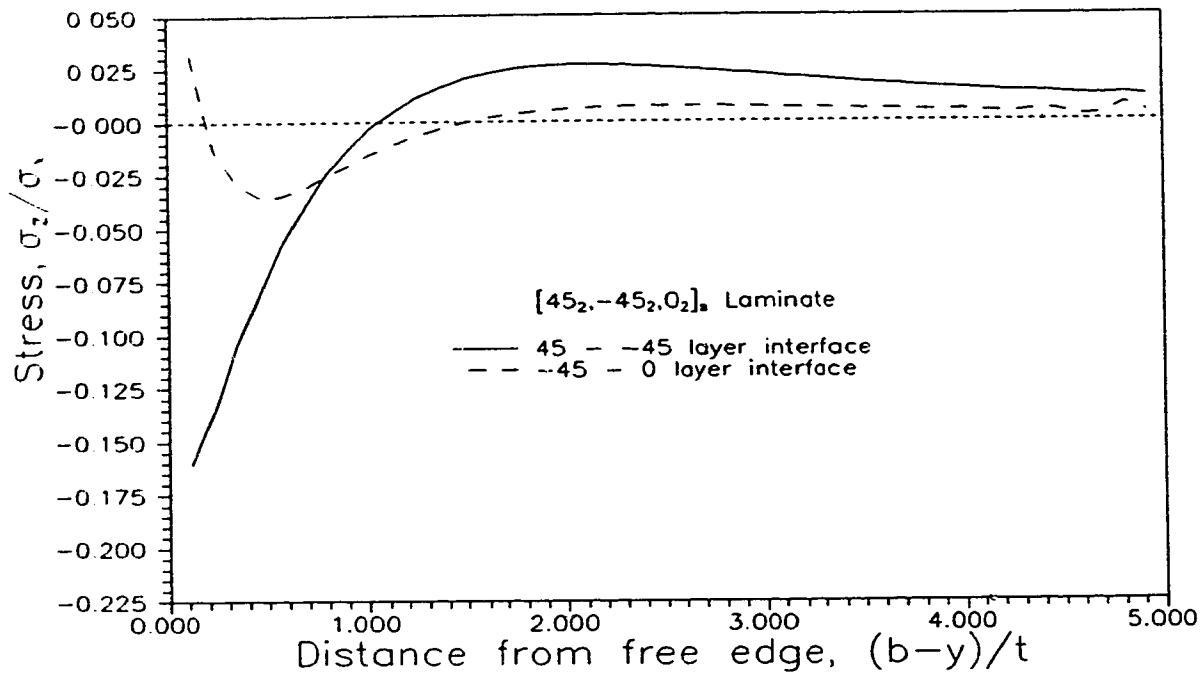
Figure 3.9 Interlaminar Normal Stress for a $[45_2,-45_2,0_2]_s$ Laminate
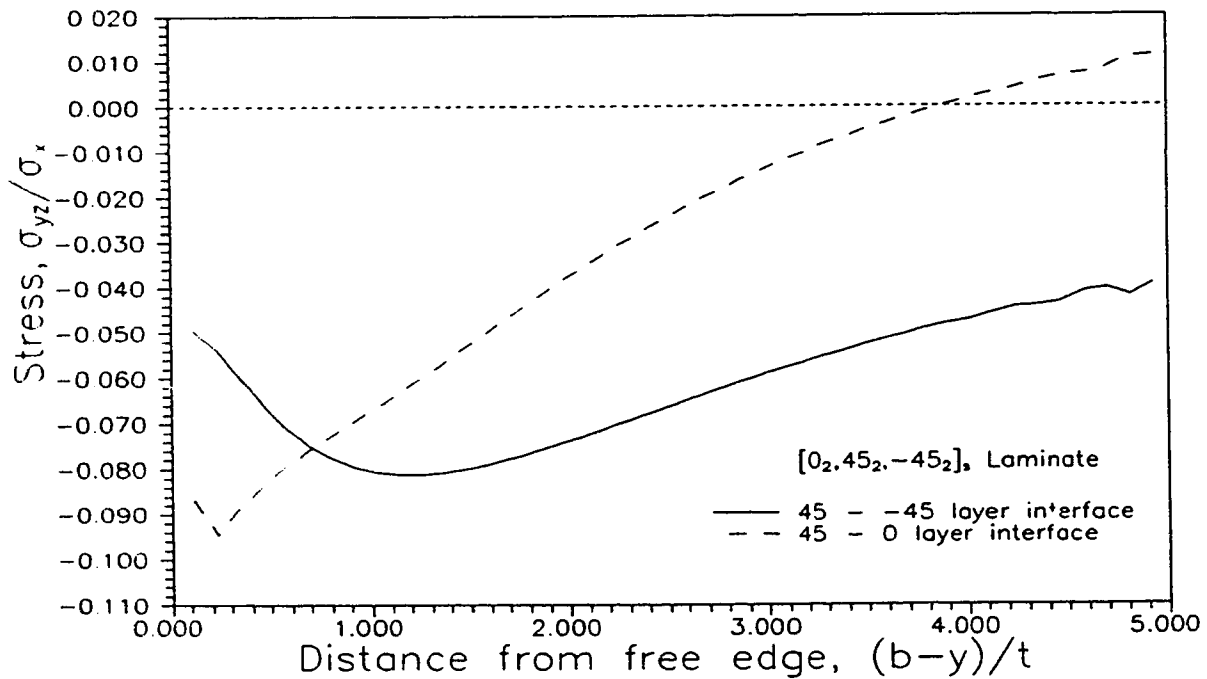
Figure 3.10 Normalized Interlaminar Shear Stress, σ_{yz}/σ_x, Verses Normalized Distance From Free Edge, (b-y)/t, for a $[0_2,45_2,-45_2]_s$ Laminate

46
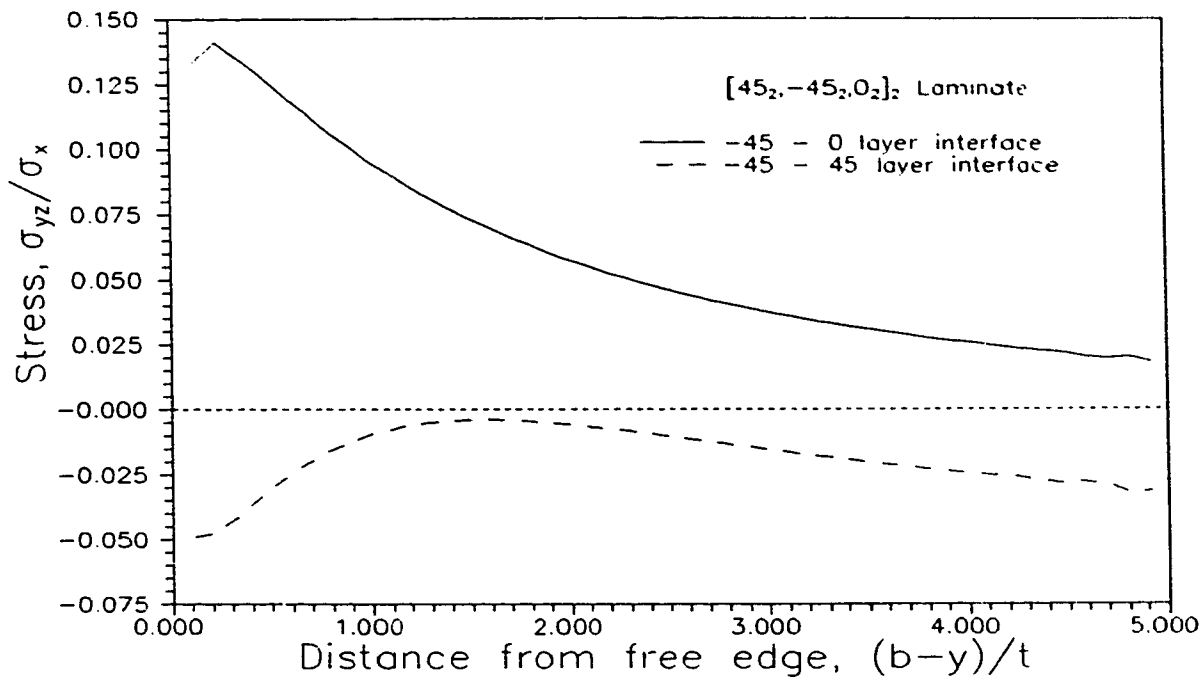
Figure 3.11 Interlaminar Shear Stresses for a $[45_2,-45_2,0_2]_s$ Laminate
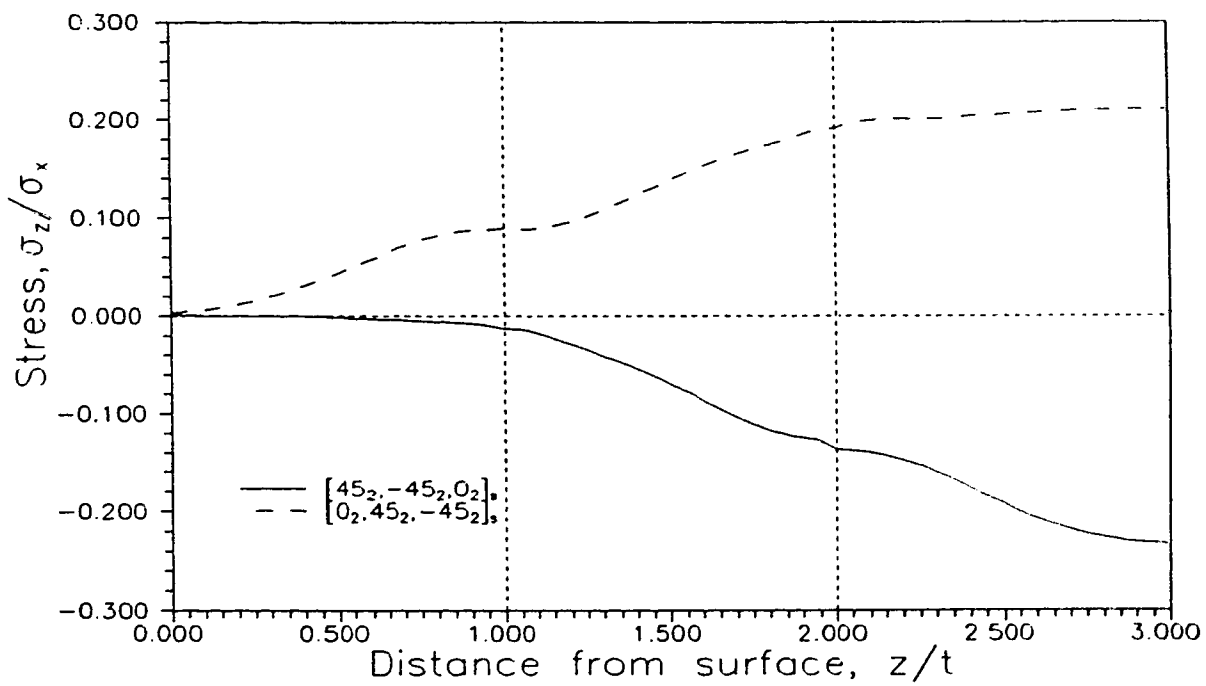
Figure 3.12 Normalized Normal Stress, σ_z/σ_x, Verses Normalized Distance Along the Free Edge, z/t
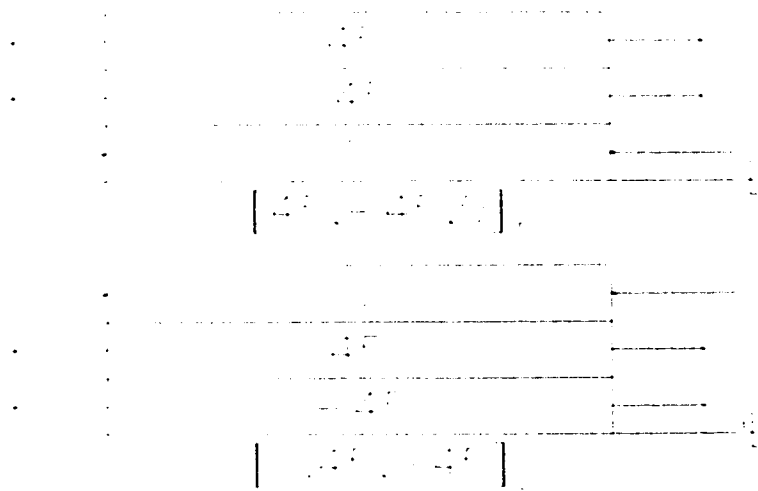
Figure 3.13 Ply Constraint Effect

CHAPTER 4

BIAXIAL TESTING APPARATUS AND TESTING PROCEDURE

4.1 Introduction

A biaxial testing apparatus was developed in order to apply the desired loading to the filament wound tubes. A high pressure system was added to a MTS axial load machine in order to produce biaxial loading. In addition, an advanced control and data acquisition system was developed to facilitate the execution of precise and informative tests. Figure 4.1 illustrates the complexity of this system.

Fibre reinforced plastic is generally regarded as a brittle material and stress concentrations are important in brittle materials because local stresses cannot be redistributed and relieved by yielding and plastic flow. For this reason attention must be given to all stress concentrations caused by defects, damage, other outside sources such as strain gages and extensometers and especially gripping systems.

Specially developed end grips were fitted on the specimen in order to apply the axial tension and compression loading and achieve a high pressure seal. Considerable time was spent designing these grips because of the inherent problems with gripping brittle composite materials with metal grips. The main problem is the development of damaging stress concentrations at the transition between the end of the grip and the specimen. This difficulty has been approached in different ways in the past, however, the proposed solutions have not been completely successful, causing failures close to the

49

grips and away from the test section.

Most of the grip designs have involved modification to the specimen itself. The addition of end reinforcements in the form of circumferential overwinding with E-glass fibre reinforced epoxy resin was used by Soden et al. (1993) in his biaxial testing of filament wound composite tubes. The ends of the tubes were built up gradually in order to minimize stress concentrations and prevent end failures caused by the grips. These built up ends were mounted in aluminum inner and outer grips with cast epoxy resin. Failures outside the test section were still observed in this study.

Another approach used by Soden et al. (1978) was to cast threaded ends onto the tubular specimens for gripping. These threaded ends where mounted in a standard threaded end grip for axial testing machines. These built up sections do not alleviate the problem of stress concentrations especially when the addition is an axisymmetric step as with the threaded built up section and when the loading involves internal pressure which induces high axial stresses close to the grips.

Lee et al. (1989) performed tests specifically designed to investigate the effects of axisymmetric steps on failure strengths. The study also involved the use of finite element analysis to model the stress concentrations caused by the steps. It was determined that if internal pressure was present, high axial stresses developed at the end of the step or grip in the form of tensile stresses on the inside surface and compressive stresses on the outside surface. This type of loading is very damaging to the tube at the stress concentration and can cause failures an order of magnitude lower than the typical failure strength.

Although a gradual built up section is one way to alleviate most stress concentrations, this was not possible to do in our testing. The test specimens were cut from a pre-made long section, therefore, the work involved in reinforcing the ends to facilitate effective gripping was deemed uneconomical. In addition, a gripping system that was relatively easy to assemble and disassemble was required. This involved the development of a system utilizing friction as the means of transferring the load from the grips to the specimen instead of the frequently used cast resin method.

4.2   Testing Apparatus

A requirement of successful biaxial testing of FRP tubes is that the cost of equipment and testing process must not be prohibitive. The biaxial testing apparatus used in this investigation was developed through some economical modifications to existing equipment and manufacturing of most new equipment at the University of Alberta.

The axial load frame was developed from an existing MTS axial loading machine pictured in Fig. 4.2. This machine is capable of 375kN axial load in tension or compression. Specially developed grip adapters were used to mount the grip-specimen unit into the machine with six 5/8in diameter high strength bolts securing the grips to the machine. The control system on the MTS axial testing machine was modified so we could perform the desired tests. This MTS machine utilizes servo valves in a closed loop system to control the applied load. The servo valves are controlled by a MTS model 405.10 servo controller and this receives the load signal from a modified MTS model 410

51

digital function generator pictured in Fig. 4.3. This function generator was able to provide the appropriate signal for all the tests performed in this investigation.

In order to achieve the biaxial state of stress of interest in this investigation, internal pressure was added to the loading on the tubes. A servo controlled pressure system was developed which includes: pressure intensifier, servo valve, control unit, and pressure transducer. This high pressure unit (Fig. 4.2), used to develop the internal pressure needed for this investigation, was slightly more complicated to develop. It was determined that 82.7MPa would be adequate to fail the FRP tubes under any loading condition and therefore we needed to multiply the available 20.5MPa high pressure line. This was achieved be modifying an available 1:10 pressure intensifier to a 1:4. The 1:10 intensifier would have been adequate but an increase in the volume was desirable. The existing intensifier was modified by boring out the slave cylinder to a diameter of 22.2 mm. Considering the master cylinder with a bore of 44.5 mm an intensifying factor of 4 was obtained.

In order to apply a controlled pressure for the biaxial tests a control system was developed. A MTS servo valve, Fig. 4.2, was incorporated into the high pressure system. This enabled the control of flow into the intensifier and therefore control of the pressure. This servo valve was controlled by a specially developed servo controller pictured in Fig. 4.3. The signal used to control the pressure was produced by the same digital function generator that the axial load machine used.

The pressure unit, intensifier, servo valve, transducers, and necessary tubes and valves, are located on the frame of the MTS axial loading machine as pictured in Fig.

4.2. This location was chosen so the length of high pressure stainless steel tubing used was as short as possible. The reason for this is the fact that there is only a small volume of oil, 65×10^3 mm^3, in the pressure intensifier and any expansion in the tube would detract from the available oil for the specimen. In addition, the location aided in the filling of the specimen since it was necessary to manipulate valves on the pressure unit and play close attention to the bleed valve on the top of the gripping system.

An error detection circuit was developed in order to determine when the test should stop. This circuit monitors the difference between the desired pressure and the actual pressure determined with the pressure transducer. An error signal occurs when this difference reaches a predetermined value. In addition, this circuit monitors the position of the cross head on the piston of the axial testing machine. If the position is greater or less than a predetermined range an error occurs. When an error occurs the system does not shut down the testing machine as most interlock error detection systems do, it returns all loads to zero and waits for further instructions. Additional interlocks are present beyond these levels that will shut down the testing machine for safety reasons. This error detection system was developed in order to protect the tubular specimens from additional damage after initial failure occurs.

It is important to note that the axial and hoop loading was uncoupled mechanically by the control system. As with all cylinders with fixed ends the pressure vessel loading conditions are present. This means that the internal pressure not only produces hoop stress but axial as well because the internal pressure applies force to the end grips. This stress is always 1/2 the hoop stress and therefore, the control system always applies the

appropriate compressive load in order to cancel this induced axial stress.

4.3 Grip Design

Friction grips to hold and seal the tubular specimens have been designed and used successfully in this experimental study as illustrated in Fig. 4.4. Since the tubes have no built up section it is very important to minimize stress concentrations caused by the grips and because they use friction it is important to create high normal stresses. This gripping system achieves this through the incorporation of a double collet configuration. The collets used are cylindrical sections with one surface tapered to a specific angle, shown in Fig. 4.5.b and 4.5.c, 8° and 2° respectively. Each collet has eight vertical slits cut most of the way through and one cut all of the way through in order to facilitate expansion and contraction of the surfaces.

The grip consists of a high strength steel (AISI 4340) mandrel with a conical end shown in Fig. 4.5.a, with a tapered flexible steel collet placed around it. The outside surface of the collet has been sandblasted in order to increase the friction coefficient between the steel and the epoxy matrix of the FRP tube. These components are inserted in the tube. Another tapered flexible sandblasted steel collet is placed around the outside of the specimen with the taper facing the opposite way. The mandrel, collets, and tube are then inserted into a heavy steel collar (Fig. 4.5.e) that has a conical inside surface that matches the taper on the outside collet. A steel ring (Fig. 4.5.d) is then bolted to the collar compressing the outside collet and creating significant normal forces on the

54

outside surface of the specimen. A nut is then threaded on to the mandrel and tightened against the collar applying tension to the mandrel which in turn causes the conical surface on the mandrel to force the inside collet outward subsequently applying a normal force to the inside of the tubular specimen.

In order to increase the normal force on the surface of the specimen the unit is placed in an INSTRON axial loading machine and an additional 155 kN is applied to the gripping system. The collar is constrained with a secure steel frame while the tensile load is applied to the mandrel forcing the inside collet to expand and apply an additional normal force of approximately 275 MPa to the inside of the specimen.

The normal and friction forces created by this gripping technique are sufficient to secure the tubular specimen for rigorous biaxial testing. This configuration works very well in tension and compression. In addition, no slippage, pull out or failures close to the grips have been observed. In the case of internal pressure some damage develops at the transition between the grip and specimen. Interlaminar delamination is observed but primary failure still occurs in the test section. The reason for this damage has been explored by Lee et al. (1989) and will be discussed is section 5.3.5c.

In addition to gripping the specimens, they must be tightly sealed in order to apply the high pressures needed to achieve failure. A brass piston (Fig. 4.5.f) was manufactured to very close tolerance to achieve a clearance on the inside of the tube of less than .12 mm. A high durometer 3/16in o-ring was placed on the piston. The clearance is quite large because the inside diameter is not perfectly circular. The pistons are attached to the end of the mandrel with the o-rings located in parallel with the top

of the outside collar. The reason for this location is the fact that the clearance for the o-ring must remain very small otherwise the o-ring will extrude through the clearance gap and the seal will fail. The outside collet constrains the radial displacement and therefore the clearance stays within acceptable values. The high pressure oil is transported to the tubular specimen through a stainless steel tube located through the mandrel and sealed with a small o-ring where the piston screws into the mandrel as illustrated in Fig. 4.4.

The gripping system, illustrated fully assembled in Fig. 4.4, has been proven to 275kN tension, 220kN compression and 82.7MPa. internal pressure.

4.4   Data Acquisition

An extensive data acquisition system was developed in order to record all variables of interest. An IBM PC with a data acquisition card with eight input channels facilitates the gathering of data efficiently. The variables monitored are: load, pressure, axial strain, transverse strain, and change in oil volume. Load and pressure readings are gathered from the existing transducers, the strain is obtained using three different methods: strain gages, extensometers and axial cross head position and oil volume information is gathered by monitoring the position of the piston in the pressure intensifier.

The axial load was measured by a load cell located at the bottom of the grip assembly pictured in Fig. 4.2. This load cell is an integral part of the control system as

well as for data acquisition because all the experiments are load controlled.

The pressure is measured with an Omega model PX613 transducer. This transducer is located underneath a manifold located after the pressure intensifier. The transducer is used for control purposes as well as for data acquisition.

Strain of the tubular specimens was measured using three different techniques. The first was with specially developed axial and transverse extensometers. These extensometers, pictured in Figs. 4.6, 4.7.a and 4.7.b, were manufactured at the Mechanical Engineering machine shop. They are made out of 6061 T6 aluminum and incorporate 350Ω strain gages in full bridge configurations. The axial extensometer, Fig. 4.7.a, has a gage length of 50.8 mm and is fastened to the specimen utilizing knife edges and springs as illustrated in Fig. 4.6. The diametral extensometer has adjustable set screws with sharp ends to facilitate attachment with a spring applying the inward force. Both of these extensometers have a resolution of .001% strain and a range of approximately -5% to +5% strain.

Another method of measuring axial and hoop strain on the specimen is the use of long gage length strain gages. Micro Measurements 12.7 mm gage length 350Ω strain gages were applied to the specimen. There was significant preparation made to the surface of the specimens in order to apply the strain gages in the form of sanding and chemical treatment, but, very consistent measurements resulted. One gage was applied in the axial direction and one in the transverse direction and both were in a quarter bridge configuration. They had very low excitations, approximately 2V, in order to avoid specimen heating and subsequent change in sensitivity of the gages. In addition,

57

the gain was low so the data acquisition system could accommodate ? gage output for ±5% maximum strain. This was the limit of the linear range of these gages. The measurements from the strain gages were compared to the extensometer measurements and the results correlated very well.

As an additional backup, the stroke of the axial load machines piston was monitored. This gave us the displacement of the entire tubular specimen and gripping system. A compliance calibration curve was developed in order to correlate the crosshead displacement with strain on the specimen test section. The resolution of this measurement technique was not as good as the other two methods.

Three strain measurement techniques were used in order to provide backup measurements when systems failed. The extensometers were not used when violent failures were expected and the strain gages failed when cracking developed on the outside surface of the tubes. The monitoring of the stroke provided a final backup for axial strain measurements. In most cases appropriate strain measurements were acquired but some extrapolation was necessary on the experiments with very high strain.

The position of the piston in the pressure intensifier was monitored to provide information on oil volume accumulated in the system. This oil volume measurement was used to determine the change in volume in the tubular specimens and to help predict when leakage of fluid through the specimen wall initiated.

All of this data was collected by an IBM PC with a Metra Byte Das-8 data acquisition card. The data was collected and displayed as the test progressed and upon completion the data was stored on hard disk drive for later manipulation. This is an

improvement to Soden et al.'s (1993, 1989, 1985) method which involved the pausing of the test while strain data was collected. A program, appendix D, was written in Quick Basic in order to facilitate data collection and a few control tasks.

4.5 Specimen Preparation and Testing Procedure

A procedure for biaxial testing of FRP tubular specimens has been developed. This procedure involves a number of steps: specimen preparation, grip assembly, strain gage application, grip mounting, testing machine set up, running of experiment, removing tested specimen from grips, analysing specimen and data analysis.

The tubular specimens used in this experiment originated from a long section. One foot lengths were cut from the section and then prepared for effective gripping, assembly into grips and for strain gage application. Each end of the tubular specimen, approximately 75 mm, was modified in a lathe. A body file was used to smoothen the surface so there was more surface area contact in the grips. The excessive epoxy coating on the pipe was removed but no fibres were damaged. In addition, small areas in the test section were prepared for the strain gages using a small grinder. The areas were sanded smooth and cleaned with special solvents designed to prepare plastic surfaces for strain gages. The ends of the tubular specimens were rounded in order to make the insertion of the mandrel and brass piston easier and to prevent damage to the o-ring.

The grip is assembled in a predetermined order. First of all the brass piston is attached to the mandrel and a high durometer o-ring is placed on the piston. The

mandrel and piston are then forced in one end of the specimen using a rubber mallet followed by the small inside collet which slides into place over the conical end of the mandrel. The outside collet is then fitted to the specimen and the entire unit is inserted into the heavy collar. The restraining ring is then bolted to the collar, paying careful attention to the alignment of the ring, compressing the outside collet. Before the other side of the grip can be assembled the restraining ring must be placed over the specimen. Bolts are threaded on to both mandrels and tightened in order to activate the grips. After the grips are assembled they are preloaded using the previously discussed technique.

Strain gages are then applied to the prepared areas on the test section of the tubular specimen. These long gage length strain gages are secured to the specimen with glue and lead wires are soldered to them. Since the gages are only being used once in each test it is not important to protect them from the environment.

The grip specimen unit is then mounted into the testing machine. The machines cross head is raised to the maximum height and the unit is placed on the bottom grip adapter. The stainless steel tubing used for the high pressure line is then attached to the fitting at the bottom of the grip and the specimen is filled with oil. A cap is placed on the top fitting after all of the air has been bled, in order to seal the specimen. The cross head is then lowered until it is possible to attach the grip to the top grip adapter. The extensometers are then placed in their respective positions as picture in Fig. 4.6. A Lexan shield is then placed around the specimen for our protection and confinement of oil and fragments from the filament wound tubes resulting from failure.

At this stage in the procedure all data acquisition needs to be verified. the loads

zeroed and testing loads calculated. Initially a program is run on the IBM PC that displays all values of interest so that the strain gages and extensometers can be balanced, the piston in the intensifier can be with drawn all the way for maximum available volume and the load is as close to zero as possible. Then the primary data acquisition and control program is run. The loading condition for the test is entered into this program which returns the appropriate settings for the axial and pressure servo control. Once these values have been applied the program coordinates the start of the test and begins to take data and display it. The program monitors the interlock errors and stops taking data. stops the testing machine and saves all the data on the hard disk drive if any error occurs.

The removal of the specimen from the grips involves a few steps. The grips, separated or still attached, are removed from the testing machine. The remaining section of specimen is cut from the grips using a cut off saw. The grips are then placed back in the preloading frame and loaded to the original preload of 155 kN in order to remove the bolt from the mandrel. With the collar still restrained the mandrel is placed into compression and forced out the other end of the grip. The inside collet can then be removed simply by slipping it through the open end of the grip. The remaining section of specimen and the outside collet is forcefully removed utilizing a punch and a hammer with the four holes located on the back of the collar which expose the specimen and collet.

The test section of the tubular specimen which was initial cut out is then investigated using a couple of different methods. On the macro scale the specimen is

investigated for type of failure and visible damage. On the micro scale small sections of the test section are removed, placed in epoxy, polished, and observed under a microscope. Pictures are taken of all these results. These techniques and observations will be discussed extensively in section 4.8.

4.6   Tests Performed

The biaxial testing apparatus and procedure developed is used to test the FRP tubular specimens under various stress conditions. In order to properly define the failure envelopes associated with biaxial testing, specific test were performed. Recalling the capabilities of the testing apparatus; axial tension, axial compression and internal pressure, this type of loading can only achieve biaxial states of stress in the positive hoop stress and positive and negative axial stress quadrants. To define the biaxial failure envelopes efficiently and effectively, monotonic loads were applied to the specimens assuming a stress ratio, hoop stress to axial stress. In each test the ratio of internal pressure to axial load was maintained constant at a predetermined value while the load increased at a steady rate until failure as illustrated in Fig. 4.8. Five stress ratios were used to adequately define the shape of the failure envelope. The tests performed had the following stress ratios: zero hoop stress to one axial tensile stress (0H:1A), tension only test, one hoop stress to zero axial stress (1H:0A), zero hoop stress to one compressive axial stress (0H:-1A), compression only test, one hoop stress to one axial tensile stress (1H:1A) and two hoop stress to one axial tensile stress (2H:1A). The first three ratios

test the uniaxial loading strength and characteristics of the tubular specimens, the fourth ratio is determined by netting analysis to be the strongest ratio for the multidirectional tubes if only the ±45° fibres are considered and the fifth ratio is determined by netting analysis to be the strongest ratio for the ±55° tubular specimens. Netting analysis is discussed in chapter 2. In summary, the five stress ratios are as follows:

OH:1A - tension

1H:1A - netting analysis (±45°)

2H:1A - netting analysis (±55°)

1H:0A - internal pressure

OH:-1A - compression

The multidirectional tubes were also tested with the stress ratio of 1H:-1A in order to help define the shape of the envelope. This ratio was decided on after the envelope was initially defined in order to determine the shape of the envelope more effectively.

In most previous biaxial tests the tubular specimens were loaded by the application of a constant strain rate to failure, discussed in chapter 2. This experimental investigation, in addition to defining the shape of the failure envelopes, explores the time dependent characteristics of the FRP filament wound tubular specimens. This means that time or rate of loading becomes a variable in the experimental program. The testing apparatus was designed to operate under load control in order to imitate service conditions closely and therefore, the rate of loading is defined by the stress. As

illustrated in Fig. 4.8, the change in stress over the change in time remains constant for each specific test. Three different values for $\delta\sigma/\delta t$ were chosen in order to investigate the time dependent effects in the composite. At each rate, $\delta\sigma/\delta t$, all five stress ratios were tested. For each specific stress ratio a "von Mises" type equivalent stress was calculated, equation 4.1, and $\delta\sigma/\delta t$ was applied accordingly, equation 4.2.

$$\sigma_{eq} = \beta\sqrt{\sigma_1^2 - \sigma_1\sigma_2 + \sigma_2^2} \qquad (4.1)$$

$$\dot{\sigma} = \frac{\delta\sigma_{eq}}{\delta t} \qquad (4.2)$$

The three rates used were approximately: $\dot{\sigma}_1 \approx 500\text{kPa/sec}$, $\dot{\sigma}_2 \approx 50\text{kPa/sec}$ and $\dot{\sigma}_3 \approx 5.0\text{kPa/sec}$ ($\dot{\sigma}_1 \approx 7^1\text{psi/sec}$, $\dot{\sigma}_2 \approx 7^0\text{psi/sec}$ and $\dot{\sigma}_3 \approx 7^{-1}\text{psi/sec}$). These rates were chosen because it is possible to apply them consistently and precisely with the developed apparatus, data acquisition can keep up with the test and the length of the longest test, approximately one day, is not too long. The rates varied slightly between stress ratios but for each ratio the three tests rates consistently differed by an order of magnitude.

In summary, the testing of the $\pm55°$ filament wound tubes involves 15 tests; three stress rates with five stress ratios at each rate. The multidirectional tubes are tested under the five initial stress ratios and the additional ratio with one stress rate, approximately 300kPa/sec.

4.7   Experiments

The failure of the filament wound tubular specimens is defined as any transmission of oil through the thickness of the wall of the tube whether it is through weepage of liquid, localized fracture or wall fracture at a distance away from the grip. Therefore, even the stress ratio's with no hoop stress have a slight internal pressure of approximately 1MPa.   Any leakage of oil through the end grips or grip slippage constitutes an invalid test. This occurrence was observed a few times and was attributed to damaged o-rings.   Specifically, wall fracture is defined by a break in the tube wall causing immediate loss of pressure and continuous loss of fluid at essentially zero pressure; localized fracture is defined by the leakage of fluid through the wall thickness at a rate that is measurable by the volume transducer, and weeping is defined as the gradual loss of fluid through microcracks and other non visible damage.

In order to qualify a test as valid results, discussion of the actual experiments is necessary.   All satisfactory specimens failed within the test section and there were no tests influenced by stress concentrations at the grips.   In addition, there was no slippage in the grips or oil leakage through the o-rings.

Because of the limited tests performed on these tubes, it is difficult to quantify scatter.   It is assumed that the scatter was rather small because of the general trends observed in the results.   The low scatter can be attributed to the manufacturing of the tubes.   They have a very consistent geometry and material properties with respect to volume fraction of fibres, voids and distribution of fibres in the epoxy matrix.   These

properties can be attributed to the automated process for manufacturing the tubular sections from which the specimens are cut. In addition, some other causes of scatter may be varying sensitivity in strain gages used for strain measurement, bending in the tubes induced in the specimen by misaligned grips or unnoticed damage in the specimens.

In general, with respect to the most recent relevant experimental investigations (Soden et al., 1993), a marked improvement has been made in the gripping, load control and data acquisition systems.

4.8   Additional Procedures

4.8.1   Specimen Analysis

Specimen lay-up, layer thickness, fibre volume and void content were determined in order to properly define the make up of the tubular specimens. The following procedures were performed in this analysis.

The fibre volume and lay-up of the specimens was arrived at by cutting a small section of composite material from the tubing. The volume was then measured by water displacement and the mass of the sample was determined with an electronic scale. The sample was then placed in a 630°C (1200°F) kiln for 10 minutes to burn off all the epoxy resin and weighed again. The following formula (eqn. 4.3) was used to determine the fibre volume fraction:

$$\frac{Fibre\ Vol.}{Composite\ Vol.} = \frac{Fibre\ Mass}{Composite\ Mass} * \frac{Composite\ Dens.}{Fibre\ Dens.} \qquad (4.3)$$

Specimen lay-up was then investigated by separating the individual layers of the burned

sample and the orientation of each ply was measured.

The void content and thickness of each layer was determined with the aid of an

optical micrograph, section 4.8.2, of the cross-section of the tubes. Void content was

noted and compared between the two filament wound tubes. The thickness of each layer

was measured on a photograph of the cross-section of the specimen.

4.8.2 Micrograph Preparation

In order to make observations of damage on the micro scale, specimens needed

to be cut and properly prepared for inspection under an optical microscope. A

representative area was cut from the tubes, Fig. 4.9, using a small abrasive circular saw.

For each tube an area in the longitudinal plane and transverse plane was cut. These

micrograph specimens were cut from the tubular specimens at least 25.4mm from the

grips and as close to visible damage as possible. The pieces of tube were then

encapsulated in polyester resin. Once the resin has hardened the pieces were polished

in order to eliminate any damage to the specimens from the cutting. A 120 grit belt

sander was used to remove excess resin and approximately 2mm of the tube specimen.

The specimen was then polished with a 240 grit belt sander followed by 240, 320, 400

and 600 grit pressure sensitive abrasive paper. The specimen was polished for about one minute on each grit. The 600 grit paper was used until the direction of the polishing was not apparent which involved frequent rotation of the specimen. The specimen was then fine polished using two cloth wheels impregnated with 5.0 micron levigated alumina oxide powder and .05 micron gamma alumina powder. Using the .05 micron powder the fibre ends could be polished without breakage and good contrast between, fibres, resin and cracks could be achieved.

All the following micro graphs have a scales in the top right hand corner and have a magnification of approximately 20 X.
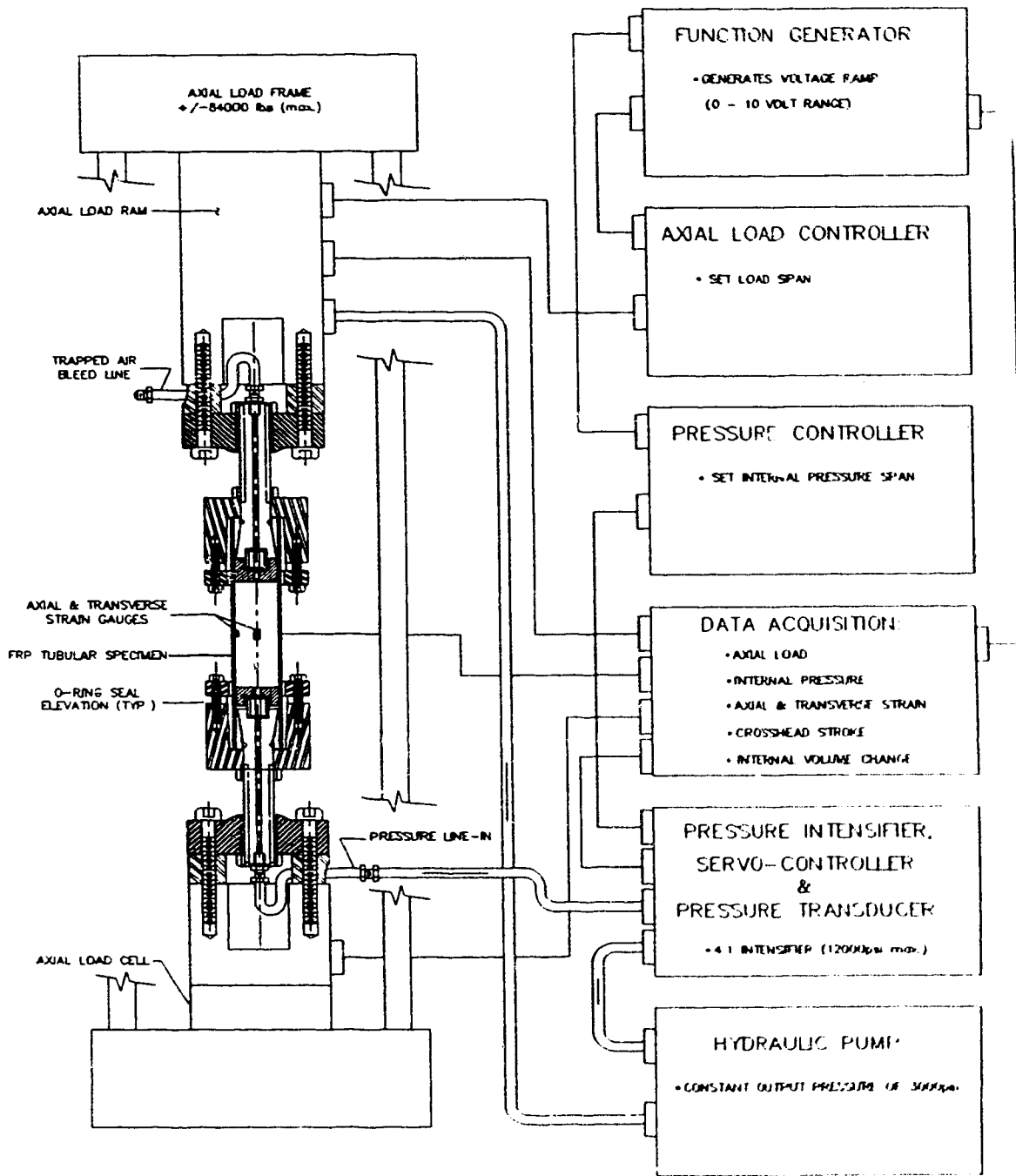
Figure 4.1 Schematic of Testing Apparatus
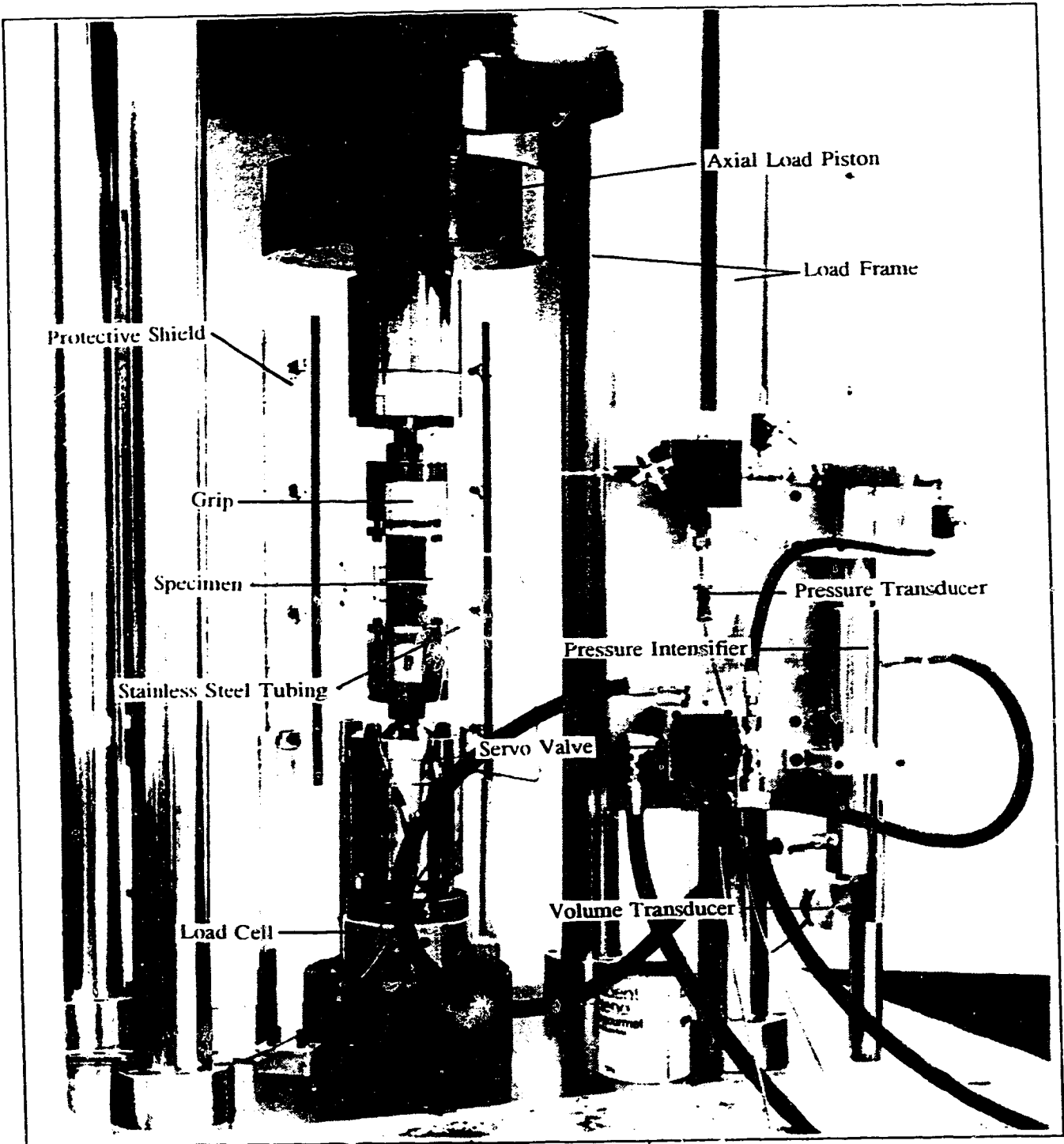
Figure 4.2 Biaxial Testing Machine

70
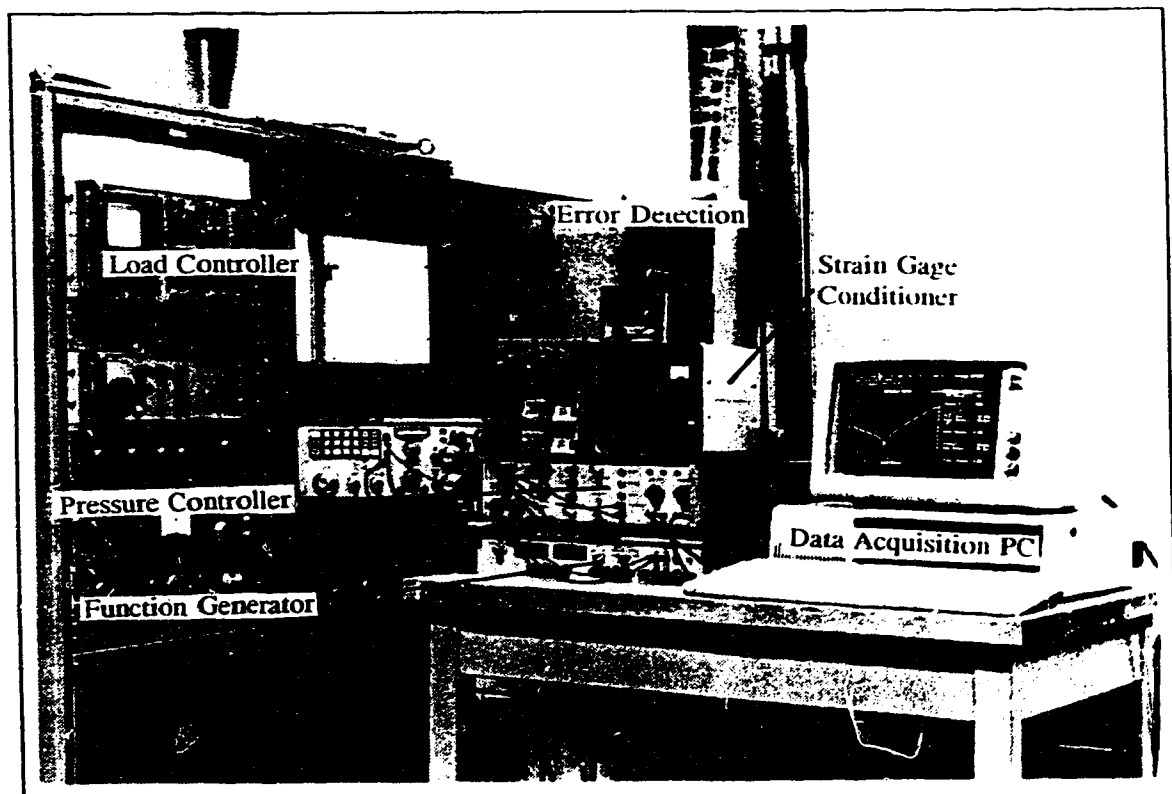
Figure 4.3 Control and Data Acquisition Systems
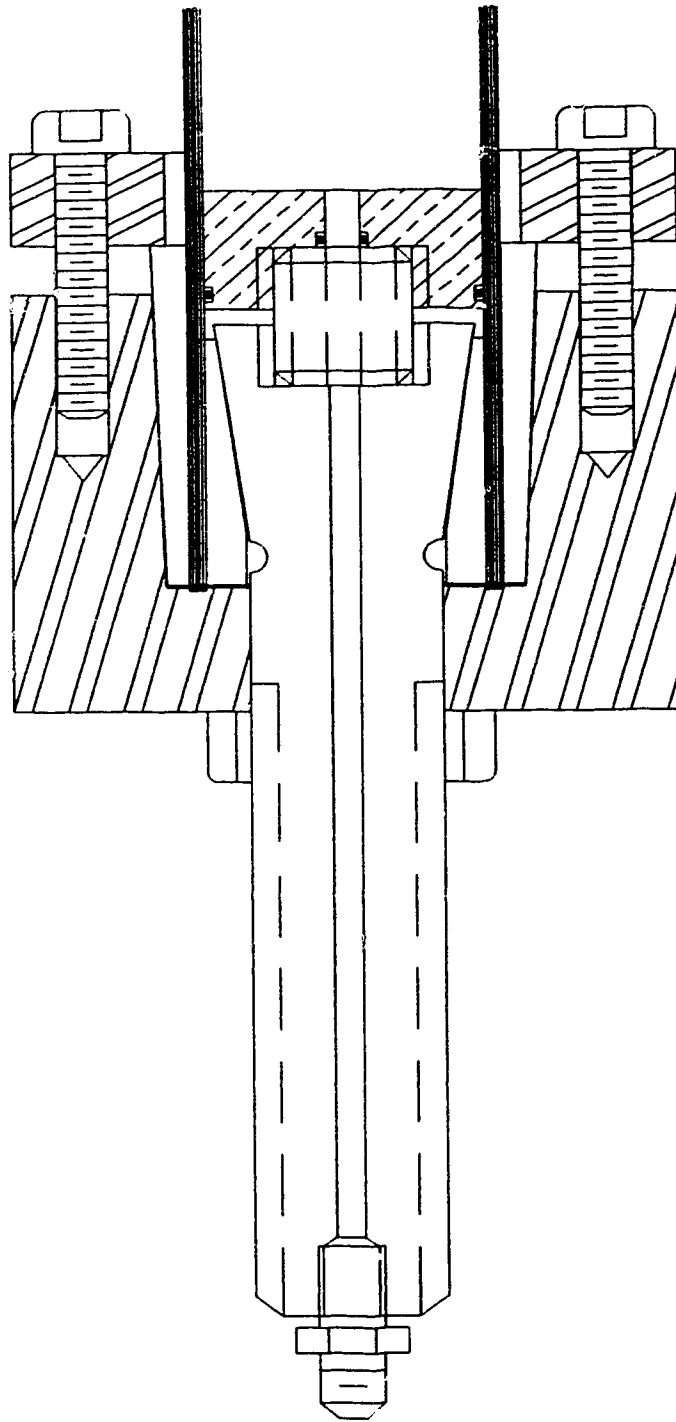
Figure 4.4 Schematic of Grip Assembly

72

f. Brass Piston
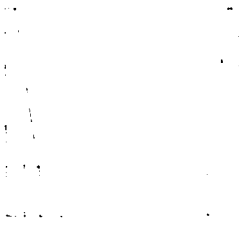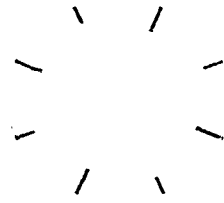
b. Inside Collet
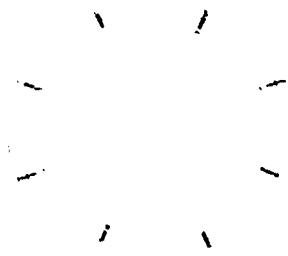
c. Outside Collet
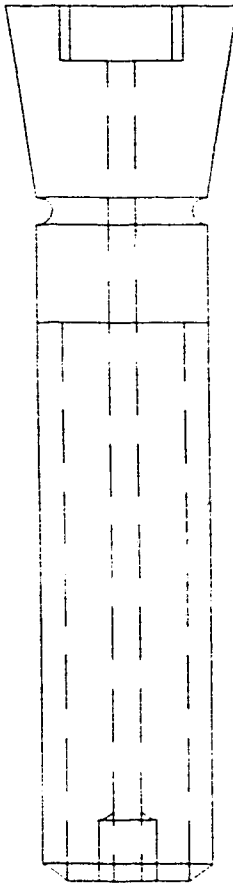
d. Restraining Ring

e. Collar

a. Mandrel
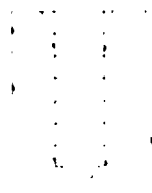
Figure 4.5 Disassembled Grip

73
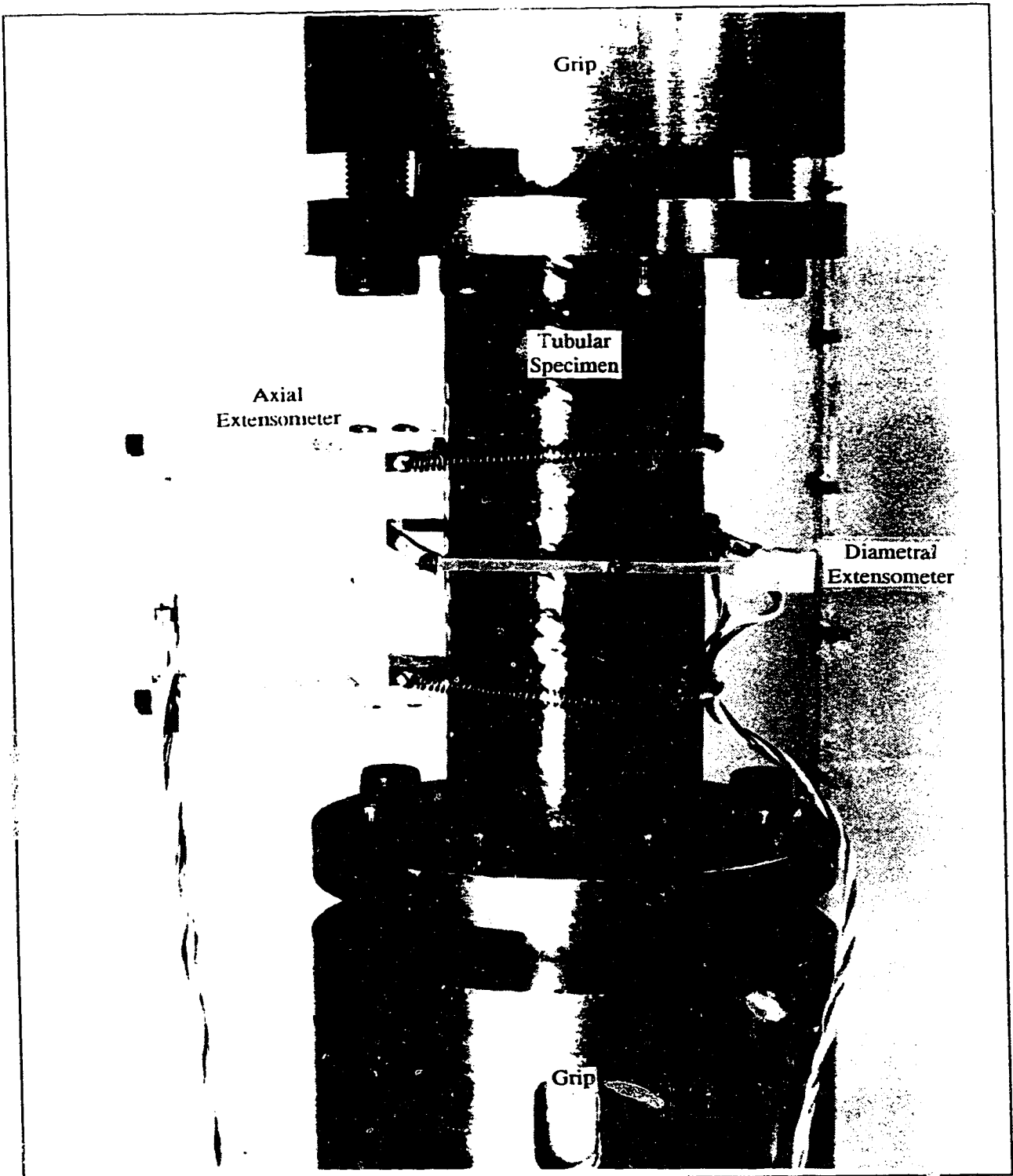
Figure 4.6 Grip and Extensometer Locations

74
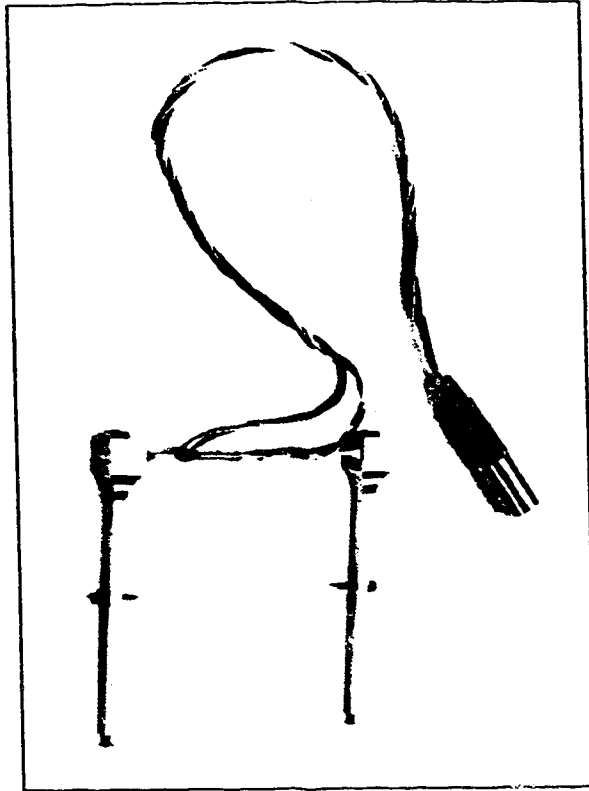
Figure 4.7.a   Diametral Extensometer
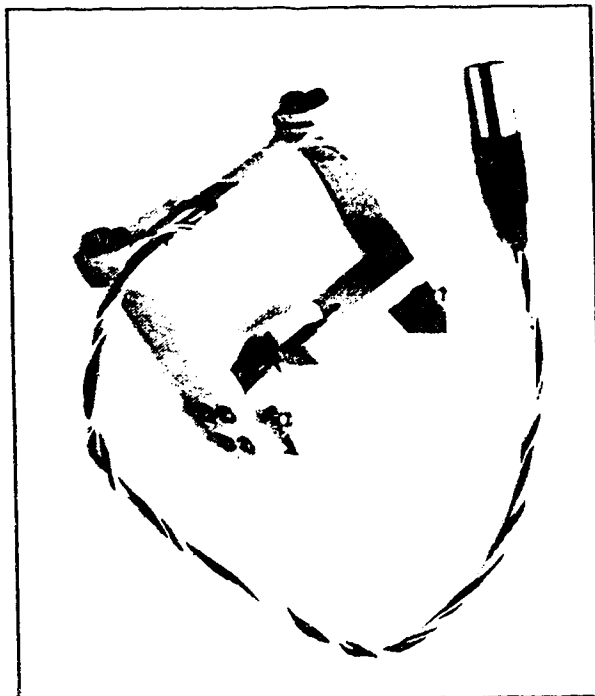
Figure 4.7.b   Axial Extensometer

$$S = \delta\sigma_A/\delta\sigma_H = \text{constant}$$

$$\delta\sigma/\delta t = \text{constant}$$
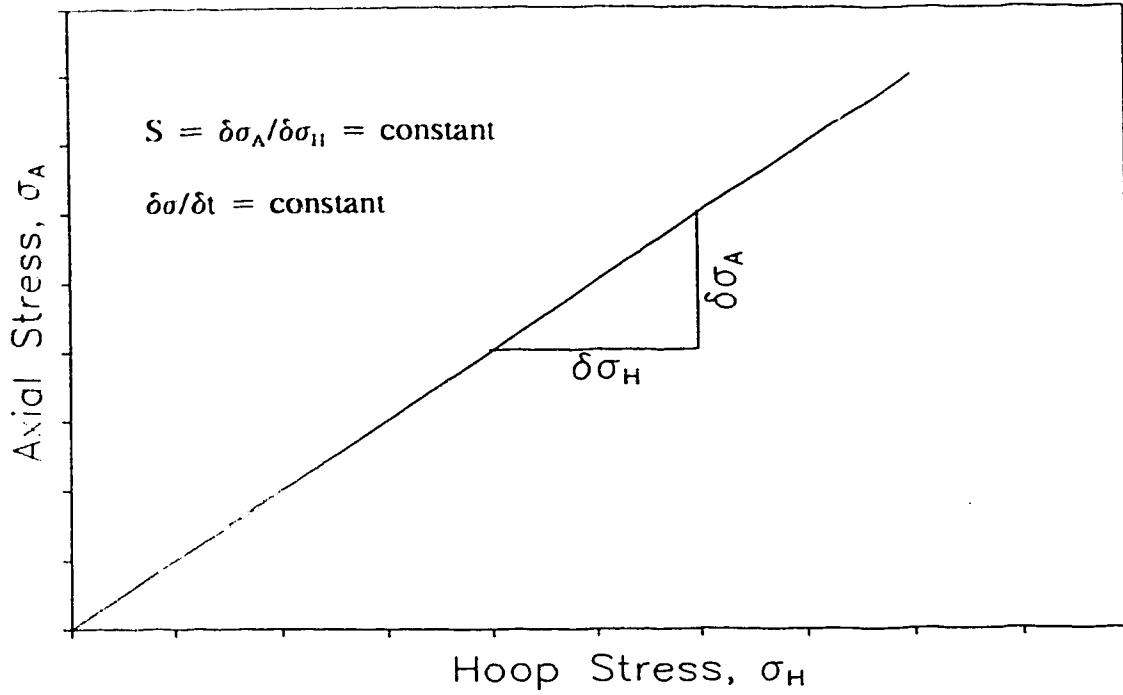
Figure 4.8 Monotonic Biaxial Loading
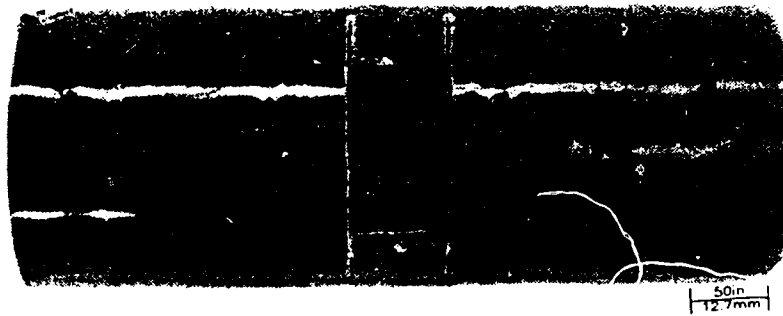
Figure 4.9 Specimen Cut for Micrograph

76

CHAPTER 5

BIAXIAL TESTING OF ±55° TUBULAR SPECIMENS

5.1   Introduction

The characterization of the filament wound tubular specimens involves the analysis of the stress and strain data gathered during the experimental program. This analysis enables the development of an elastic model and defines biaxial failure envelopes. These results and subsequent analysis provide insight into the behaviour of filament wound tubes with respect to stress-strain relationships, linear and nonlinear behaviour, time dependent properties and filament wind angle and lay-up.

As discussed previously in section 4.4, a number of variables were recorded during each experiment. Specifically, the axial load and strain, internal pressure and transverse strain were recorded using a few different methods as discussed in chapter 4. The load and pressure data is converted into stress assuming thin walled cylinder theory using the following simple equations:

$$\sigma_A = \frac{Load + Pressure(\pi r_i^2)}{\pi(r_o^2 - r_i^2)} \tag{5.1}$$

$$\sigma_H = Pressure * \frac{(2r_o - t)}{2 * t} \tag{5.2}$$

Where r_i is the inside radius, r_o is the outside radius of the tubular specimens and t is the thickness of the tube wall. The thin walled cylinder assumption essentially means that

77

all stresses through the thickness of the tubes are constant. This assumption was used in order to simplify calculations and because thick walled calculations for anisotropic materials need constants unavailable to us in this study.

5.2   Material and Specimens

The FRP filament wound tubes have been reinforced with glass fibres wound at angles of $\pm 55°$. Fourteen layers with an average thickness of 0.273 mm (0.0011")/layer, of alternating $55°$ and $-55°$ angle of fibre orientation with respect to the axis of the tubes, were present in each tube tested as illustrated in Fig. 5.1 and pictured in Fig. 5.2.a. Highly accurate processing equipment was used to manufacture these tubes producing the following dimensions, an inside diameter of 49.50 ± 0.01 mm (1.949 ± 0.002") and an outside diameter of 57.4 ± 0.1 mm (2.26 ± 0.02"). The reason for less accuracy in the outside measurement is the fact that the outside surface is not smooth. Each foot long test section was cut from a long section of tube. The volume fraction of fibres in the first set of filament wound tubes was determined to be 58%.

Figure 5.2.b is a micrograph of an undamaged $\pm 55°$ specimen. It can be observed that voids are small and evenly spaced in the specimen indicating high manufacturing standards. A thin protective resin coating is present on the outside surface of the tube and fibre distribution through out the tube is fairly consistent.

5.3   Test Results

5.3.1   Stress-Strain Curves

A general discussion of the stress-strain curves follows. Each graph presents the axial and transverse strain compared to the average stress in the tube wall. The linear elastic behaviour of the tubes is also presented and will be discussed thoroughly in section 5.4.1. The linear elastic range is defined by the 0.2% offset method which is frequently used for metals.

Figure 5.3 shows the axial stress compared to the axial and transverse strain for the three stress rates used in the investigation of the $\pm 55^\circ$ tubes for the stress ratio of 0H:1A. It can be observed that the tube follows typical behaviour for a pure tensile test, the axial strain is positive while the transverse strain is negative. The failure stresses are 101 MPa, 83 MPa and 76 MPa for the three stress rates tested respectively with failure strains of approximately -1.0% in the transverse direction and 2.3% in the axial direction. It is observed that the experimental curves follow linear elastic behaviour for only very low stress . . . i.e. approximately 1/3 of the final failure stress, and strains less than .25% in both directions. The viscous, time dependent, characteristics of the tubes are present in these curves in addition to a strongly nonlinear stress-strain relationship. It can be observed that the failure stress is lower for the slower tests and the strains are proportionally greater for lower stresses which is typical of time dependent plastics.

Figure 5.4 shows the stress-strain curves for the test with hoop stress only on the ±55″ tubes. Again, as expected the transverse strain, change in diameter, is positive while the axial strain is negative with increasing internal pressure or hoop stress. The failure stresses are 405 MPa, 362 MPa and 350 MPa for the three stress rates respectively, with failure strains extrapolated to approximately 7.0% in the transverse direction and -10.0% in the axial direction. The transverse strains are extrapolated past 5.0% strain with the aid of curve fitting. The axial strains beyond 5.0% are determined by the stroke position except for the fastest rate which is extrapolated from curve fitting. The linear elastic behaviour is plotted against the experimental data. It is observed that the experimental curves follow linear elastic behaviour for only very low stress values corresponding to approximately 1/5 the final failure stress and strains less than 0.25%. In addition, the examination of the axial strain curves reveals the existence of viscous effects but it is observed that there is limited time-dependent behaviour in the transverse strains. This fact demonstrates the complexity of the time-dependent behaviour present in glass filament wound tubes.

Figure 5.5 shows the stress-strain curves for the ±55° tubes for the test with the stress ratio of 1H:1A. The failure stresses are 199 MPa, 195 MPa and 165 MPa for the three stress rates tested with failure strains between -1.0% and -2.0% in the transverse direction and approximately 4.0% in the axial direction. Under this loading condition it is observed that the transverse strain is almost constant at 0% strain in the linear elastic range and the axial strain is positive. The linear elastic behaviour of the experimental curves occurs in the first 1/3 of the final failure stress. Again, it is observed that the

linear range of the experimental curves follows the linear elastic behaviour. Examination of the curves for the different loading rates reveals the existence of time-dependent properties.

Figure 5.6 shows the stress-strain curves for the tests with the stress ratio of 2H:1A as determined by netting analysis for the ±55° tubes. The hoop failure stresses are approximately 488 MPa for the three rates tested with strains of approximately -0.5% in the axial direction and 2.5% in the hoop direction. It is observed that under this stress condition the axial strain is approximately zero in the linear range of the stress-strain relationship and the transverse strain is positive. The linear elastic portion of the transverse stress-strain curves follows the linear elastic behaviour but the axial curve does not correspond to the elastic equation. In addition, it is observed that there is very little time-dependent behaviour. The reason for this lack of viscous behaviour is the fact that the principle direction of stress is close to the direction of the fibres in the tubular specimens, 55°. Therefore, the fibres will carry almost all of the load applied to the pipe and since glass fibres have no time-dependent properties none will be observed in the tubular specimens.

Figure 5.7, the last of the stress-strain curves for the ±55° tubes, illustrates the results for the axial compression tests. Typical negative axial strain and positive transverse strain is observed for this loading condition. The failure stresses are -146 MPa, -131 MPa and -124 MPa for the three rates tested with failure strains of approximately 4.0% in the transverse direction and failure strain approximately -7.5% in the axial direction. The linear elastic behaviour is only valid for approximately 1/4

the final failure stress. Time dependent behaviour is also observed and is similar to the other axially dominated loading conditions.

Failure stresses are summarized in appendix B.

5.3.2 Biaxial Failure Envelopes - Stress and Strain

The characterization of the filament wound tubular specimens involves the presentation of data in meaningful ways. The biaxial failure envelope is a graph of the axial failure strength versus the hoop failure strength point for each loading ratio. These points define a biaxial failure envelope which, in general, can be used to predict the biaxial loads a composite structure can withstand. Figure 5.8 illustrates the biaxial failure stress envelope for the fastest tests on the $\pm 55^\circ$ tube. The curve is fitted by eye to show the trend observed. It can be noted that this failure envelope is asymmetrical. This can be attributed to the fact that the stress ratio of 2H:1A yields the highest failure stresses, and the axial and transverse behaviour of the tubes is significantly different.

Figure 5.9 pictures the biaxial failure envelopes for the $\pm 55^\circ$ tubes for the three different loading rates. These envelopes demonstrates the time-dependent properties of the filament wound tubular specimens. It can be observed that as discussed previously the 2H:1A load ratio does not exhibit any noticeable viscous effects for the failure times chosen here. Therefore, it can be concluded that the failure envelopes not only change size with different loading rates but they change shape as well.

Another meaningful way to present the strain data is through the development of

a strain envelope. as shown in Fig. 5.10. This is a graph of the hoop strain vs. the axial strain for the fastest rate tested. Again the asymmetry of the envelope demonstrates the complex behaviour of these filament wound tubes. This graph will be discussed with respect to failure modes and damage accumulation in section 5.3.5.

5.3.3 Oil Volume Changes

The change in oil volume is another way to monitor the behaviour of the tubes. Figures 5.11 and 5.12 show the percent of available oil volume used with respect to the normalized time to failure for the medium rate and the slowest rate of loading respectively. It can be noted that the tests with low constant pressure. HO:A1 and HO:A-1. have a relatively constant oil volume. The tests with high pressure involved. H1:A1, H2:A1 and H1:A0. show an increase in oil volume as the tests progress. Change in slope of these curves indicates leakage of fluid which may correlate to a failure in the tubes. This can be observed in the last part of the curves for the 0H:1A and 1H:1A tests. The curves for the 2H:1A tests are not valid because under very high pressure some fluid is lost within the pressure system through the seals.

5.3.4 Failure Observations

The strength of fibre reinforced epoxy materials is based on the strength characteristics of two constituent elements: fibres and matrix. and the bond between the

two governs the behaviour of the composite as a whole. In addition, these components do not fail at the same time because of their individual properties. This fact complicates the failure of these materials because damage accumulation, initial and final failure depends on how the constituents fail.

The full characterization of the filament wound tubular specimens involves the investigation of the type of failure observed under the different loading conditions. The failures observed will be discussed based on initial damage, extent of damage, final failure mode, and failure location. These phenomena are explained with the aid of macro examination and low magnification optical micrographs. The particular failures will be related to the behaviour of the tubes on a strain basis.

5.3.4a Macro Observations

Observation of the macro failure mechanics of the filament wound tubular specimens is based on naked eye inspection. Fig. 5.13-5.14 show pictures of specimens after testing under their respective loading conditions.

In general, there are five types of observable macro failures in the ±55° tubes that are related to specific strain behaviours and stress rate. In addition, there are only three types of damage accumulation which are independent of stress rate. Each of these failures and damage accumulations is discussed individually based on the strain and stress rate of the specimens.

The tests with axially dominated loading, i.e. 0H:1A and 1H:1A, both have

84

positive axial strains. This axial strain enables the matrix in the specimens to develop cracks parallel to the direction of the fibres as the loading progresses. Observable matrix cracking occurs with these stress ratios at all loading rates although, the speed at which this damage accumulates depends on the stress rate. The final failure mode is dependent on the stress rate as observed in Fig. 5.14. In Fig. 5.14.a, the fastest stress rate, a complete failure of the matrix is observed. This loading condition enables a saturation of matrix cracks through the thickness of the tube wall and subsequently the matrix does not have any useful physical properties and does not bind the fibres together. Therefore, the fibres in the tube basically unwind from the inside out as the tube is stretched because the fibres are shortest on the inside wall.

Inspecting Fig. 5.14.b and 5.14.c. reveals that similar matrix cracking is present but it has not reached the saturation stage as previously discussed. Since failure is defined as a loss in containment of liquid as soon as any leakage or loss in pressure is detected, the pipe is considered to have failed. This leakage was detected with the naked eye and later verified with the change in oil volume. The slower stress rates produced failures that involved leakage of liquid through the pipe wall while the structural integrity of the pipe is intact. The medium rate test had more visible damage than the slow test with the same type of failure at higher stress values. These weepage type failures observed in the slower rates are similar to the initial failure observed in Soden et al.'s (1989) investigation. The damage accumulation will be discussed based on micro observations later on in this chapter.

All the tests with a stress ratio of 2H:1A had similar failure modes to the one

85

pictured in Fig. 5.14.d. These tubes had very small axial strains and relatively small hoop strain when compared to the pure hoop stress tests. The failure of these tubes possibly involved a localized fibre fracture which led to a section of the tube being blown out by the internal pressure. Fibre breakage was the probable cause of the localized fracture because there was no whitening of the surrounding matrix to indicate resin damage. In all of Soden et al.'s (1989) failures there was an apparent whitening of the matrix around the failed location. The tubes were still able to hold limited axial load after failure. Damage accumulation was not observable with the naked eye as the tests progressed with this stress ratio under any of the tested stress rates. This can be attributed to the fact that the axial strain did not allow the development of any matrix cracking and ultimately led to failure of the fibres.

Hoop stress only, 1H:0A, produced interesting failures because more than one mode of failure was evident. The exact site of the initiation of failure and the order of failure mode is not obvious. As the test progressed, under any stress rate, a apparent whitening of the pipe was observed along with very high hoop strains and negative axial strains. The whitening of the pipe was possibly caused by micro cracking developing in the resin. The negative axial strain prevented any visible matrix cracking from developing parallel to the fibres and led to a rupture possibly initiated with the failure of fibres. On the inside wall of the tube where the hoop stress is highest, the tubes fractured in a longitudinal direction shown in Fig. 5.15. The reason for this is the fact that the principal stress is in the hoop direction and wants to tear the tube in the longitudinal direction. This fibre breakage propagates through the wall thickness until

a second mode of failure occurs, delamination (Fig. 5.13.b.). Delamination may take over from fibre breakage because as the longitudinal fracture line propagates through the wall thickness, interlaminar stresses may develop because of the induced asymmetry through the wall of the pipe. This failure was violent under all loading rates because of the amount of energy stored in the tube with large strains. Violent failures for tests with high internal pressures have been previously documented in literature.

The tests with axial compression produced similar damage accumulation as the pure internal pressure tests but different failure modes. Under any stress rate a whitening of the tube occurs until failure. Failure involves the shearing of the pipe in the direction of the fibres with an angle of 45° through the wall thickness which corresponds to the maximum shear stress (Fig. 5.13.c.). This particular failure was observed under all three stress rates under similar strains and different failure stresses as previously discussed. Since the matrix provides all the shear strength to the component it can be assumed that this failure was matrix dominated. The axial compression tests in Soden et al.'s (1989) investigation produced some failures caused by buckling. This phenomena was apparently alleviated by increasing the wall thickness of his specimens which subsequently produced similar shear failures to ours.

In summary, the failure modes can be related to strain behaviour. For positive axial strains matrix cracking parallel to the fibres was possible and led to final failure. For negative axial strain matrix cracking was not apparent parallel to the fibres but a overall whitening of the tube was observed. For high internal pressure, violent failures were observed incorporating delamination and fibre breakage. For compression, the final

failure was a matrix dominated shear failure. The 2H:1A load ratio which had low strains in both directions apparently failed by fibre breakage. Figure 5.16 summarizes the behaviour of the tubes by relating the damage accumulation to the biaxial failure stress envelope defined in section 5.3.2.

5.3.4b Micro Observations

Optical micrographs provide a medium to observe damage that has occurred in the filament wound tubulars. In general, matrix cracking and delamination are the most readily observed damage and any combination of the two constitutes most failures. Matrix cracking is found in two forms transverse and longitudinal to the fibre direction. Transverse cracking is initiated at or near fibre matrix interfaces and propagate through the resin around fibres (Jones, 1979). Longitudinal cracking is apparent in some specimens but interlaminar delamination is usually dominant in that direction.

The tests with positive axial strain have the same type of damage accumulation as discussed in the previous section. Figure 5.17.a and 5.17.b. present the two extremes of damage present in the fastest and the slowest tests respectively. It can be observed that in each picture transverse cracks and delamination are present but far less damage is apparent in the slow stress rate tests. The fast test final failure occurred when the resin could not bind the fibres together any more. This failure coincided with the leakage of fluid through the thickness of the tube wall. In the slower case the final failure was weepage of oil through the cracks observable in the wall. It is possible to

88

trace a path the oil could follow in the specimen if sufficient time is given. In the first case the stress rate is 2 orders of magnitude faster and therefore much more damage must be present in order for there to be any leakage of fluid. An explanation for the difference in the amount of damage may be the fact that at a slower rate the stresses have more time to redistribute themselves through the viscous properties of the matrix. If these properties were not present the failure stress of the slower rates may be considerably lower because of stress concentrations.

Figure 5.18.a presents the optical micrograph of a typical shear failure in the tests with pure axial compression. It can be observed that there is no apparent visible damage other than the actual fracture line. As discussed previously the specimens sheared along the direction of the fibres in one layer, i.e. -55° or +55° and the through wall shear angle can be observed to be approximately 45° which is the direction of the maximum shear stress. Although whitening of the tube was observed during testing, the micro cracking associated with this type of damage is not visible under the optical microscope.

Figure 5.18.b shows the optical micrograph of the typical failure observed in the 2H:1A tests. Inspection of the micrograph reveals the fact that there is delamination and matrix cracking present. It is not possible to tell whether the damage modes occur after the initial fibre breakage or before. It can be assumed they happened after the fibre breakage based on the fact that no visible damage is present away from the localized fracture.

Figures 5.19.a and 5.19.b show delamination from two different tests, the 2H:1A stress ratio and the 1H:0A stress ratio respectively. Both of these delaminations are a

result of the initial failure of the tubular specimen. In the 2H:1A stress condition the localized fracture can be assumed to have initiated the delamination. as previously discussed. which propagated between layers. In the pure hoop stress condition the delamination also occurred after the initial failure which involved the development of a longitudinal fibre fraction line on the inside wall of the specimen. It is interesting to note that the delamination occurs at similar locations with respect to wall thickness. This may be attributed to the fact that both of these stress ratios involve high internal pressures and therefore relatively high compressive radial stresses. This compressive stress may inhibit the delamination at locations closer to the inside surface of the wall.

In summary. these micrographs present damage observable in the ±55° tubular specimens. The axial tension dominated tests reveal different accumulations of transverse cracking and delamination for diffrent . This indicates one reason why the tubes fail at different stress levels. The angle of shear failure is vri   b in the direction of maximum shear stress. Large delaminations are observed but in general are a result of other failures. Additionally, when a localized fracture is observed. as in the 2H:1A condition. many different types of damage are apparent but no definite conclusion to which initiated the failure can be made.

5.3.4c Micro Observations - Grip Damage

Grip damage. as discussed in chapter 4. is a major consideration in the design of

a gripping system. Therefore, observation of damage close to the grips was investigated on a micro scale. Samples from all loading conditions were taken and observed under the microscope. The only stress ratio that exhibited any damage that was obviously caused by stress concentrations in the grips was the 1H:0A ratio. Figure 5.15 shows the location of the micrograph and Fig. 5.20 shows the damaged caused by the end of the grips.

The end of the grips can be considered an axisymmetric step which has been investigated by Lee et al. (1989). The damage results from a high stress gradient caused by the step. Although this damage seems quit extensive, the tubes still fail in the test section. It can be observed that matrix cracking and delamination is present, originating from the outside surface. The reason for this is the fact that the stress concentration is located at the outside surface where the grip ends. The damage propagates through the wall thickness but arrests before the inside wall. Therefore, there is no path for the fluid to leak through the wall at this location and the tube can still hold pressure at this point. Additionally, the specimen adopts a barrel shape when loaded under high internal pressure and therefore the high hoop strains are not present close to the end grips. The 1H:0A tests all failed because of excessive hoop strains for both the ±55° and the multidirectional tubes.

This damage developed by the grips demonstrates a need to consider such axisymmetrical steps carefully. A simple way to fix this problem would be to bevel the inside top corner of the outside collet on the gripping system.

5.4   Interpretation of Data

5.4.1   Linear Elastic Behaviour

The stress conditions present in the tubes will be discussed based on loading conditions and linear elastic response. The hoop stress is not constant through the thickness in these tubes. It has a maximum tensile value at the inside surface of the pipe and a minimum value on the outside surface. The difference of the values is approximately 17% for the $\pm 55^\circ$ tubes following an inverse second order relationship, $(1-1/r^2)$, if we assume the tubes are made from an isotropic material. In addition, the radial stress, σ_r, varies through the thickness with the maximum compressive stress on the inside surface equal to the internal pressure and the minimum value equal to 0 on the outside surface. It has been determined by careful experiments that the axial strain in a thin and thick walled cylinder is constant through the thickness for an isotropic material (Higdon, 1985). This will hold true for an anisotropic material if the plane perpendicular to the axial loading direction has symmetric material properties.

The composite tubes under investigation have an axis of anisotropy that is aligned with the longitudinal axis of the tubes. All directions intersecting the axis at right angles are equivalent. In addition, all directions parallel to the axis and all directions orthogonal to the first two directions are equivalent as illustrated in Fig. 5.21. This type of anisotropy is called cylindrical if it contains these properties. If we assume a cylindrical

92

coordinate system, r, θ, z, utilizing the generalized Hooke's law for cylindrical anisotropy (Lekhnitskii, 1963) we obtain the following equations:

$$\epsilon_r = a_{11}\sigma_r + a_{12}\sigma_\theta + a_{13}\sigma_z + a_{14}\tau_{\theta z} + a_{15}\tau_{rz} + a_{16}\tau_{r\theta}$$
$$\epsilon_\theta = a_{12}\sigma_r + a_{2r}\sigma_\theta + \ldots + a_{26}\tau_{r\theta} \qquad\qquad (5.3)$$
$$\vdots$$
$$\gamma_{r\theta} = a_{16}\sigma_r + a_{26}\sigma_\theta + \ldots + a_{66}\tau_{r\theta}$$

If a plane of symmetry exists at each point on the z axis, then the coefficients a_{14}, a_{24}, a_{34}, a_{46}, a_{15}, a_{25}, a_{35}, a_{56}, are equal to zero. In addition, if there are two planes of symmetry, radial and tangential, then the coefficients a_{16}, a_{26}, a_{36}, a_{45}, are also equal to zero. Therefore, assuming a heterogenous material the stress-strain relationship for an orthotropic body with cylindrical anisotropy is expressed in the following form:

$$\epsilon_r = \frac{1}{E_1}\sigma_r - \frac{\nu_{21}}{E_2}\sigma_\theta - \frac{\nu_{31}}{E_3}\sigma_z, \qquad \gamma_{\theta z} = \frac{1}{G_{23}}\tau_{\theta z}$$

$$\epsilon_\theta = -\frac{\nu_{12}}{E_1}\sigma_r + \frac{1}{E_2}\sigma_\theta - \frac{\nu_{32}}{E_3}\sigma_z, \qquad \gamma_{rz} = \frac{1}{G_{13}}\tau_{rz} \qquad (5.4)$$

$$\epsilon_z = -\frac{\nu_{13}}{E_1}\sigma_r - \frac{\nu_{23}}{E_2}\sigma_\theta + \frac{1}{E_3}\sigma_z, \qquad \gamma_{r\theta} = \frac{1}{G_{12}}\tau_{r\theta}$$

A few additional assumption are made in order to simplify our calculations of the linear elastic behaviour of these tubular specimens. The radial stress is ignored because the radial stress is small compared to the stresses in the axial and hoop directions, i.e. in the test with pure internal pressure on the ±55° tubes approximately 62.0 MPa is applied which corresponds to the maximum radial stress, and a hoop stress of approximately 345 MPa is achieved. In addition. the radial stress approaches 0 at the outside surface of the tube where the hoop stress is only slightly less on the outside surface than the maximum stress value on the inside wall surface as previously discussed.

93

The final elastic stress-strain equations, Eqn. 5.5, use the convenient subscripts H (hoop) and A (axial) which correspond to the previous subscripts 3 and 2 respectively.

$$
\epsilon_H = \frac{\sigma_H}{E_H} - \nu_{AH} \frac{\sigma_A}{E_A}
$$

$$
\epsilon_A = \frac{\sigma_A}{E_A} - \nu_{HA} \frac{\sigma_H}{E_H}
$$

(5.5)

Where E_H and E_A are the elastic moduli in the hoop and axial directions, respectively, and ν_{AH} is the Poisson's ratio which characterizes the strain in the hoop direction due to the stress acting in the axial direction and ν_{HA} is the Poisson's ratio which characterizes the axial strain due to the stress acting in the hoop direction. With the use of the appropriate elastic constants determined from the stress-strain data, this stress-strain relationship has been used successfully to describe the linear elastic behaviour of the $\pm 55°$ filament wound tubes under various loading conditions, illustrated in Figs. 5.3-5.7.

The stress-strain curves produced from the data gathered through out the experimental program proved to be invaluable in the characterization of the FRP tubes. To determine the elastic constants used in the stress-strain relationship, Eqn. 5.5, the tests with the appropriate loading conditions need to be analyzed. The stress-strain curves for the test with pure axial tension, depicted in Fig. 5.3, will give us the global elastic properties in the axial direction for the $\pm 55°$ tubes. The graphs present the existence of linear and nonlinear behaviour. Time dependent behaviour is also more pronounced in the first graph and will be discussed later on. The elastic constant E_A and ν_{AH} can be determined from the linear part of the stress-strain curves using best fit polynomial curve fitting. The first order term of this curve fitting is assumed to be a

94

good approximation of the linear elastic response of the stress-strain relationship. It was determined that for the $\pm 55^\circ$ tubes, the elastic modulus, E_A, is 14.4 GPa and the Poisson's ratio, ν_{AH}, is 0.28, 0.43, 0.47 for the three rates approximately 270 kPa/sec, 23 kPa/sec and 1.4 kPa/sec respectively. Soden et al.'s (1993) study revealed a similar Young's modulus of 14.82 GPa and a slightly higher Poisson's ratio of 0.333 for the $\pm 55^\circ$ tubes. Soden's loading rate is similar to our fastest although not rigorously controlled.

Figure 5.4 illustrates the stress-strain curves for the tests involving pure hoop stress. The elastic constants in the hoop direction can be determined from these curves in a similar manner to the axial tests. It was determined that for the $\pm 55^\circ$ tubes the elastic modulus, E_H, is 19.1 GPa in the hoop direction and the Poisson's ratio, ν_{HA}, is 0.62, 0.75, 0.88 for the three rates approximately 465 kPa/sec, 53 kPa/sec and 4.7 kPa/sec, respectively. Soden et al.'s (1993) study revealed a higher Young's modulus of 25.98 GPa and a slightly lower Poisson's ratio of 0.55. This may be due to the fact that Soden's tubes were thin walled.

It is observed in the $\pm 55^\circ$ tubes that the elastic modulus is independent of loading rate but the Poison's ratio does have a significant time dependent relationship. Additionally, it is observed that the ratio of ν_{AH} to ν_{HA} is approximately 0.5 for the three different rates tested on the $\pm 55^\circ$ tubes but the ratio of E_A to E_H is equal to 0.75. The relationship presented in eqn. 5.6 does not hold true because of the apparent time dependent properties observed in the elastic behaviour of the tubes.

95

$$\frac{E_A}{E_H} = \frac{v_{HA}}{v_{AH}}$$

5.4.2   Discussion of Failure Envelopes

The following discussion will focus on the failure envelopes defined in this experimental study. Comparisons with similar results and analysis assuming thin and thick walled equations will be presented.

The comparison of these results with previous investigations exposes some interesting relationships. Data is available for the strength of filament wound tubes tested under uniaxial and pressure vessel conditions but there is limited data available for the biaxial stress conditions considered in this investigation. Three experimental investigations performed by Soden et al. (1993,1989,1985) have studied biaxial failure stresses for filament wound tubes.

Figure 5.22 presents the study of Soden with filament wound epoxy tubes compared with the short term failure envelope define by our data. Soden's results are presented with respect to an initial failure envelope defined by the weeping failure points of his tubes and a final failure envelope which is determined from specimens that have been lined with rubber to prevent weeping of liquid. Soden's investigation involved the use of thin walled specimens with 2 layers of $\pm 55°$ fibres with an approximate wall thickness of 1 mm loaded at a similar rate to our fastest test. We will only consider the final failure stress envelope because few weepage failures were observed in our testing.

It can be seen that there is quite a difference in the final failure stresses for

certain stress conditions. this can be attributed to a few factors. The wall thickness of the tubes used in our investigation are considerably thicker, approximately 4mm. Based on the uniaxial tests in tension and compression it can be observed that similar failure stresses have been attained. The reason for this is that in general the axial strain is constant through the thickness of the tube wall no matter how thick it is (Higdon, 1985). The failure stress in the compression loading condition is slightly higher in our case because the greater wall thickness ensures the specimen does not fail by buckling.

It is also observed that the tests involving significant internal pressure or hoop stress have considerably lower failure stresses. The fact that our tubes have thick walls contributes to the lower failure stresses. If one considers ϵ_θ, Eqn. 5.7, to be known on the outside surface of the tube and ϵ_r, Eqn. 5.8, is considered to be constant through the thickness, then it can be determined that the inside of the wall will have a greater ϵ_θ which corresponds to a greater hoop stress.

$$\epsilon_\theta = \frac{u}{r} + \frac{\partial v}{r \partial \theta} \qquad (5.7)$$

$$\epsilon_r = \frac{\partial u}{\partial r} = constant \qquad (5.8)$$

If the geometry of the tubes in Soden's and this investigation are considered, ±55°, it can be determined that the inside of the wall has a strain value 1% and 16% greater, respectively. This clearly demonstrates that the inside of the tube wall will have a significantly higher hoop stress if the wall thickness is large. This indication is verified by the observed failure mechanisms in the thick walled specimens. Through a simple

97

calculation it can be determined that the inside wall stress is higher and therefore failure occurs at a lower pressure.

Tsai (1987) analysis compares thin and thick walled solutions for pressure vessels with a winding angle similar to our tubes. He determined that the thick wall pressure vessel cannot hold as much internal pressure as a thin walled pressure vessel, when considering equivalent wall stresses. Therefore, for b/a = 1.16 for $\pm 55^\circ$ tubes, where a is the inside radius and b is the outside radius, which qualifies as thick walled, the Tsai thick walled solution predicts significantly lower failure pressures for the 2H:1A stress condition. This is readily observed in the comparison of our experimental failure envelope with that of Soden et al.'s. It is interesting to note that Tsai determined that no significant increase in failure pressure is achieved when the wall thickness is b/a > 1.30. This essentially means that the failure is not self arresting and once it occurs on the inside wall it will propagate through the tube no matter how thick the wall may be.

Another observation in the comparison of Soden et al.'s and our envelopes for the $\pm 55^\circ$ tubes, reveals a discrepancy between the shape of the envelopes in the area where the stress ratio is between 2H:1A and 1H:0A. This suggests that a point should have been tested in that area with a stress ratio of ,for example, 3H:1A. It was impossible to know that this ratio needed to be tested because the netting analysis used predicted 2H:1A as the strongest point on the envelope. It is possible that it is the strongest axial point on the envelope but with the inspection of S. 'en et al.'s envelope it is obvious that the highest hoop stress is at a stress ratio of 3H:1A.

5.4.3 Extrapolation of Failure Stresses

The time-dependent properties of the filament wound tubular specimens exhibit an overall trend with respect to failure strength. Figure 5.9 indicates that the failure stresses are lower for all of the stress ratios tested except the 2H:1A with decreasing stress rate or increasing loading time. This trend of lower failure stress with respect to slower loading rate is demonstrated in Fig. 5.23 where the normalized failure stress is plotted against normalized rate. This figure shows that most of the difference occurs when the normalized stress rate is close to zero. A log-log scale is more appropriate as illustrated in Fig. 5.24. Figure 5.25 clearly demonstrates the failure trends with respect to decreasing normalized stress rate for all stress ratios and facilitates the extrapolation of the failure stress for considerably lower rates or longer loading times. Usually it is assumed that extrapolated stress levels should be limited to one order of magnitude of rate although, the probable behaviour of the tubes for longer loading times is as shown. The graph illustrates the failure stresses up to a loading rate which corresponds to approximately ten years time which can be a typical service life for these types of tubes in industrial use. The failure stress graph of the 2H:1A stress ratio, Fig. 5.24, as observed before, has no change in failure stress over the test time. Extrapolation beyond an order on magnitude may not be valid in this case.

The extrapolated failure stresses are illustrated on another failure envelope graph, Fig. 5.26, that includes the short term test, the linear elastic range of this test and the extrapolated failure stresses. The worst case scenario is chosen as a conservative factor

to define the extrapolated envelope. In this case it is approximately 50% the short term envelope as defined by the behaviour of the tubes under the stress ratio of 0H:1A. The use of this type of approach to describing long term performance of tubular products needs further investigation and verification.

5.4.4 Failure Criteria

The prediction of composite behaviour has been approached by many investigators as summarized by Labossiere (1986, 1987) and Fawaz (1992). In general, by carrying out extensive tests on a material, a phenomenological failure criterion can be established. Our experimental study enables the definition of failure stresses in the axial tension, axial compression and hoop directions. These stresses can be used to define a criteria which will help to predict the failure stresses under different loading conditions. Only one failure criteria will be discussed to demonstrate the advantages and limitations of using such models.

In addition to Soden et al.'s failure envelope, the Tsai-Wu Criteria (Tsai, 1971) is used to gain an insight into the shape of the failure envelope. The Tsai-Wu criteria is a very adaptable failure criteria designed for laminated composites under multiaxial loading conditions. It has the following generalized tensor form:

$$F_i \sigma_i + F_{ij} \sigma_i \sigma_j = 1 \qquad (5.9)$$

With our biaxial loading conditions it has the following form:

$$F_1\sigma_1 + F_2\sigma_2 + F_{11}\sigma_1^2 + F_{22}\sigma_2^2 + 2F_{12}\sigma_1\sigma_2 + F_{66}\sigma_6^2 = 1 \qquad (5.10)$$

σ_6 is equal to 0 because of our tubular specimens, therefore, the equation takes the following simplified form:

$$F_1\sigma_1 + F_2\sigma_2 + F_{11}\sigma_1^2 + F_{22}\sigma_2^2 + 2F_{12}\sigma_1\sigma_2 = 1 \qquad (5.11)$$

The constants take the following form:

$$F_1 = \frac{1}{X} - \frac{1}{X'}$$
$$F_2 = \frac{1}{Y} - \frac{1}{Y'}$$
$$F_{11} = \frac{1}{XX'} \qquad\qquad (5.12)$$
$$F_{22} = \frac{1}{YY'}$$
$$F_{12} = -\frac{1}{XY}$$

Where X is the axial tensile failure stress, X' is the axial compressive failure stress, Y is the hoop tensile failure stress and Y' is the hoop compressive failure stress. Since the hoop compressive failure stress was not known it was assumed to be equal to the axial compressive failure stress. With these equations and selected failure stresses from the $\pm 55^{\circ}$ tests, a failure envelope can be constructed as depicted in Fig. 5.27. It can be observed that this envelope fits most of the experimental data quit well, except for the H/A > 2 region.

101

5.4.5 Practical Application of Failure Envelopes

The following discussion relates to the practical application of the failure envelope. The asymmetry of the failure envelope poses some interesting problems if these tubes are to be used efficiently. For example, the $\pm 55^{\circ}$ tubes perform best under the pressure vessel loading condition of 2H:1A. If these pipes are loaded in another direction they will fail at a considerably lower stress level, i.e. the failure envelope presented here shows us that if the pipe is loaded in the tensile axial direction only it will fail at a value 1/4 of the failure stress for the 2H:1A condition. In addition, it is very important to consider the actual conditions that the tube will operate under. If for example, the tubes are loaded with the optimum stress condition of 2H:1A and for some reason one of these components is lost, i.e. pressure is lost due to a pump failing, the tubes could fail because the stresses present in the tube will shift outside of the defined envelope. Therefore, it is very important to consider the loading conditions under which the tubes will operate.

5.5 Summary of Results

A significant amount of information can be gathered by the examination of the stress-strain curves for these monotonic biaxial loading experiments of filament wound tubular specimens. In addition to the determination of the failure stresses, the curves revealed important information on elastic, nonlinear and time-dependent behaviour.

From the stress-strain curves of the pure tensile loading test and the pure internal pressure test, the elastic constants E_A, E_H, ν_{AH} and ν_{HA} were determined and applied to a stress-strain equation derived from the generalized Hooke's law for cylindrical anisotropy. This equation with these constants fit the linear elastic behaviour of most of the stress ratios for the $\pm 55°$ tubes tested in this study. The linear elastic range was determined for each test and plotted demonstrating the fact that elastic behaviour in these tubes is present at very low stress levels. The time-dependent properties were observed through examination of the stress-strain curves for the three different loading rates tested on the $\pm 55°$ tubes. It was shown that the failure stresses were lower for longer tests under most stress ratios. In addition, failure stresses are extrapolated from the failure stress data in order to demonstrate the trend of failure with respect to increasing time. It can be concluded that the $\pm 55°$ filament wound tubes under long term loading may fail at stress levels 50% lower than their short term failure stresses.

A relationship between damage accumulation and failure modes and stress-strain behaviour has also been developed. It has been observed that the failure mode depends on stress ratio and rate of loading. In addition, the strain behaviour can be used to explain the damage accumulation in the tubular specimens. A failure criteria needs to be developed based on failure modes and damage accumulation in order to predict the behaviour of these filament wound tubes under multiaxial loading conditions. This failure criteria should also be time dependent.

5.6 Conclusions

The results and observations gathered in the investigation of the $\pm 55^\circ$ filament wound tubes can lead to the following conclusions:

I.   Strength and stiffness are a function of loading direction.

II.   Linear elastic behaviour of the tubes can be described by the simplified Hooke's equation.

III.   Time dependent properties are present in the linear and nonlinear stress-strain behaviour.

IV.   Failure mode depends on stress ratio and stress rate.

V.   Damage accumulation is related to stress ratio, stress rate and strain behaviour.
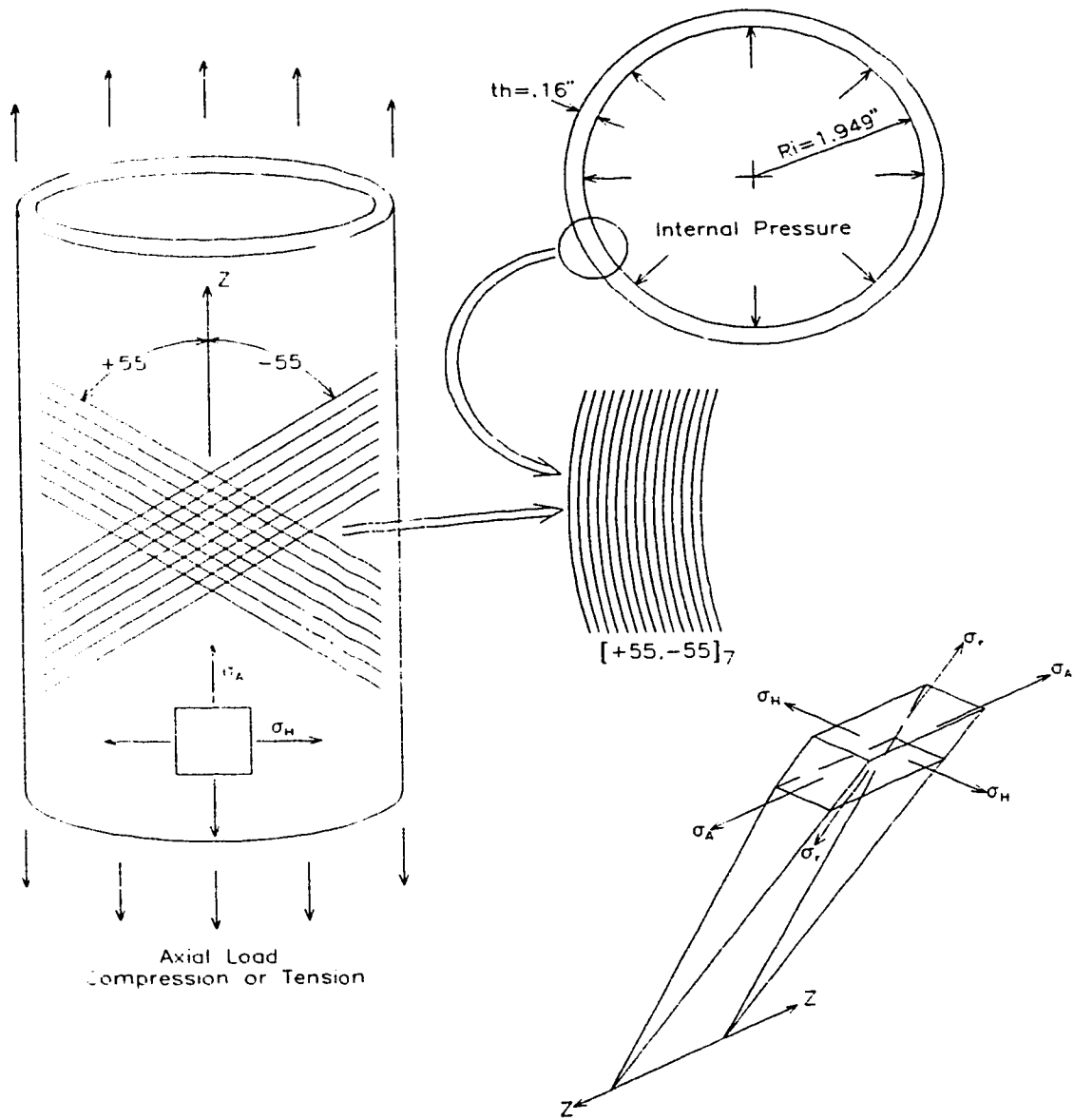
Figure 5.1 ±55° Filament Wound Tube

105
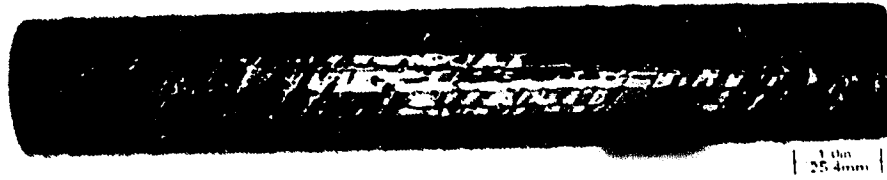
Figure 5.2.a Undamaged Specimen
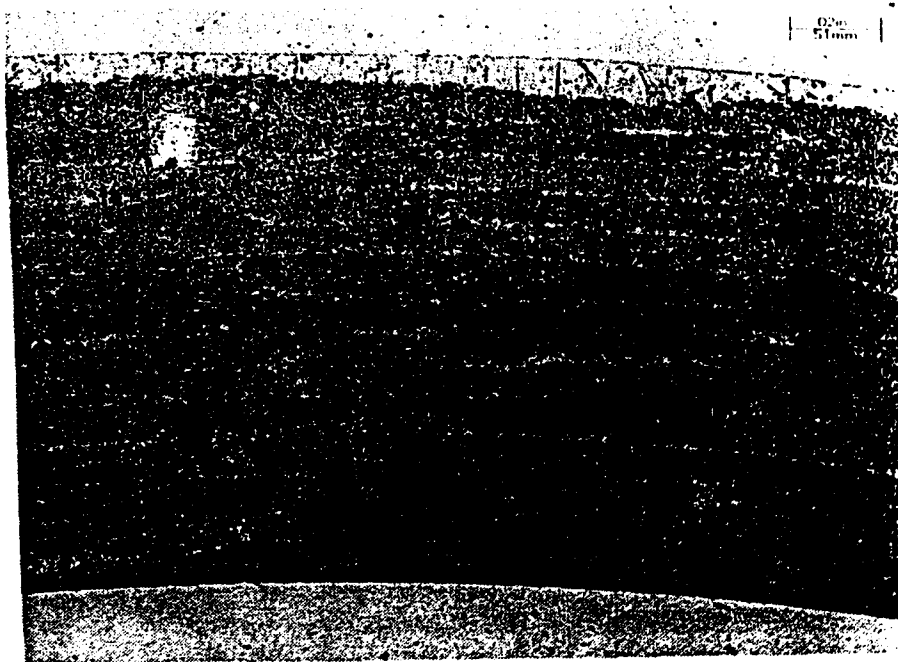
Figure 5.2.b Micrograph of Undamaged Specimen

106
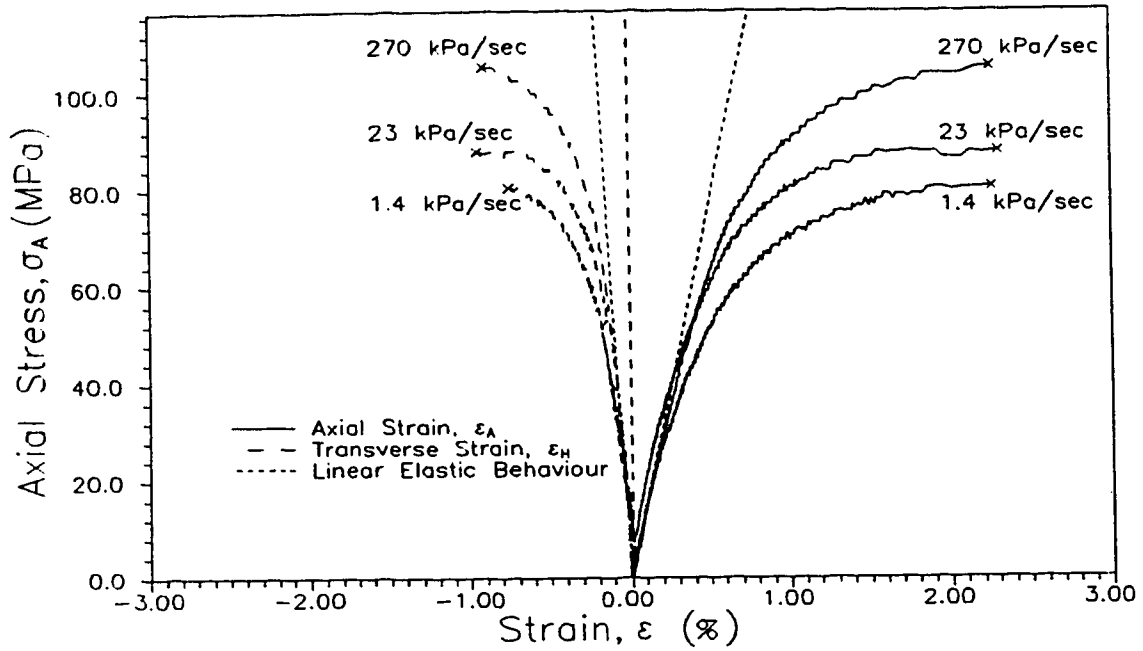
Figure 5.3 Stress-Strain Curves - Stress Ratio 0H:1A - ±55° Tubes
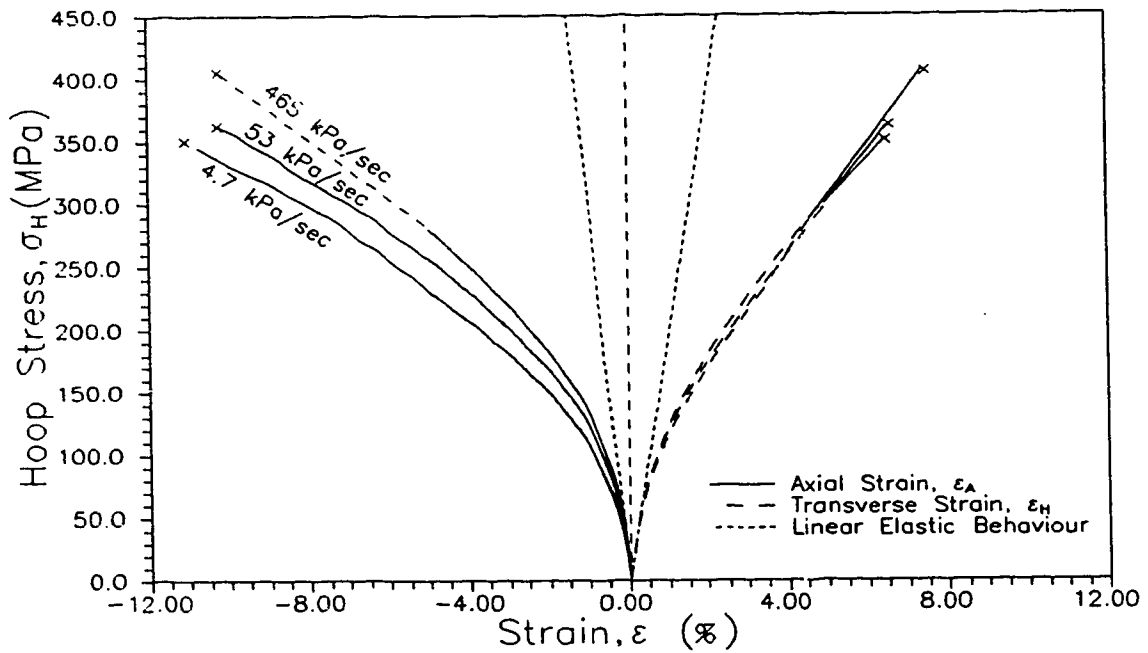
Figure 5.4 Stress-Strain Curves - Stress Ratio 1H:0A - ±55° Tubes
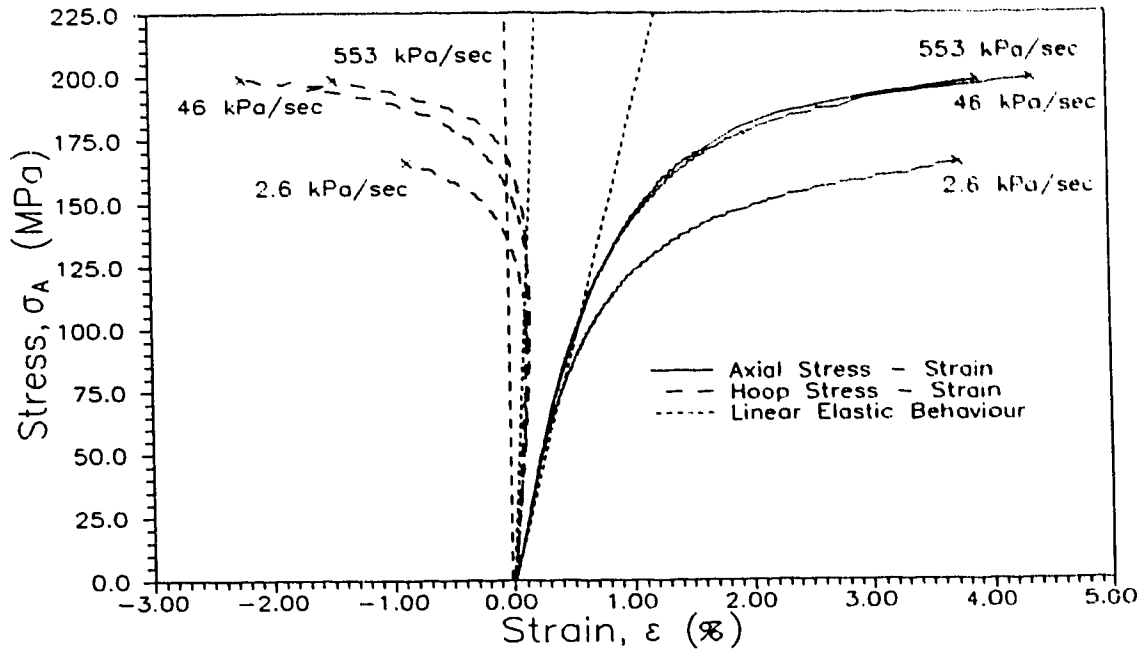
Figure 5.5 Stress-Strain Curves - Stress Ratio 1H:1A - ±55° Tubes
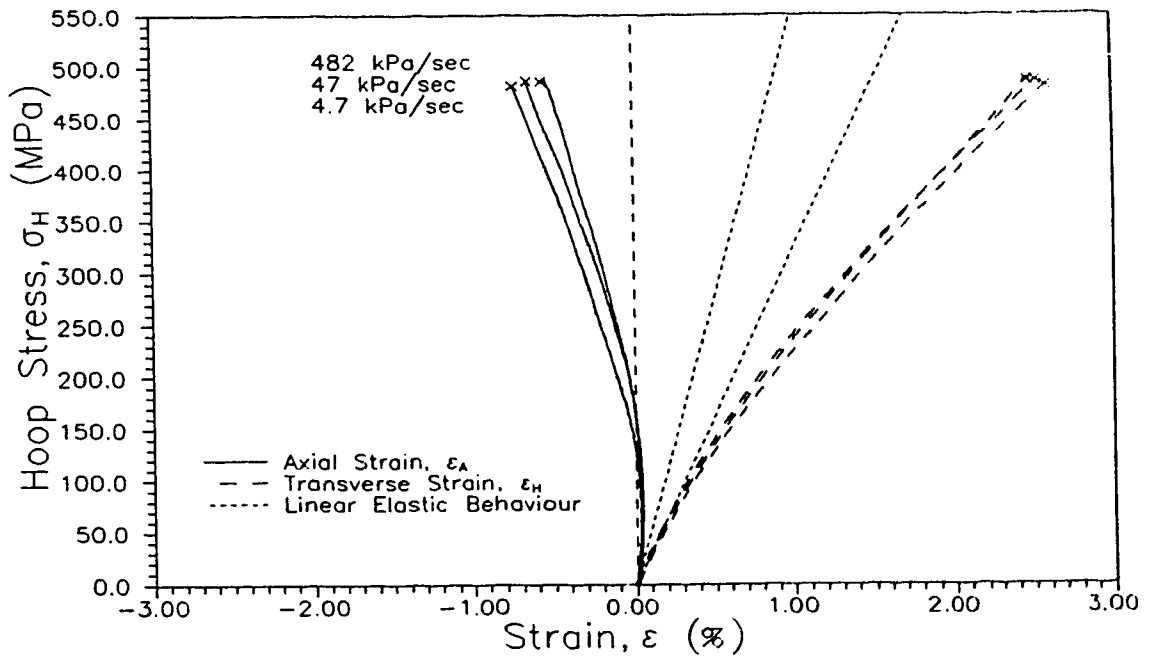
Figure 5.6 Stress-Strain Curves - Stress Ratio 2H:1A - ±55° Tubes
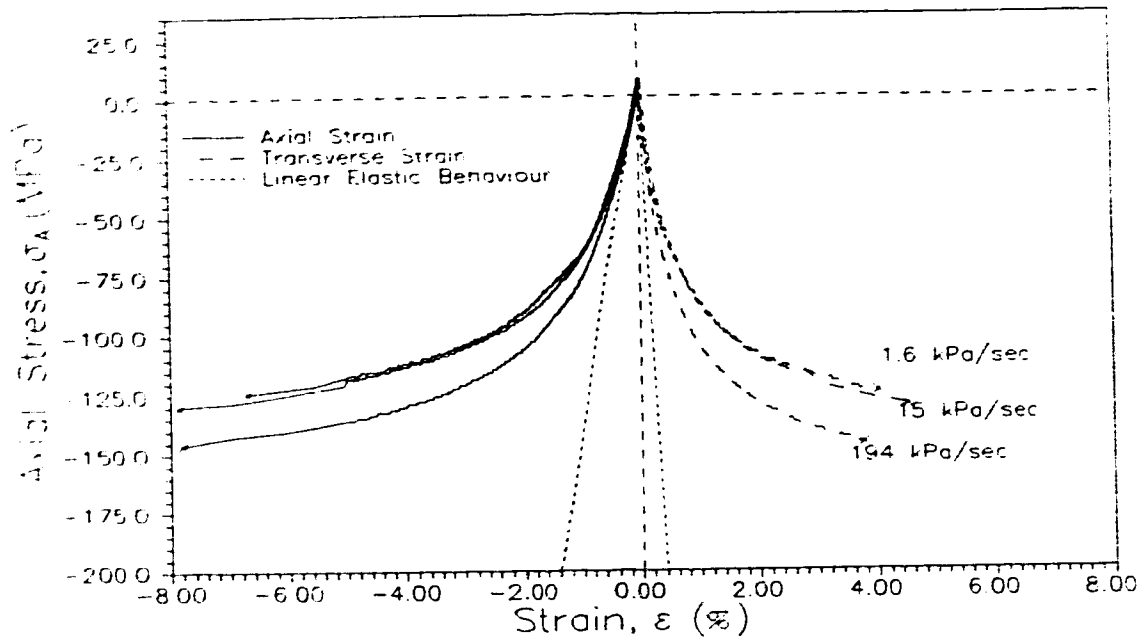
Figure 5.7   Stress-Strain Curves - Stress Ratio 0H:-1A - ±55° Tubes
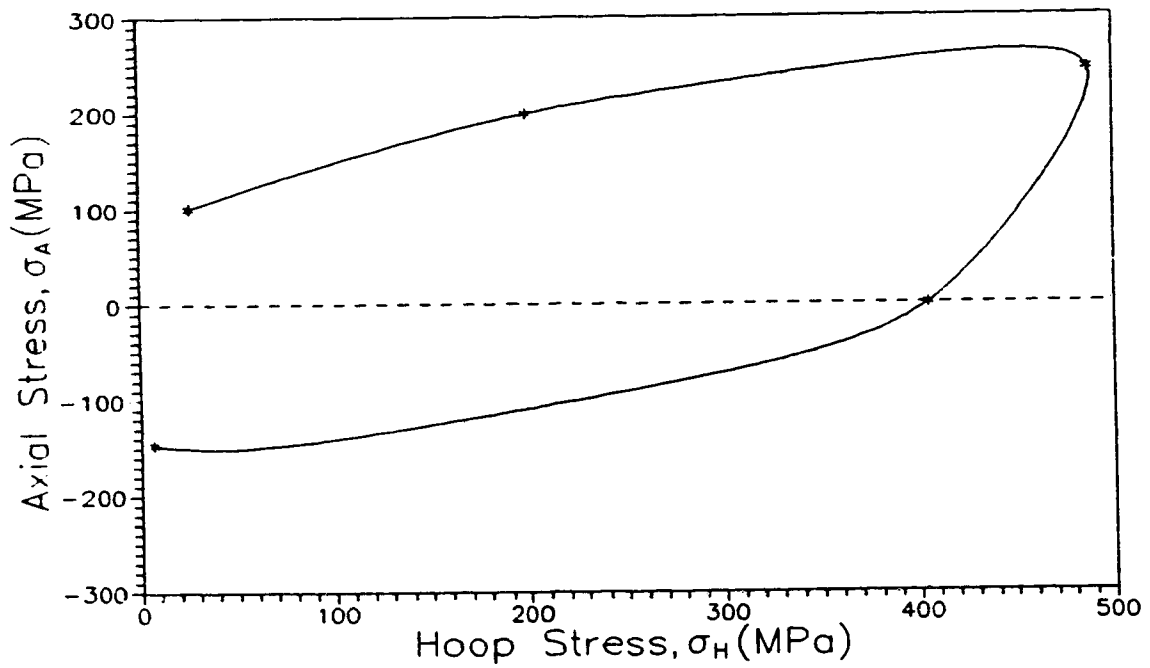
Figure 5.8   Failure Stress Envelope - ±55° Tubes - Fast Test
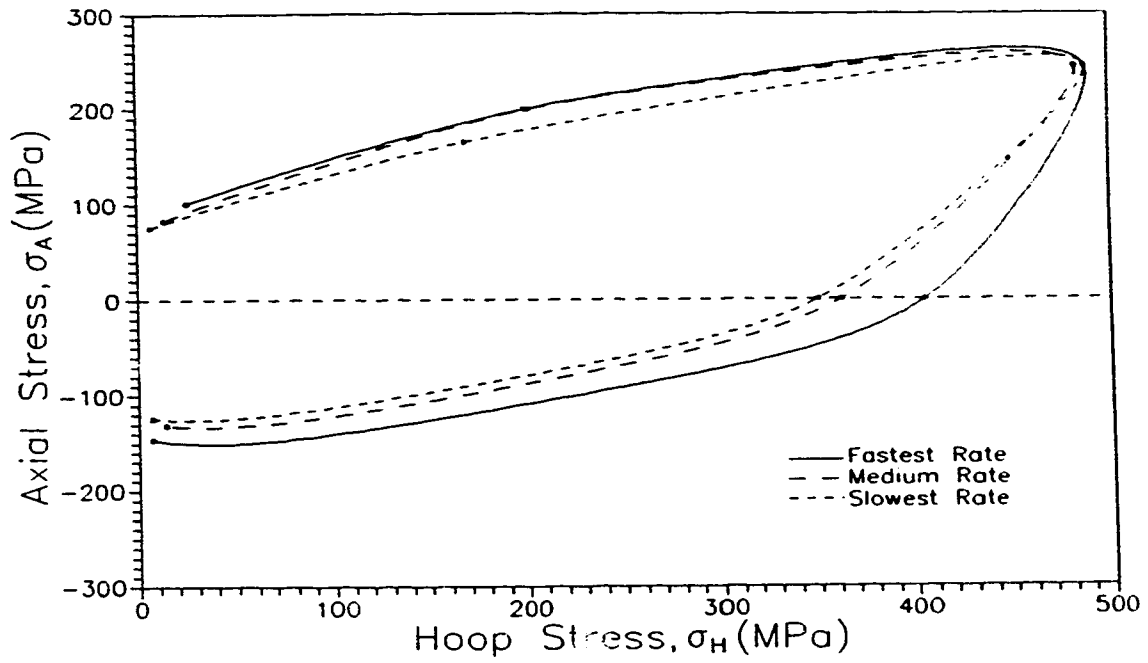
Figure 5.9 Failure Stress Envelopes - ±55° Tubes
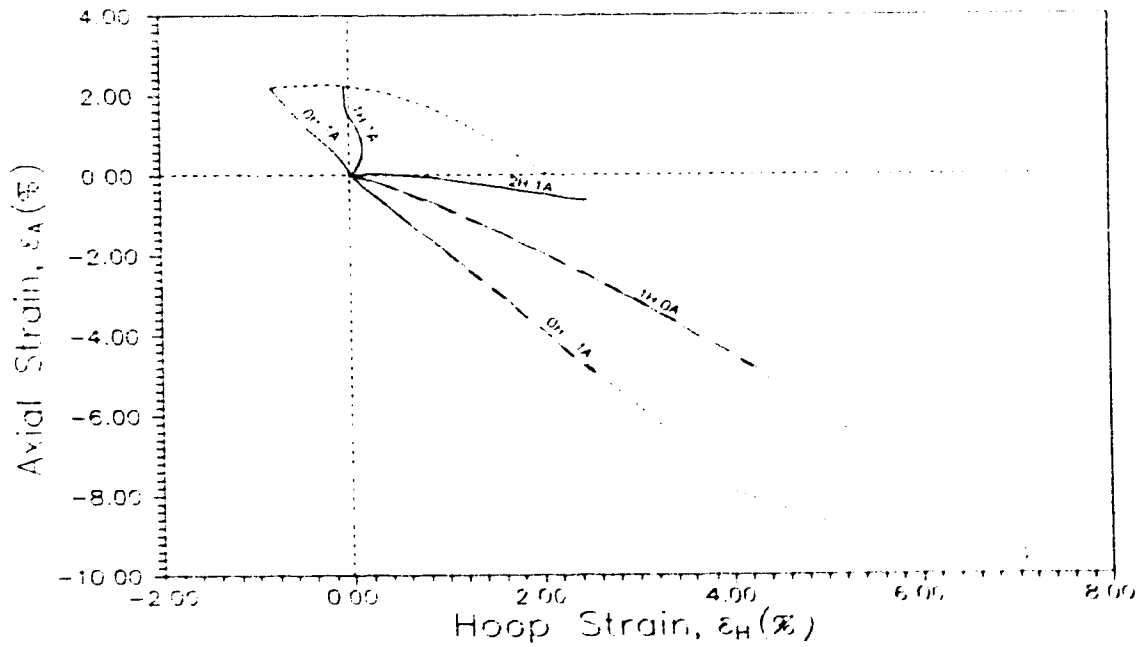
Figure 5.10 Strain Envelope - ±55° Tubes - Fast Rate

110
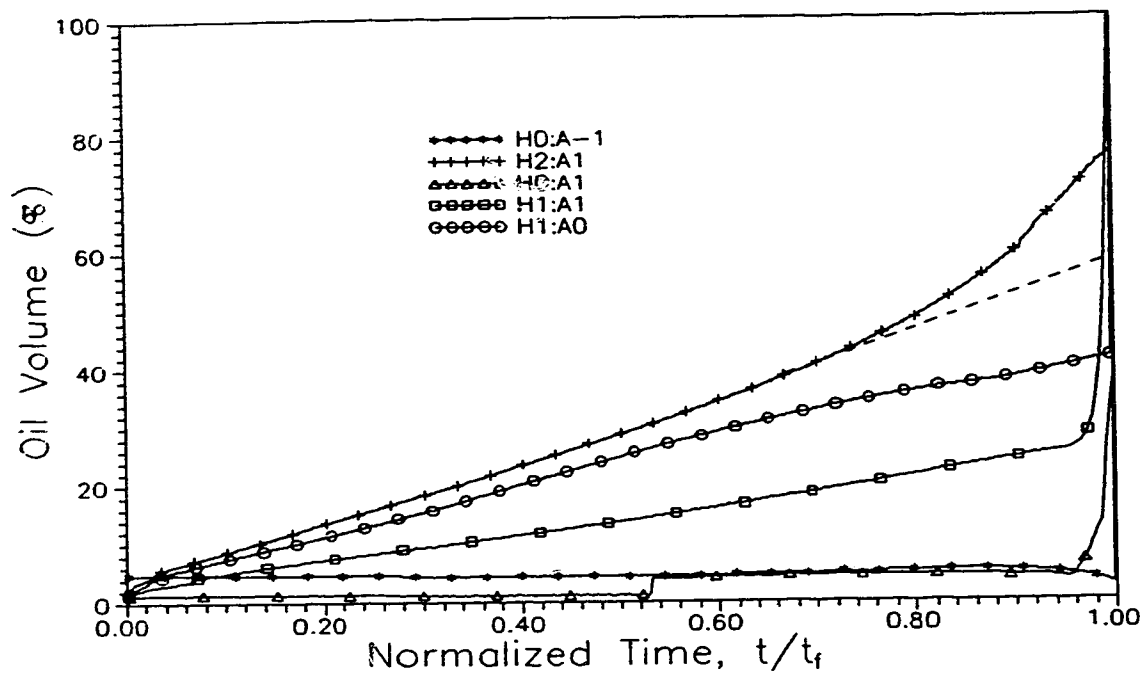
Figure 5.11 Oil Volume in ±55° Tubes - Medium Rate
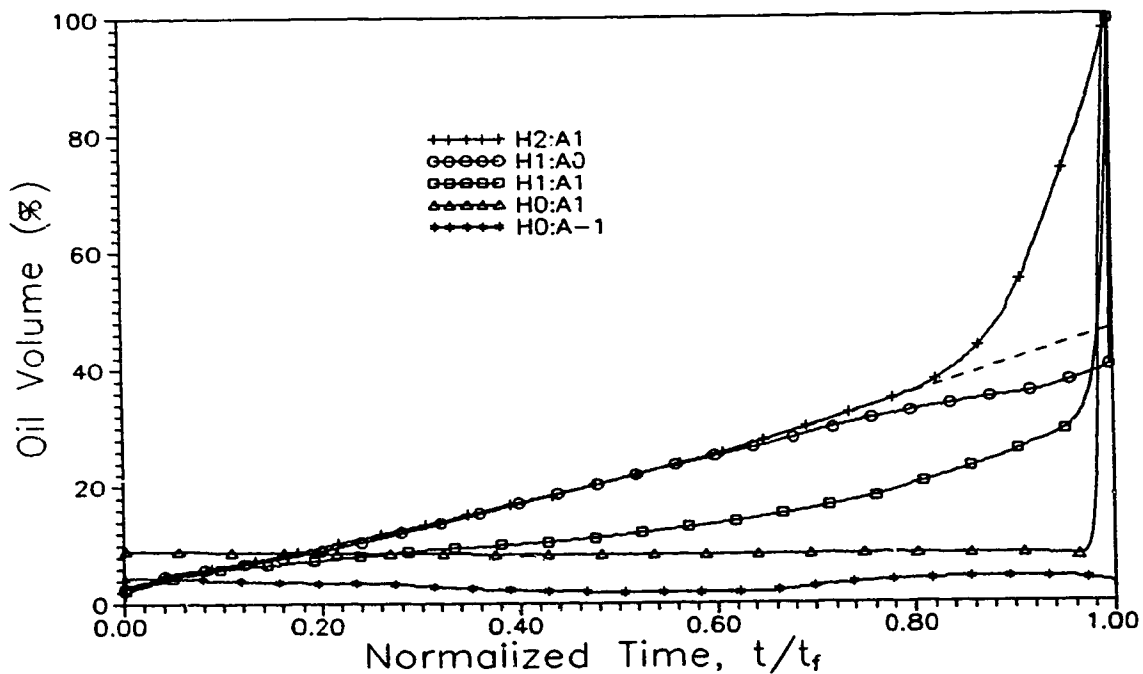
Figure 5.12 Oil Volume in ±55° Tubes - Slow Rate

a. Axial Tension
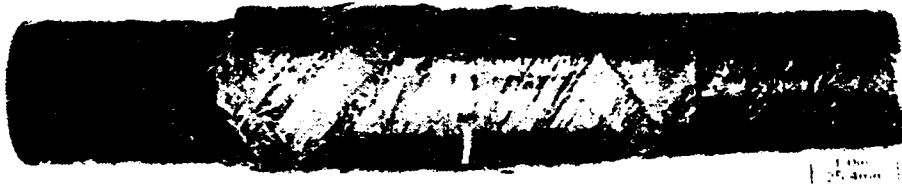
b. Hoop Stress Only
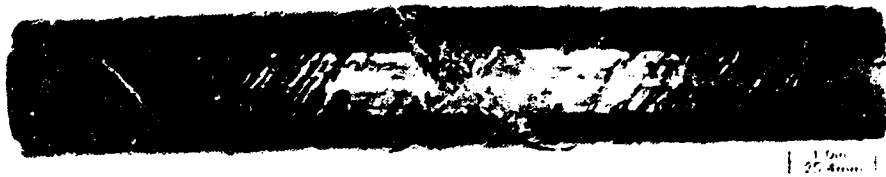
c. Axial Compression

Figure 5.13 Failures - Fastest Rate - ±55° Tubes

a. Axial Tension - Fast Rate
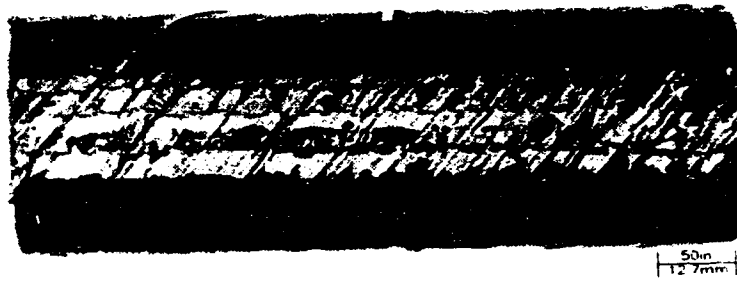
b. Axial Tension - Medium Rate
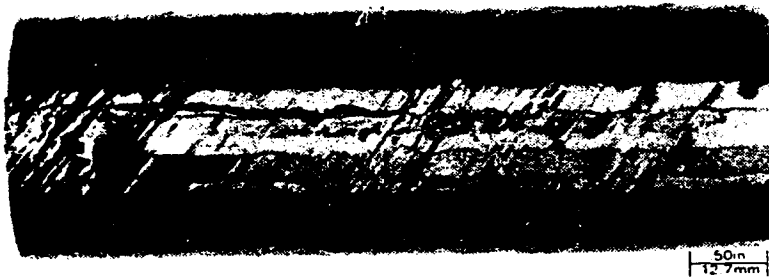
c. Axial Tension - Slow Rate

d. 2H:1A - Fast Rate

Figure 5.14 ±55° Tubes - Failures

113
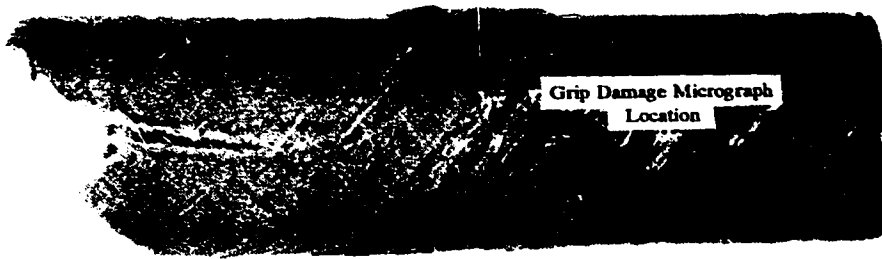
Figure 5.15   Hoop Stress - Longitudinal Fracture
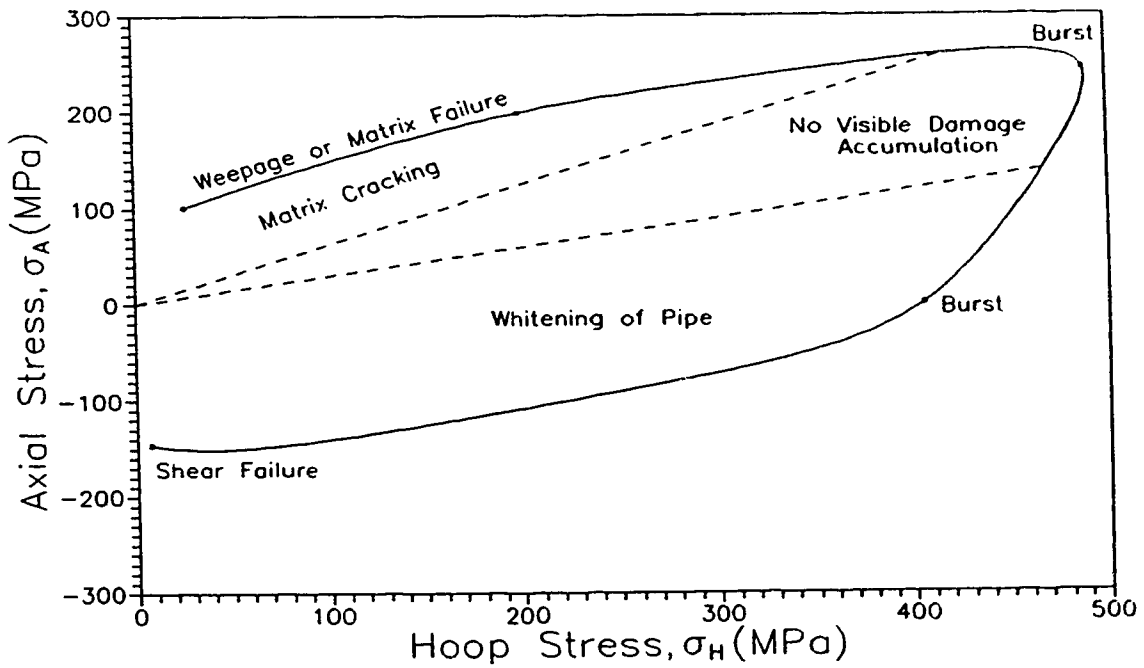
Fgiure 5.16   Stress Envelope with Damage Mechanisms and Failure Modes

114
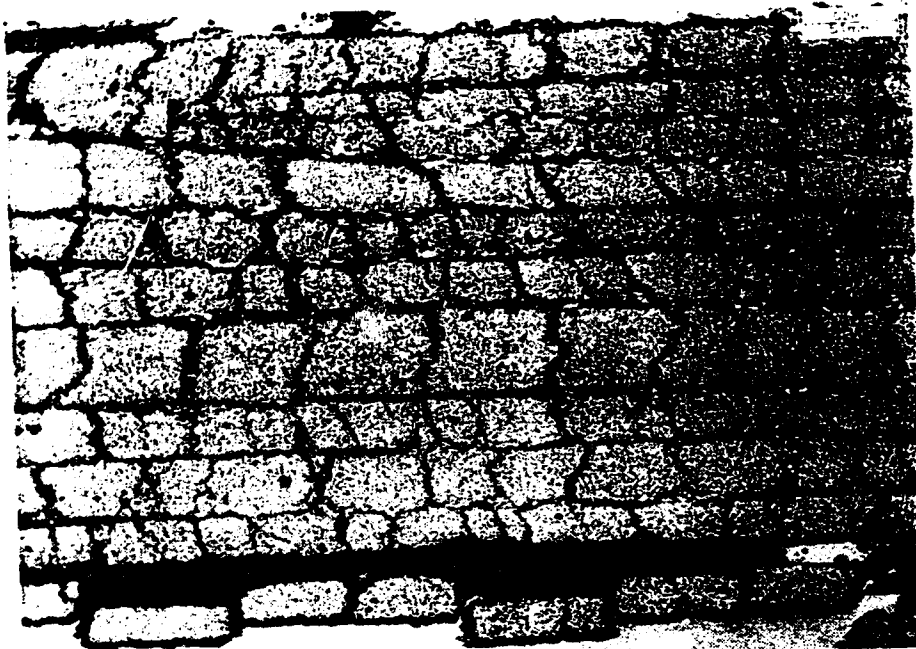
a. OH:1A - Fast Rate

b. OH:1A - Slow Rate

Figure 5.17   Axial Tension ±55° Tubes - Matrix Cracking

115

a. 0H:-1A

b. 2H:1A

Figure 5.18 ±55° Tube Failures

a. 2H:1A
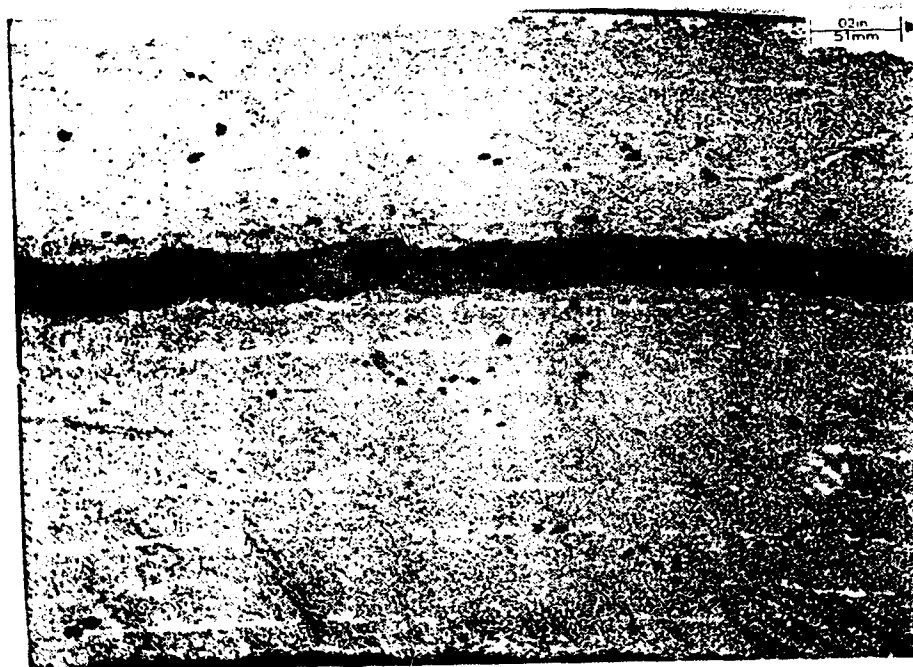
b. 1H:0A

Figure 5.19 ±55° Tubes - Delamination

117

Figure 5.20 Micrograph of Grip Damage - Stress Ratio 1H:0A

118
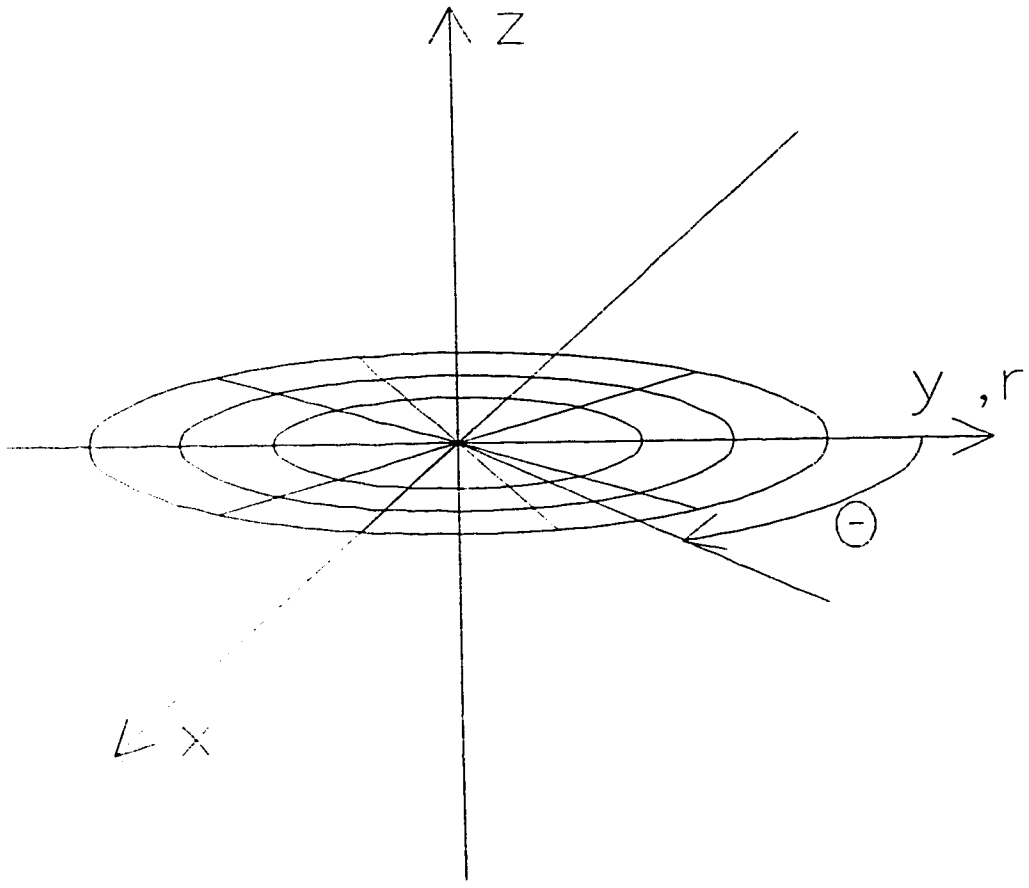
Figure 5.21   Cylindrical Anisotropy
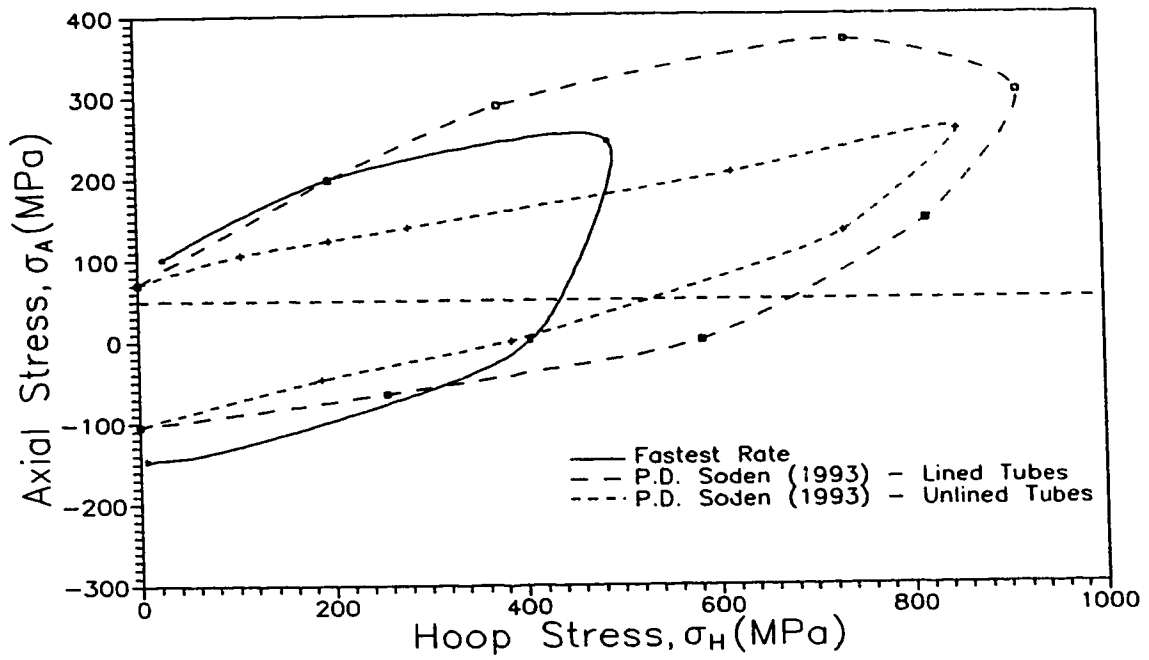
Figure 5.22 Failure Envelope - ±55° Tubes - Comparison with Literature
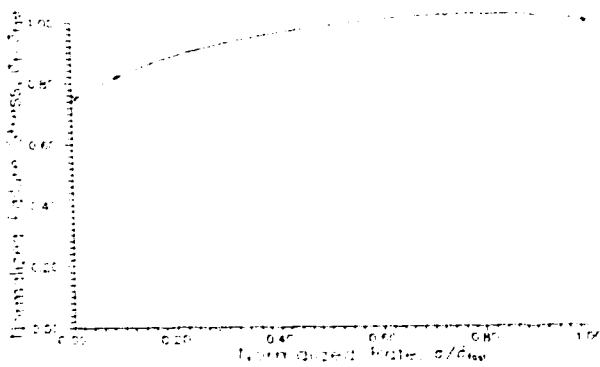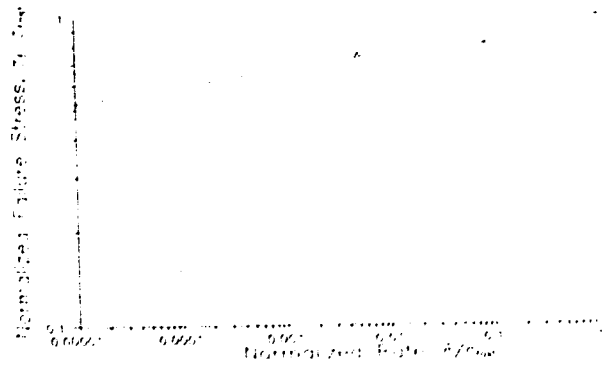
Figure 5.23 0H:1A - Rate Effect

Figure 5.24 0H:1A - Rate Effect

120
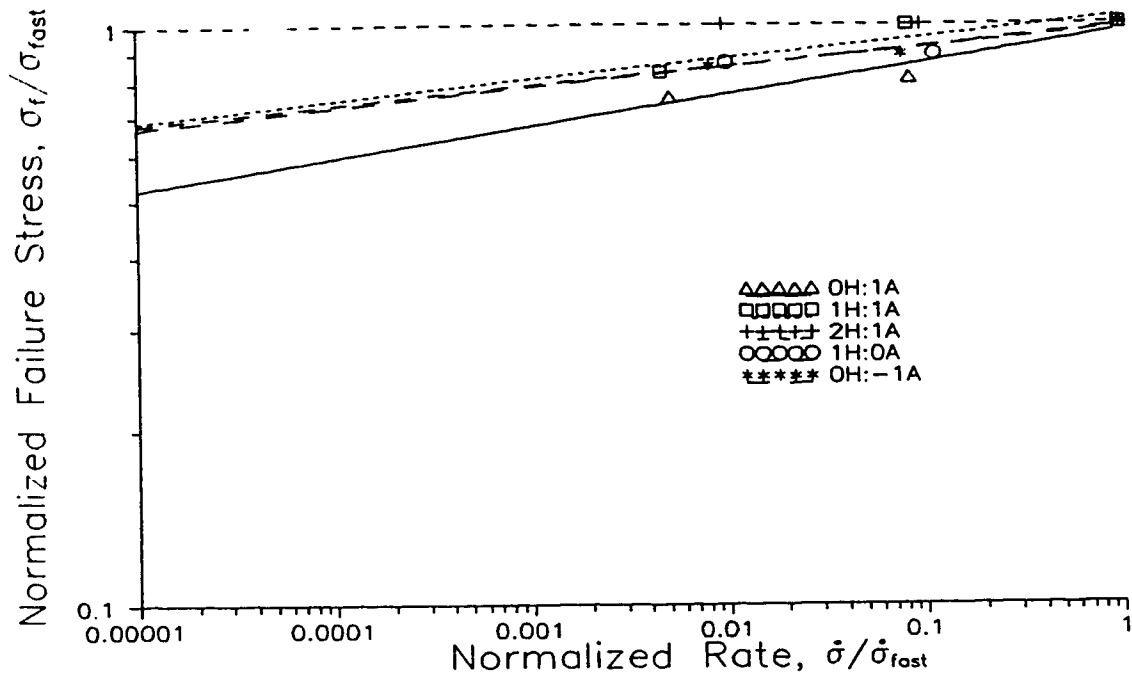
Figure 5.25   Rate Effect - ±55° Tubes
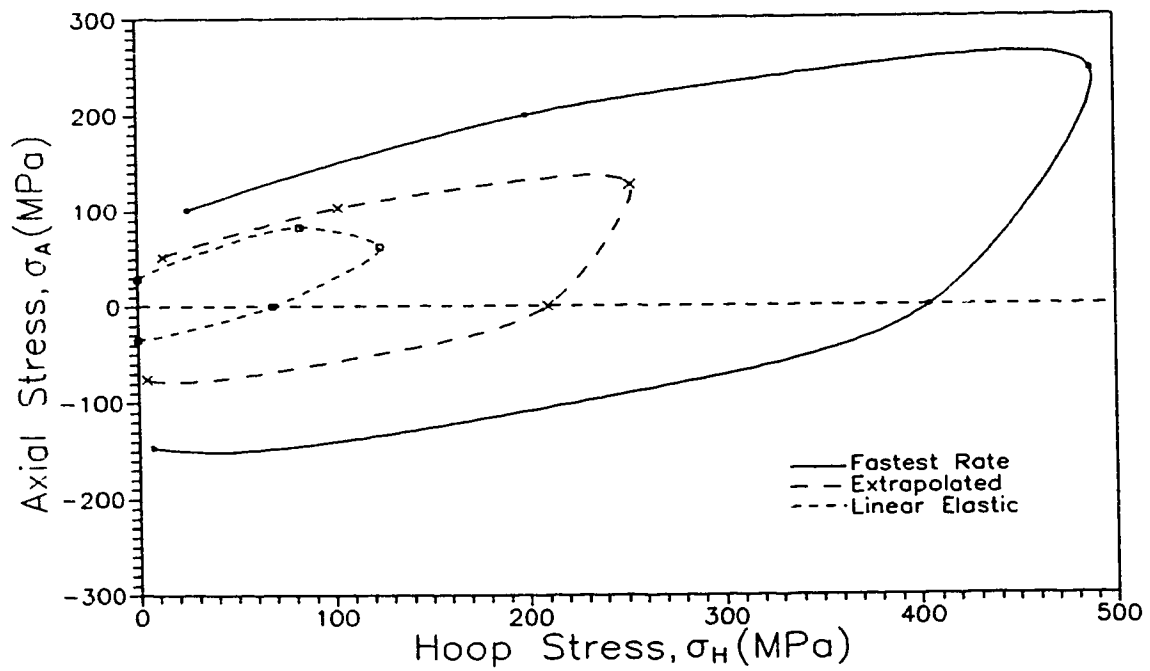
Figure 5.26   Extrapolated Failure Envelope

121
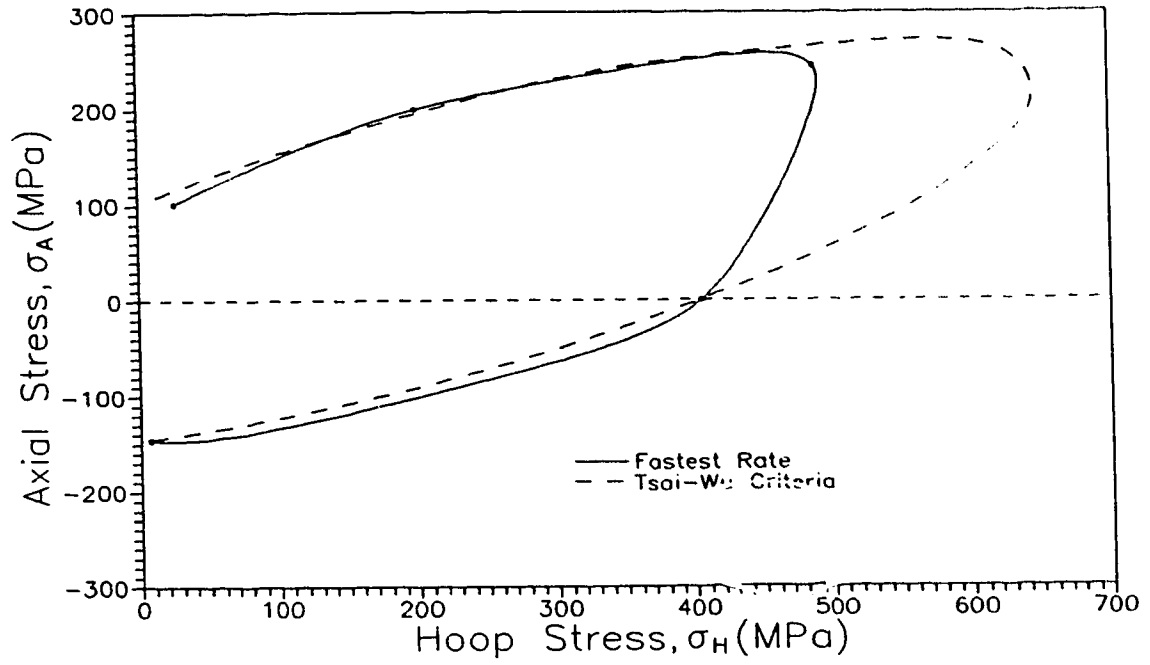
Figure 5.27 Failure Envelope - ±55° Tubes - Comparison to Tsai-Wu Criteria

CHAPTER 6

BIAXIAL TESTING ON MULTIDIRECTIONAL TUBULAR SPECIMENS

6.1   Introduction

The characterization of the multidirectional tubes is more complex than the $\pm 55^c$ tubes. This chapter presents the stress-strain data gathered from one series of tests performed on the multidirectional tubes and briefly discusses some of the properties observed. Many of the same assumptions are made as for the $\pm 55^c$ tubes, i.e. thin walled cylinder theory, and therefore, calculations are simplified.

6.2   Material and Specimens

The multidirectional filament wound tubes have a complex winding pattern as illustrated in Fig. 6.1. To precisely determine this lay-up a section of the specimen was placed in a Kiln and all of the resin was burned off. The remaining layers of glass fibres were separated, Fig. 6.2, and it was determined that three different orientations existed: $\pm 45^{\circ}$, $\pm 70^c$ and 0°. The off axis orientations were filament wound using a similar process to the $\pm 55^c$ tubes. The 0° layer was produced using a lay-up process because it is impossible to wind fibres at precisely 0°. Four inch strips were placed on the tube in a spiral pattern which over lapped the strips. This overlapping was sufficient enough so that the transfer of load was such that the fibres could be considered as continuous.

The lay-up of these pipe is $[\pm 70, \pm 45, \pm 45, 45, -70, 0, +45, \pm 45, \pm 45, \pm 45, \pm 45]$ and the fibre volume is 56%. The tubes have an inside diameter of 49.30 $\pm$0.02mm (1.937 $\pm$0.005") and an outside diameter of 60.9 $\pm$.1mm (2.40 $\pm$0.02"). Figure 6.3 shows a micrograph of a cross-section of the tube. It can be observed that there are more voids than the $\pm 55°$ tubes and some resin rich areas around the $0°$ fibres.

6.3   Test Results

6.3.1   Stress-Strain Curves

Since the multidirectional filament wound tubes were tested with only one stress rate each graph of the stress-strain behaviour only includes one curve. Figures 6.4 to 6.9 present these curves which will be discussed in a general manner with respect to linear and nonlinear behaviour and tube filament wind angles. The strains are plotted against the average stresses in the tube wall.

Figure 6.4 shows the stress-strain curve for the stress ratio of 0H:1A. These curves follow the typical behaviour of most materials under uniaxial tension. The axial strain is positive and the transverse strain is negative. The linear elastic range is approximately 40% of the final failure stress and is present under a strain of 0.40% in the axial direction and -0.35% in the transverse direction. Failure occurs at a stress of 162 MPa at an axial strain of 1.60% and a transverse strain of -1.40%. The axial failure strain corresponds to a typical failure strain for glass fibres loaded in the axial direction.

It can be concluded that the failure of the 0^c fibres in the tube caused the global failure. This is verified by the examination of a micrograph of the failure (section 6.3.4b).

Figure 6.5 shows the stress-strain curve for the stress ratio of 1H:0A. Again, the stress strain curves follow an expected path for pure hoop stress conditions. The transverse strain is positive and the axial strain is negative. The failure stress is 277 MPa with failure strains of 3.70% and -2.30% for the transverse and axial directions respectively. The linear elastic behaviour is exhibited only 22% of the failure stress with corresponding strains of 0.50% and 0.25% for the transverse and axial directions, respectively. Again, it is observed that the failure strain is small which is due to the $\pm 70^c$ fibres constraining the deformation of the $\pm 45°$ fibres.

Figure 6.6 shows the stress-strain curves for the stress ratio of 1H:1A. Both of the strains are positive and are very close in value. This is because under the 1H:1A loading condition the principal stress direction is along the 45° fibres. The failure stress is 192 MPa with small failure strains approximately equal to 0.60%. The linear elastic region of the curve extends 52% of the failure stress with a strain of 0.24% in the transverse and axial directions. When nonlinearity begins the stress-strain curves deviate possibly because of the effects of the 0° fibres and the $\pm 70°$ fibres on the behaviour of the $\pm 45°$ fibres.

Figure 6.7 shows the stress-strain curves for the stress ratio of 2H:1A. The failure stress for this loading condition is 124 MPa and 248 MPa in the axial and hoop direction respectively. The failure strains produced are very small with the axial strain almost zero, -0.10%. The linear elastic range is approximately 40% of the failure stress

125

with an axial strain of 0% and a transverse strain of 0.50%.

Figure 6.8 shows the stress-strain curves for the stress ratio of 0H:-1A. The failure stress for this loading condition, axial compression, is 226 MPa which corresponds to failure strains of -2.90% and 2.65% in the axial and transverse directions respectively. The linear elastic range is approximately 22% of the failure stress with strains less than 0.5%.

Figure 6.9 shows the stress-strain curves for the stress ratio of 1H:-1A. The failure stresses for this loading condition is 131 Mpa in the hoop direction and -131 MPa in the axial direction which corresponds to failure strains of -3.4% and 2.80% respectively. Again, the linear elastic range is very small corresponding to approximately 20% of the failure stress and strains less than 0.5%.

The failure stresses and linear elastic ranges are summarized in appendix C. The failures will discussed based on macro and micro mechanical behaviour.

6.3.2 Biaxial Failure Envelope - Stress and Strain

Figure 6.10 shows the biaxial failure envelope for the multidirectional tubes. The stress values used for the envelope are the averages of the axial stress and hoop stress through the wall. This is somewhat simplistic because the different fibre orientations have different stiffness and therefore stress values vary through the tube wall with constant strain. The distribution of stresses will be analyzed in future studies.

The strain failure envelope, Fig. 6.11, is developed in order to present the strain

data in a useful manner. Again, the asymmetry of the envelope demonstrates the complexity of the strain behaviour of the filament wound tubes under biaxial loading.

6.3.3 Oil Volume Changes

The change in oil volume can be used to describe the leakage of the tubular specimens. Figure 6.12 presents the percent of available oil volume with respect to the normalized time to failure. The tests with low pressure indicate no change in oil volume over the length of the test. The test with high pressure indicate a constant increase in oil volume. The H1:A1 and H2:A1 tests demonstrate an increase in the slope of the change in oil volume. This change corresponds to the weepage of fluid through the tube wall which was observed visually in the actual tests.

6.3.4a Macro Observations

The multidirectional tubes produced some complex failures under the loading conditions tested. These tubes are comprised of a complicated winding scheme that incorporates three different fibre angle orientations. i.e. $0°$, $\pm45°$ and $\pm70°$. The differing material properties and interaction of each angle ply contributes to the failure modes and damage accumulation observed. The tubular specimens are discussed based on mode of failure, location of failure, damage accumulation and strain behaviour.

Figure 6.13.a shows the failure of the multidirectional tubular under pure axial

127

tension. Matrix cracks developed parallel to the ±70° fibres as the test progressed. Final failure occurred when a critical axial strain was reached and the 0° fibres fractured. This caused extensive delamination between the ±70° fibres and the ±45° fibres which are hidden from view. The actual delamination will be shown later on in section 6.6.4b. Matrix cracking was also observed in the inside wall parallel to the ±45° fibres. No fluid leakage was detected because the instantaneous structural failure caused the test to stop and the pressure to drop to zero. Later tests verified that leakage occurs within a few seconds of initial failure.

The 1H:1A (not shown) and 2H:1A (Fig. 6.13.b) tests produced similar failures. Matrix cracking parallel to the ±70° fibres was observed to develop as the tests progressed. This matrix cracking apparently lead to failure by weepage of fluid through the wall thickness at multiple locations. Small drops of oil formed on the surface of the tubes which progressed into a wetting of the entire outside surface. The structural integrity of both specimens was preserved.

Figure 6.13.c presents the failure of the multidirectional tube under pure hoop loading. This tube failed when critical hoop strain caused the ±70° fibres to break. It can be observed from the figure that there is fibre breakage, matrix cracking and extensive delamination of the ±70° fibres from the rest of the tube. Fluid leakage was not observed and damage to the other layers seems minimal. Some matrix cracking is observed parallel to the ±45° fibres on the inside wall. The tube is still able to hold limited axial load but its pressure carrying capabilities were unknown. Again, later tests demonstrated that no pressure carrying capabilities are preserved after initial failure.

The axial compression test produced a failure similar to the $\pm 55^{c}$ failure under the same loading conditions as shown in Fig. 6.14.a. Again, with negative axial strain, it is obviously a matrix dominated shear failure at an angle parallel to the $\pm 45°$ fibres.

Figure 6.14.b. shows the failure of the multidirectional specimen loaded under the 1H:-1A condition. This produced a failure that involved a couple of different modes. The principal direction of loading is in the direction of the $\pm 45°$ fibres and strains are between the axial compression test and the pure hoop test. This was the only tube that failed violently in the multidirectional series. Inspecting the figure reveals actual fibre breakage in the $\pm 45°$ layers and delamination in the $\pm 70°$ layers. It is possible that there was a shear failure in the matrix similar to the axial compression test which was followed by the burst of the tube due to the high internal pressure. This failure happened in a localized form and therefore no damage is apparent on the rest of the specimen.

By relating the failure modes and damage accumulation to the strains developed on the specimens a few observations can be made. For all tests with axial strains equal to or greater than zero extensive matrix cracking developed on the outside surface of the tubes at an angle parallel to the $\pm 70°$ fibres. The final failure mode depended on the level of axial strain, i.e. for high axial strains the $0°$ fibres failed and for low axial strain the tubes failed by leakage of fluid through matrix cracks. Specimens with high negative axial strains had initial failures of shear in the direction of the $\pm 45°$ fibres. The specimen with high hoop strain failed with the breakage of the $\pm 70°$ fibres on the outside wall. Figure 6.15 summarizes damage and failure modes with respect to the failure stress envelope previously defined.

Micrographs were made from each tested specimen in order to examine the damage present.

Figure 6.16.a shows the damage present in the multidirectional tube after failure in the OH:1A loading condition. The plane of the micrograph is parallel to the tube axis because damage is more visible. It can be observed that there is matrix cracking in the ±45° layers which may have accumulated as loading increased. The other damage present, extensive delamination between the 0° layer and the ±45° layers and between the ±70° and the ±45° layers, and the apparent destruction of the internal 70° layer, probably occurred after the initial failure. From observations made during the test and on the macro scale it can be assumed breakage of 0° fibres caused this extensive damage. Differing layer stiffness creates high interlaminar shear stress and therefore delamination may result.

Delamination is also present in the failure of the multidirectional tube under pure internal pressure loading as shown in Fig. 6.16.b. This delamination, occurring between the ±70° layers and the ±45° layers, probably developed after the fibre breakage in the ±70° layers. Limited matrix cracking is also observable in the 0° layer and in the ±45° located on the inside of the 0° layer because the hoop strain is positive. This damage probably accumulated as the test progressed and ultimately would have led to fluid weepage.

Figure 6.17.a shows the damage accumulation for the 2H:1A load condition. As

130

previously mentioned this pipe failed by weepage of fluid through the wall thickness and did not have a structural failure. Extensive transverse matrix cracking is observable in all layers except the ±70°. Matrix cracking was present in the ±70° layers otherwise weepage could not have occurred. In addition, longitudinal matrix cracking is present in the 0° layer. This damage enabled the formation of a path for the oil to follow through the wall thickness. The 1H:1A test experienced similar damage.

The multidirectional tube under axial compression failed by shearing. The damage presented in Fig. 6.17.b was observed away from the shear failure. Although it is impossible to tell whether this damage occurred before or after the shear failure it clearly shows delamination between the 0° layer and the rest of the pipe. The reason for this damage may be the difference in layer stiffness. In addition, limited transverse matrix cracking is present in the 0° fibre bundles probably caused by high positive hoop strain.

The damage present in the multidirectional tubes can not be as easily related to strain behaviour as the ±55° tubes. The ±45° layers in the multidirectional tube can develop matrix cracks if positive axial or hoop strain is present. This condition is present under all loading conditions and therefore matrix cracking is possible in any test. Delamination is also present in many cases because of high interlaminar stresses created by the differing stiffness of the layers.

131

6.4   Interpretation of Data

6.4.1   Linear Elastic Behaviour

To determine the elastic constants used in the stress-strain relationship developed in chapter 5 the tests with the appropriate loading conditions need to be analyzed. By examining the axial tensile stress-strain curve the elastic modulus, E_A, was determined to be 26.2 GPa and the Poisson's ratio is, ν_{AH}, 0.8. Correspondingly, the elastic modulus, E_H, was determined to be 25.0 GPa and the Poisson's ratio is, ν_{AH}, 0.70 by examining the pure hoop stress test stress-strain curve.

The stress-strain relationship developed in the previous chapter used on the multidirectional tubes does not correlate well with the stress strain curves shown in Figs. 6.4 to 6.9 and therefore it is not plotted. The reason for this discrepancy is the fact that a complex model is needed to describe the behaviour of these tubes. The addition of 0° and $\pm 70^\circ$ fibres modifies the behaviour of the $\pm 45^\circ$ fibres in the tubes by adding stiffness in the axial and hoop directions. In addition, the $\pm 70^\circ$ fibres constrain the radial deformation of the tubes, subsequently complicating the linear elastic and nonlinear behaviour. A complex elastic model needs to be developed in order to predict the linear elastic behaviour of these tubes.

132

6.4.2 Discussion of Failure Envelopes

Figure 6.10 shows the biaxial failure envelope for the multidirectional tubes assuming an average stress through the wall. This asymmetrical envelope demonstrates the complexity of the material properties of the tubes. It can be observed that the highest positive axial stress occurs at a load ratio approximately equal to 1H:1A, the maximum hoop stress occurs under pure hoop loading conditions and the highest axial stress occurs under pure compression loading.

Figure 6.18 illustrates the difference between the two different filament wound tubes tested. This figure shows the biaxial failure stresses and the linear elastic range of each tube. It is plotted for the sake of comparison using average stresses through the tube wall. It can be observed that the multidirectional tubes are stronger in the axial direction because of the addition of the 0° fibres. The ±55° tubes are stronger in the hoop direction even though there are some ±70° in the multidirectional tubes. The linear elastic ranges are similar because the epoxy matrix is the same for both pipes.

The failure envelope for the multidirectional tubes is less asymmetric than the ±55° envelope. This enables relatively high loading under any attainable biaxial conditions. The path of loading is not as crucial because the axial failure stress does not increase by a significant amount with the addition of pressure. Any loss of pressure or axial load when operating under high stress conditions will not result in failure on the tube.

6.4.3   Failure Criteria

The complex behaviour of the multidirectional tubes can not be described by the failure criteria equation discussed in chapter 5. This demonstrates the inflexibility of this equation for all composite materials. In order to define a curve to fit the data the F_{12} constant needs to be modified. This has been done many times as summarized by Fawaz (1992) in order to fit ones own experimental data.

6.5   Summary of Results

A significant amount of information can be gathered by the examination of the stress-strain curves for these monotonic biaxial loading experiments for the multidirectional filament wound tubular specimens. In addition to the determination of the failure stresses, the curves revealed important information on elastic and nonlinear behaviour. From the stress-strain curves of the pure tensile loading test and the pure hoop stress test the elastic constants E_A, E_{II}, ν_{AII} and ν_{IIA} were determined and applied to a stress-strain equation derived from the generalized Hooke's law for cylindrical anisotropy. This equation with these constants does not fit the linear elastic behaviour of the multidirectional tubes because of their complex lay-up. The linear elastic range was determined for each test and plotted demonstrating the fact that elastic behaviour in these tubes is present at very low stress levels.

Because of the complex nature of these multidirectional tubes further study is

134

necessary to characterize them properly. The combination of fibre winding angles complicates the determination of stress distribution in the tube walls. This is obvious in the examination of the failure modes and damage accumulation because individual layers show extensive damage while others reveal no damage at all. The differing stiffness in each layer makes averaging stresses meaningless and therefore, a criteria needs to be developed in order to compensate for this. The damaging interlaminar stresses developed between layers under loading need to be analyzed in order to understand the failure modes. In addition, the time dependent properties of the multidirectional tubes need to be evaluated.

6.6   Conclusions

The results and observations gathered in the investigation of the multidirectional tubes can lead to the following conclusions:

I.   Strength and stiffness are a function of stress ratio.

II.   Linear elastic behaviour of the multidirectional tubes can not be described by a simplified Hooke's law.

III.   Failure mode depends on stress ratio.

135
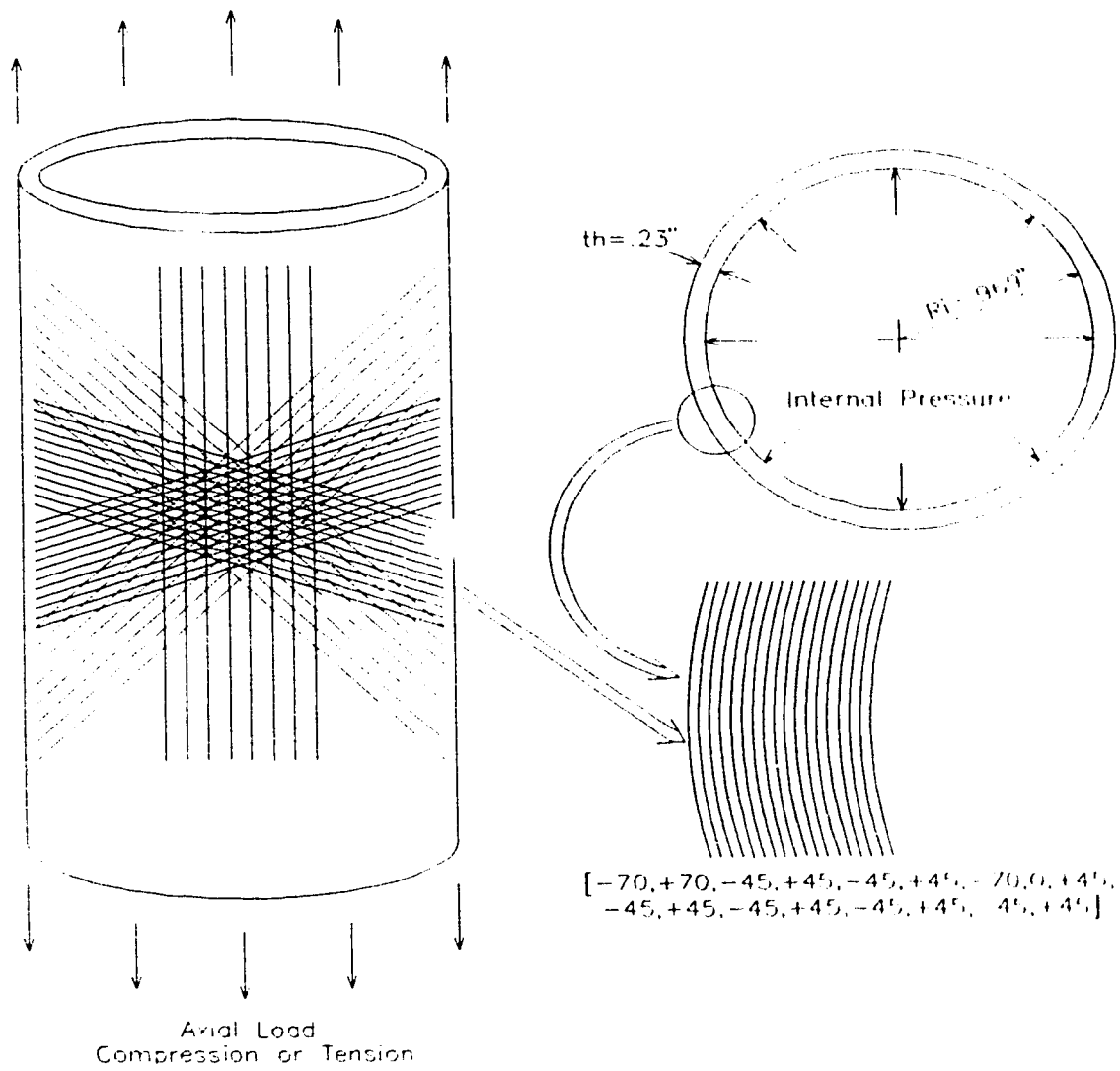
Figure 6.1 Multidirectional Tubular Specimens

136
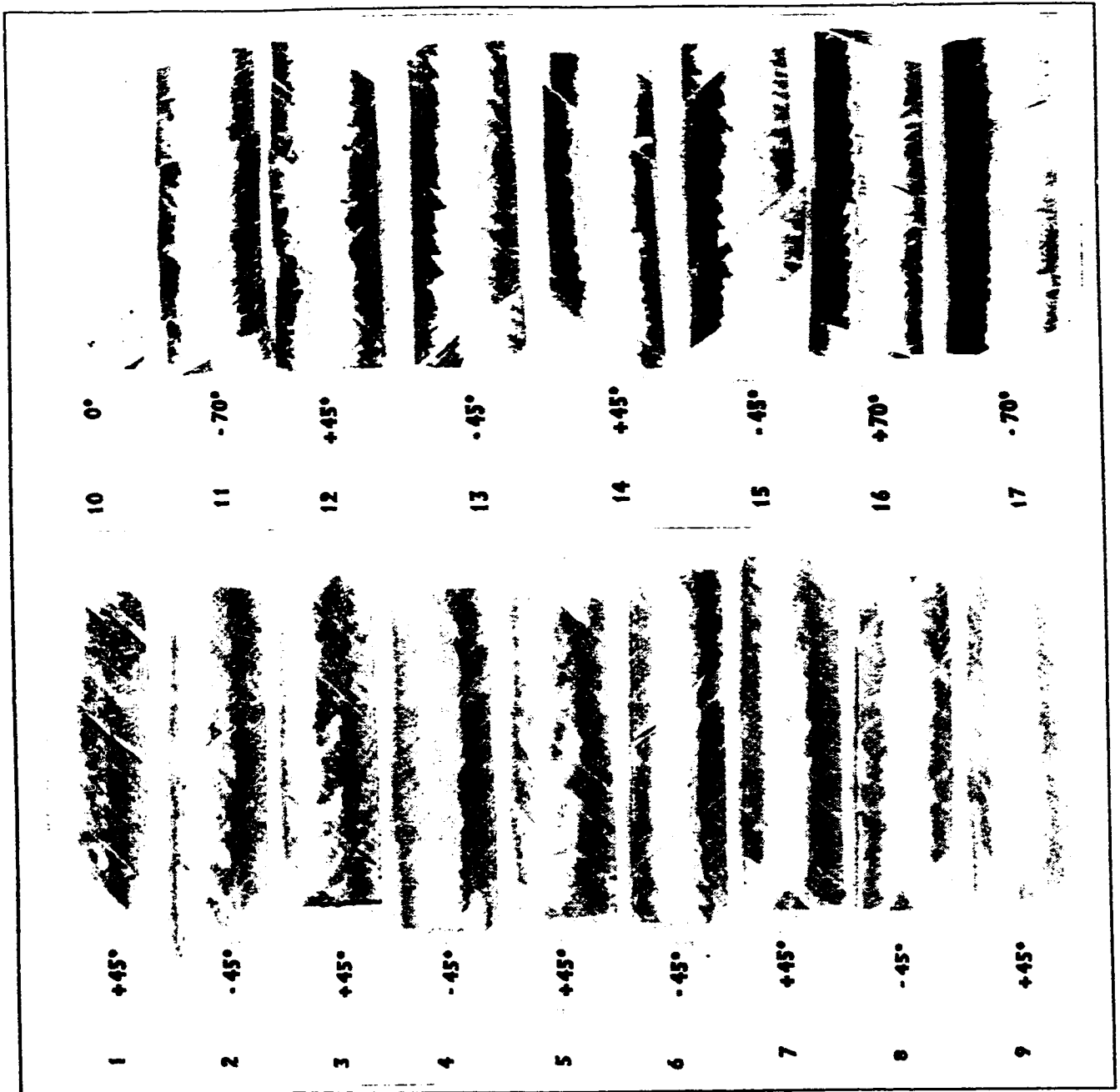
Figure 6.2 Lay-Up of Multidirectional Tubes (1 inside - 17 outside)

137
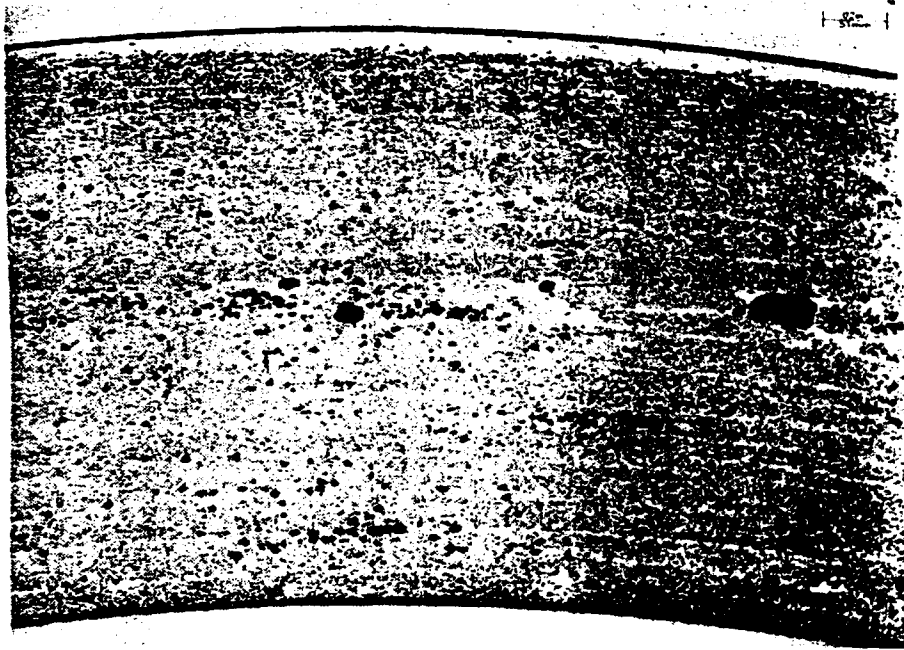
Figure 6.3 Micrograph of Undamaged Specimen
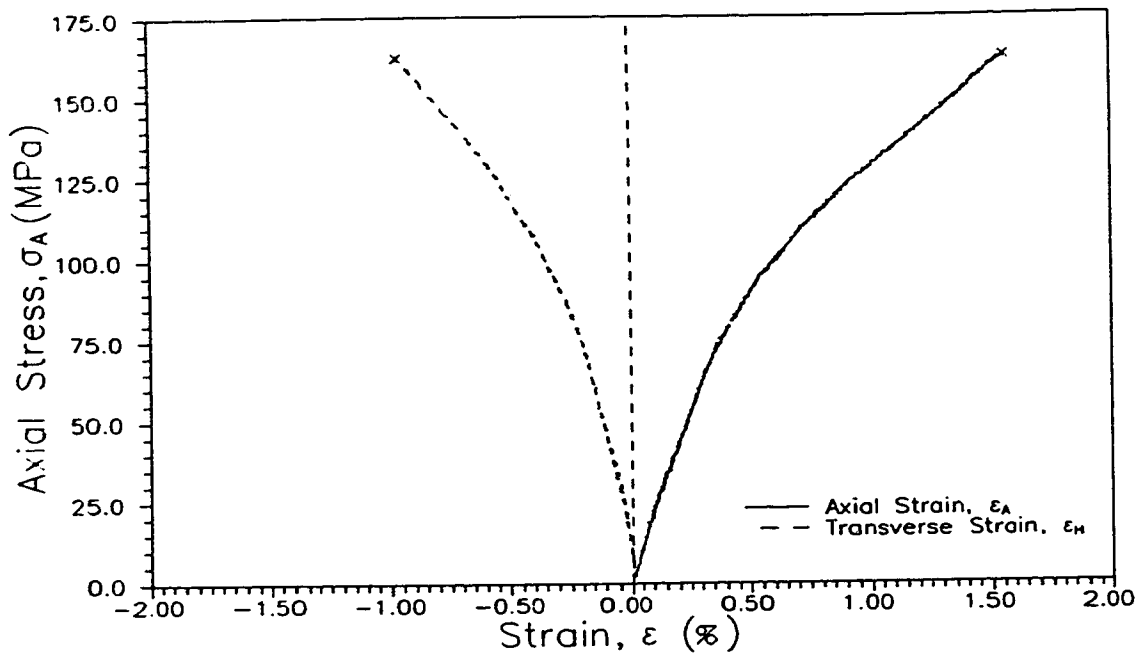
Figure 6.4 Stress-Strain Curves - Stress Ratio 0H:1A - Stress Rate 196 kPa/sec
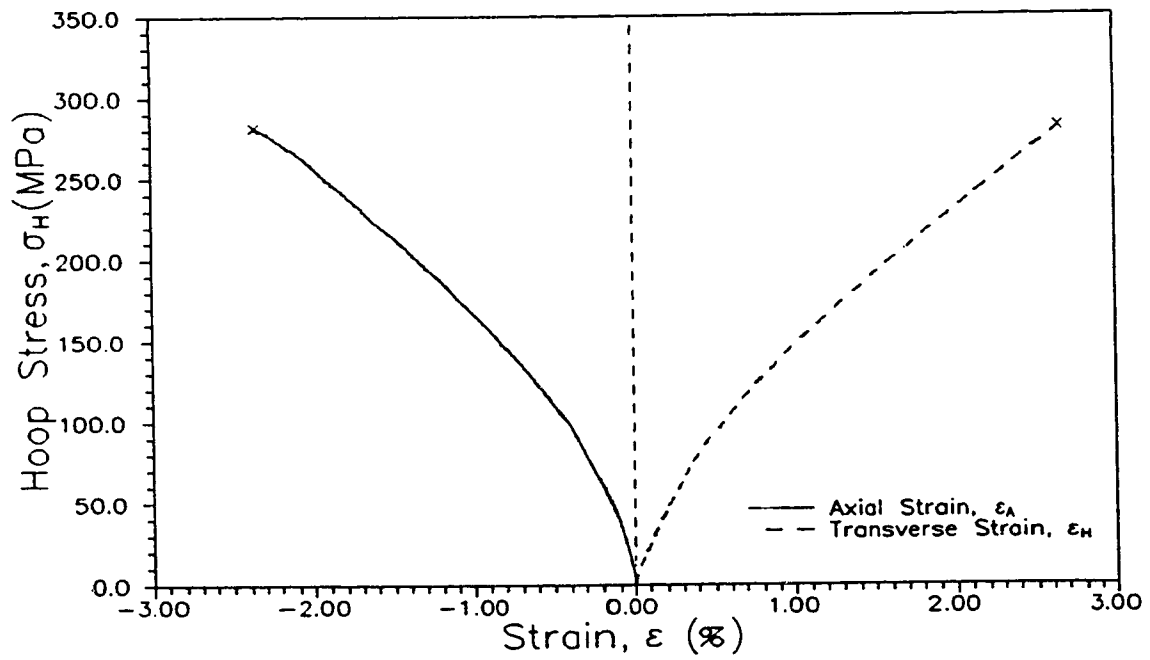
Figure 6.5 Stress-Strain Curves - Stress Ratio 1H:0A - Stress Rate 385 kPa/sec
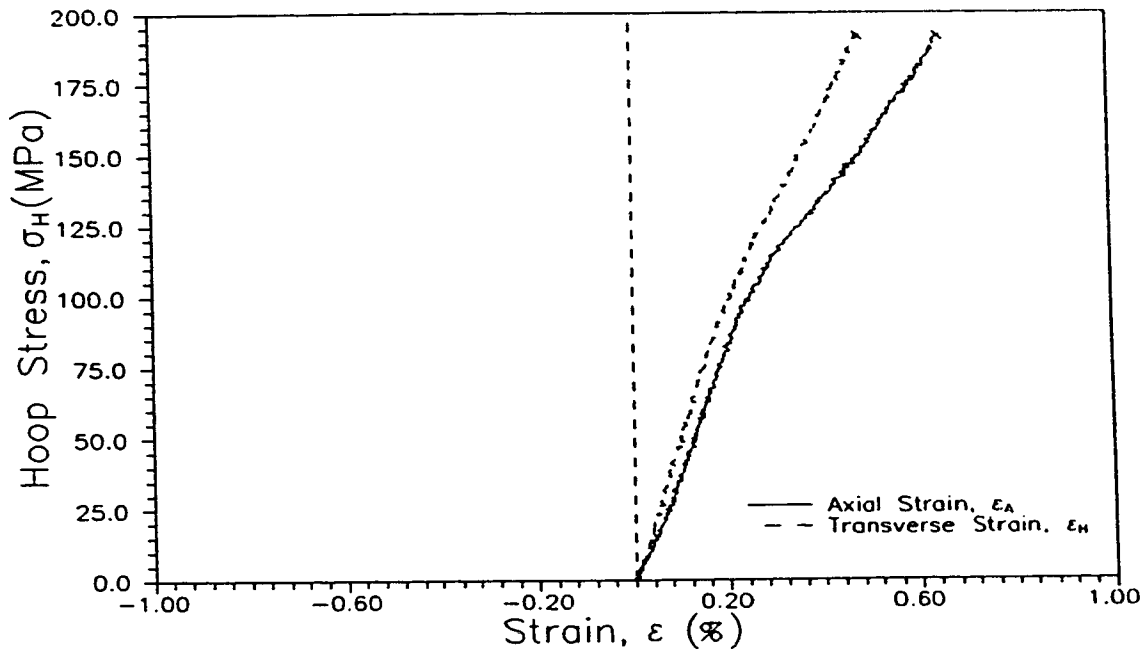
Figure 6.6 Stress-Strain Curves - Stress Ratio 1H:1A - 400 kPa/sec
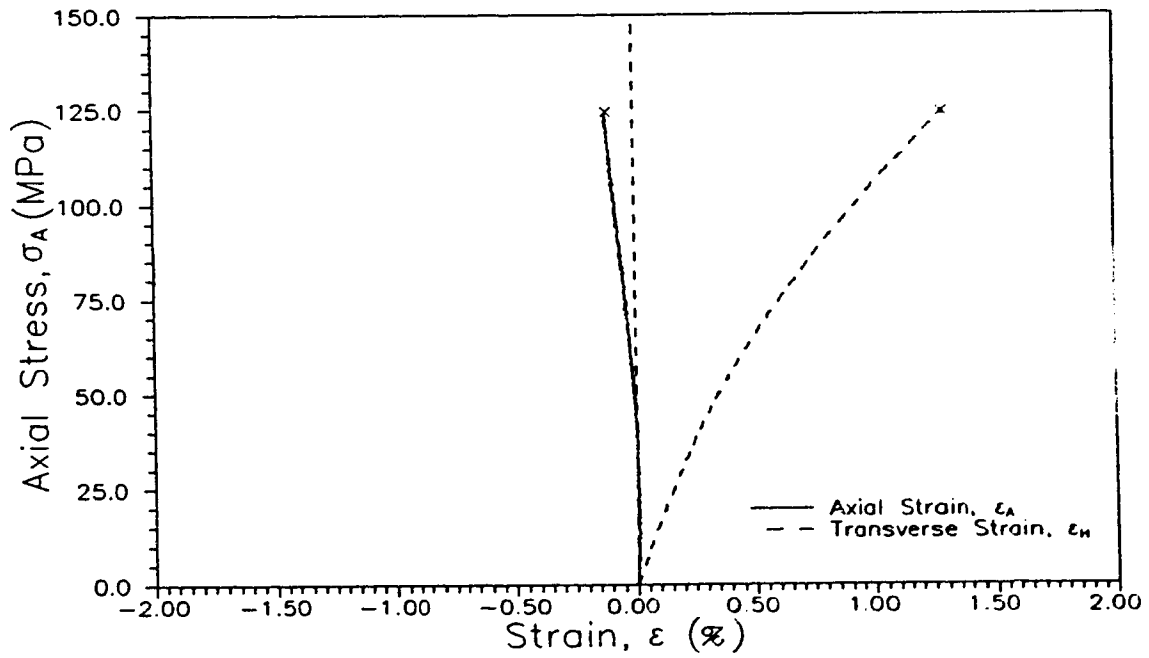
Figure 6.7 Stress-Strain Curves - Stress Ratio 2H:1A - 335 kPa/sec

140
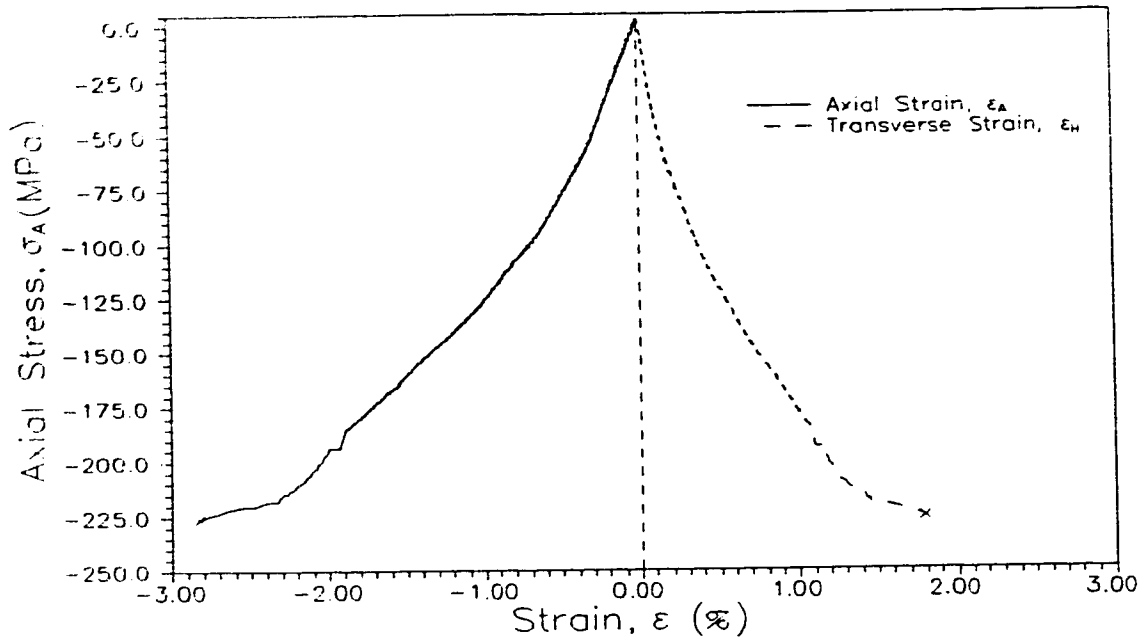
Figure 6.8 Stress-Strain Curves - Stress Ratio 0H:-1A - Stress Rate 235 kPa/sec
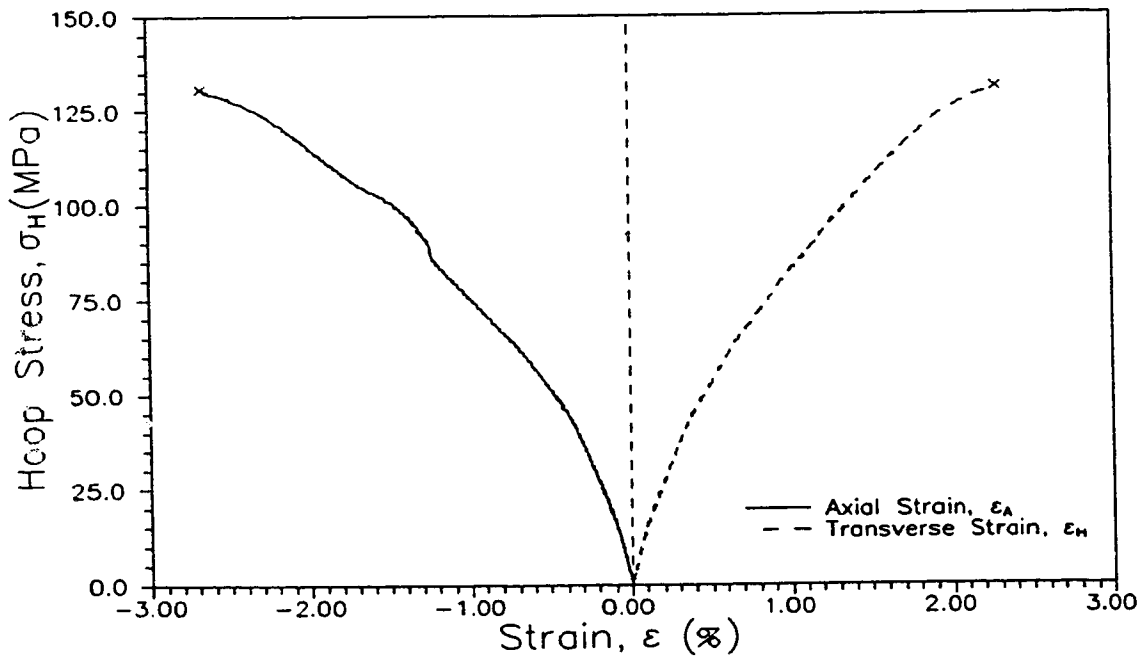
Figure 6.9 Stress-Strain Curves - Stress Ratio 1H:-1A - Stress Rate 284 kPa/sec

141
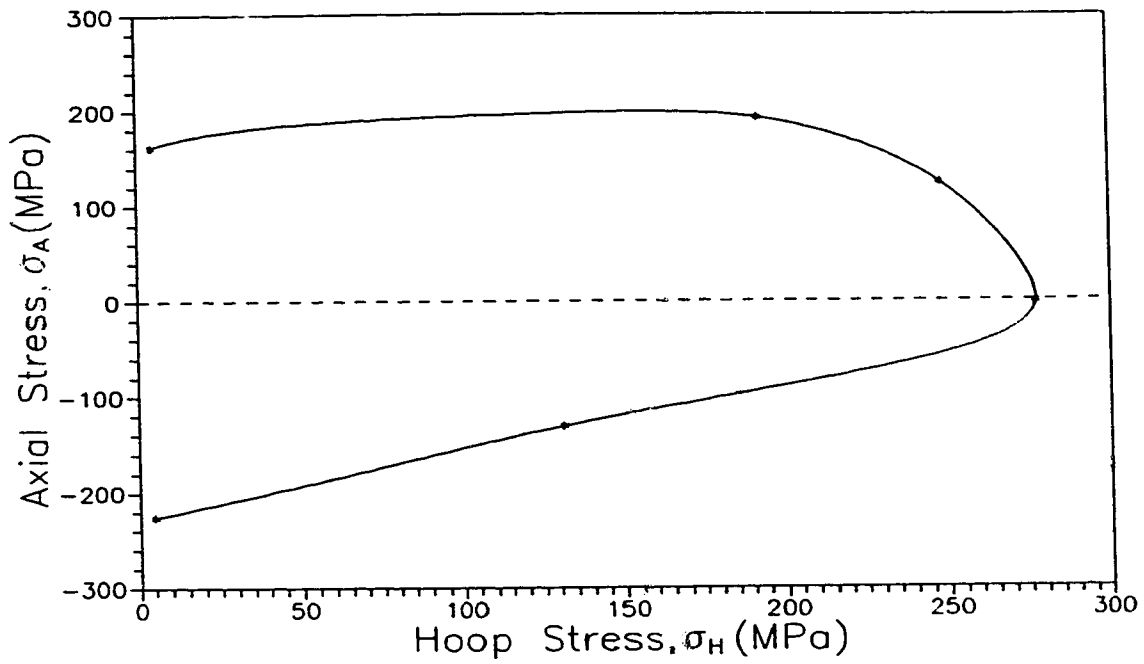
Figure 6.10 Biaxial Failure Envelope (Average Stress)
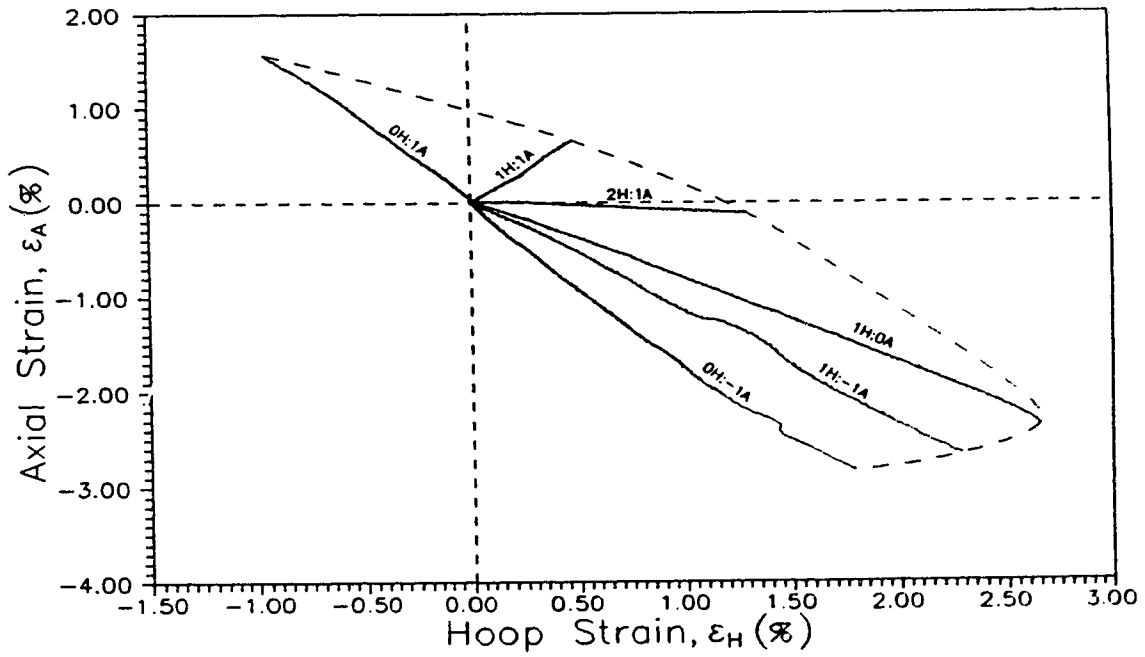
Figure 6.11 Strain Envelope - Multidirectional Tubes

142
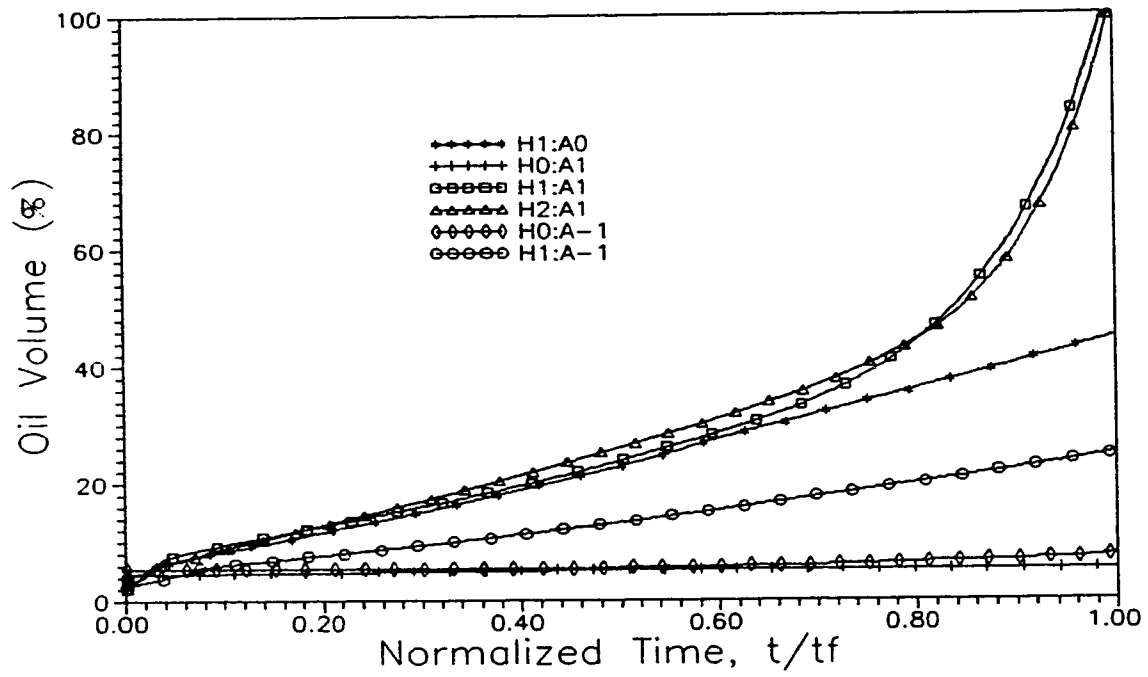
Figure 6.12 Oil Volume in Multidirectional Tubes
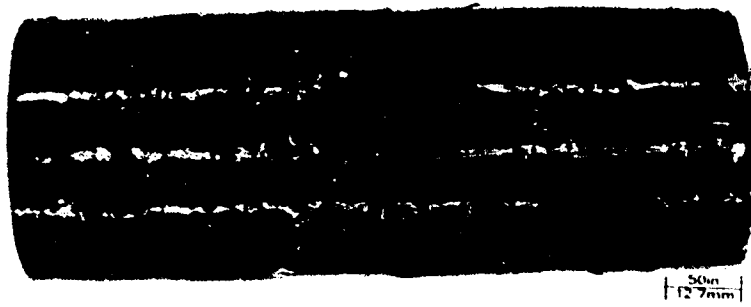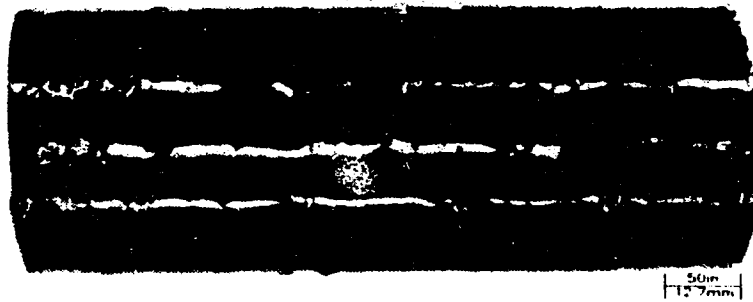
a. 0H:1A

b. 2H:1A
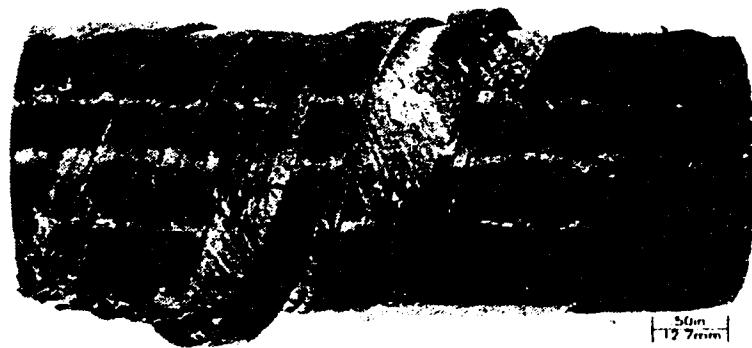
c. 1H:0A

Figure 6.13   Macro Failures - Multidirectional Tubes

144

a. 0H:-1A

b. 1H:-1A

Figure 6.14   Macro Failures - Multidirectional Tubes

145
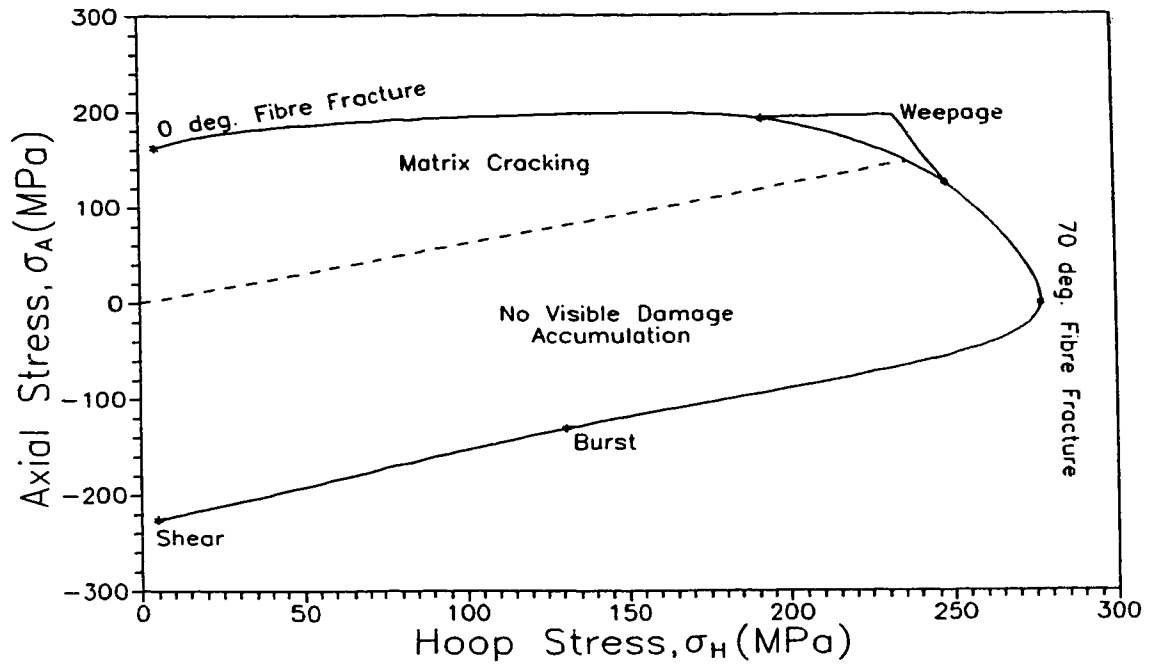
Figure 6.15 Failure and Damage with Stress Envelope - Multidirectional Tubes
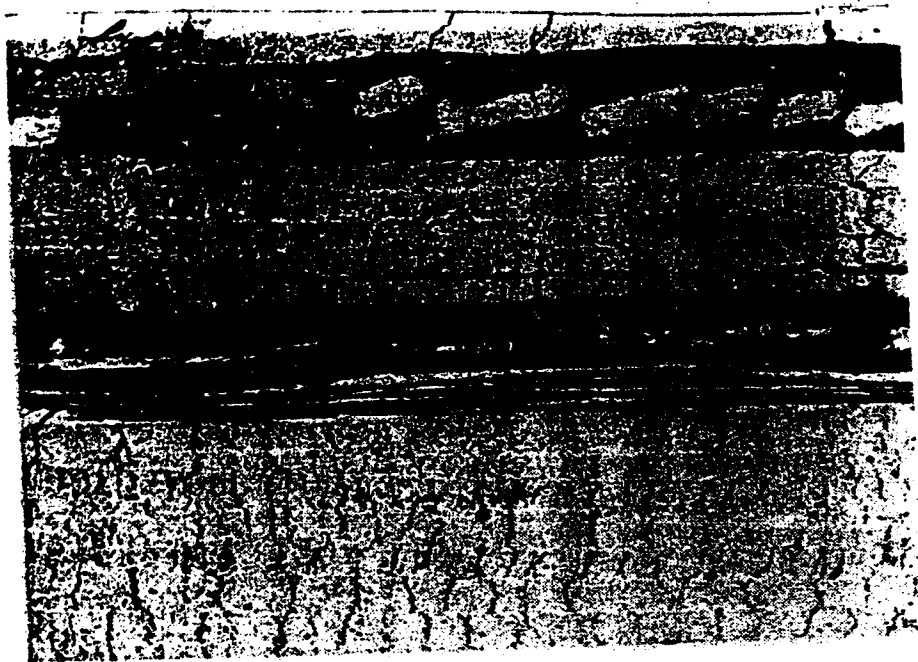
a. 0H:1A
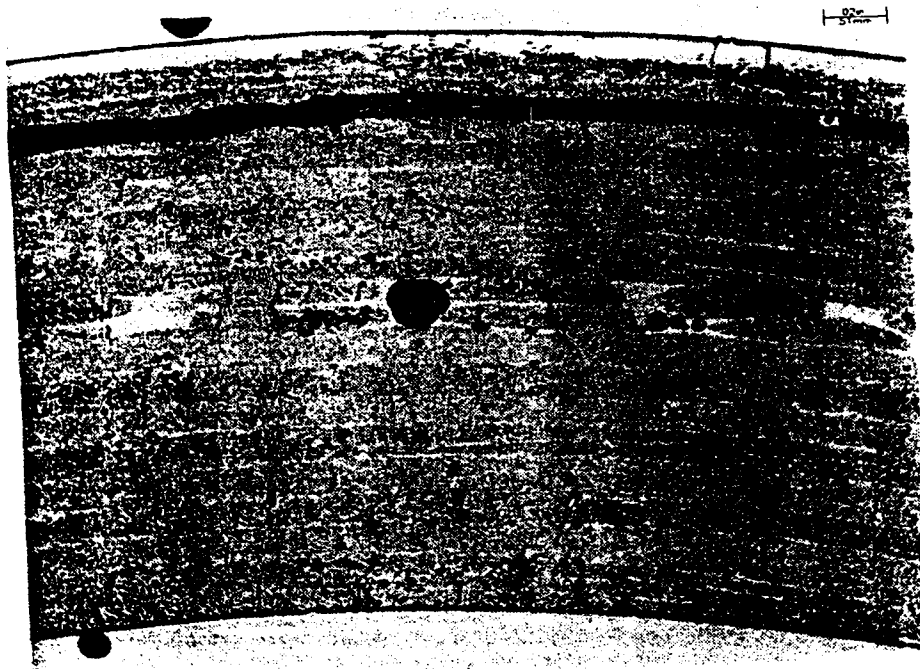
b. 1H:0A

Figure 6.16 Micrographs - Damage in Multidirectional Tubes

147

a. 2H:1A
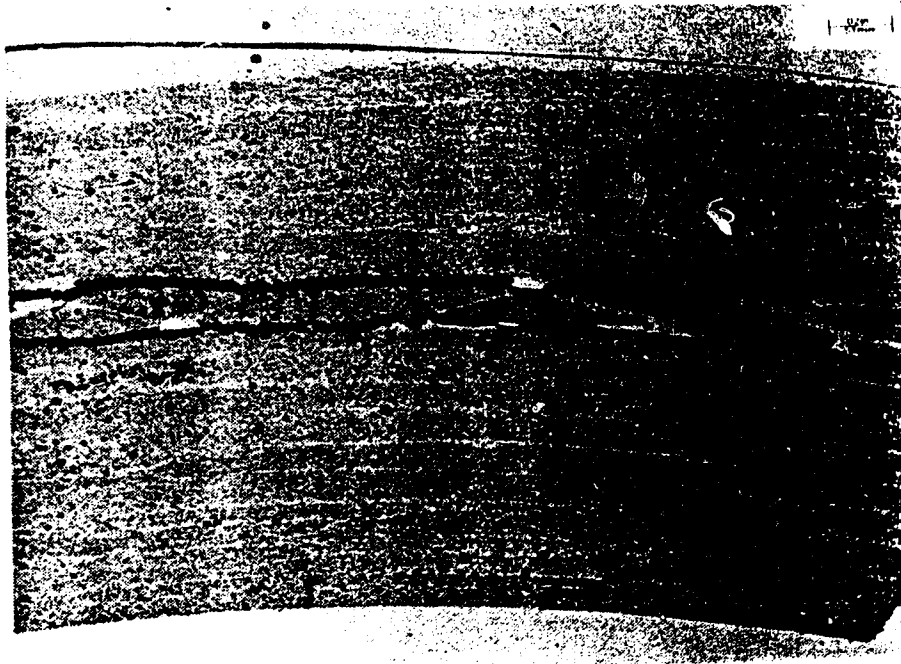
b. OH:-1A

Figure 6.17 Micrographs - Damage in Multidirectional Tubes
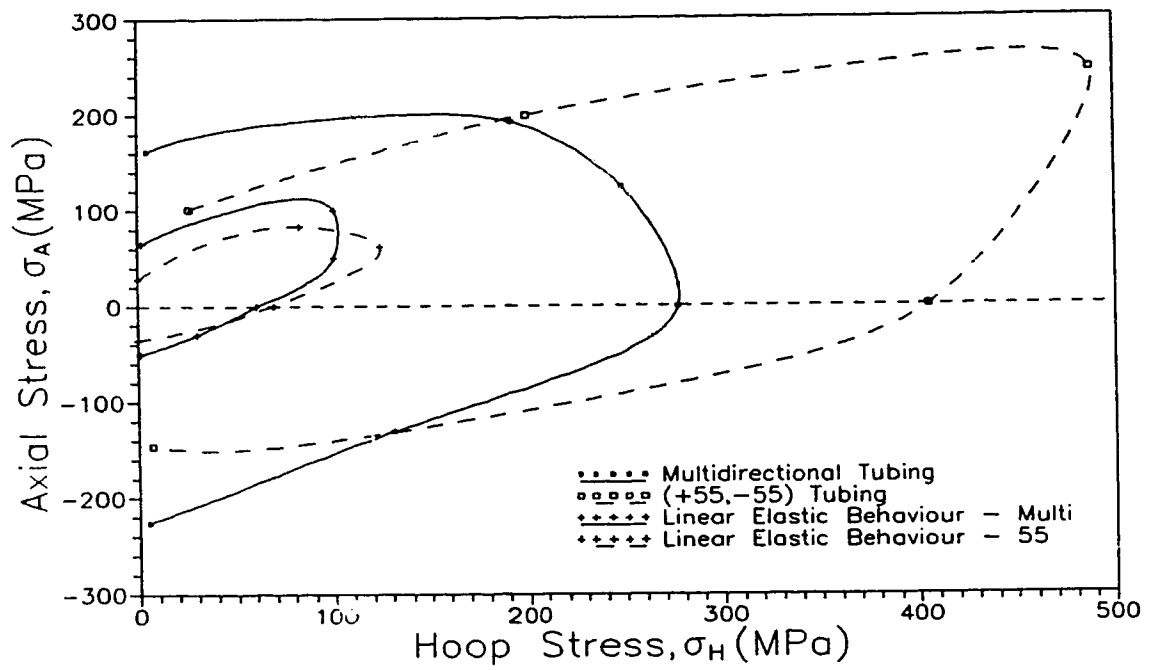
Figure 6.18 Failure Stress Envelopes - Multidirectional vs. ±55° Tubes
(Average Stress)

149

CHAPTER 7

CONCLUSIONS

7.1   Conclusions

This thesis presents an investigation of the material properties of glass fibre reinforced epoxy. The properties of interest are stiffness, strength and time dependence which are studied with respect to ply stacking sequence, fibre orientation, loading conditions, damage accumulation and failure modes.

The ply stacking sequence in fibreglass/epoxy laminates has an effect on the strength, stiffness and fatigue life. In relation to the S-N curve for fatigue life discussed in section 2.1, the monotonic strength and the slope of the S-N curve, α, change with respect to the sequence of plies in the laminate. A fatigue limit is not seen for these composite materials. No rate effect is observed in this lay-up but it has been documented in previous work for laminated composites (Ellyin et al. 1993). In addition, finite element analysis is used to investigate the interlaminar stress close to the free edge of the laminate. It is concluded that the free edge effect can cause premature delamination in monotonic loading and high stress level cyclic fatigue. The constraint effect of 0° plies is observed in low stress level cyclic fatigue.

The development of the biaxial testing apparatus was an integral part of this investigation. Chapter 4 summarizes the design and functions of the uniaxial loading frame, high pressure unit, specimen gripping system, control systems and the data

150

acquisition system. The gripping system caused few unwanted failures and was capable of transferring the highest loads to the specimen with little damage. The computerization of data acquisition was advantageous and the redundant strain measurements were useful as back ups and in determining the measurement accuracies. The load control system performed very well and all specimens were tested with the approximate desired loading ratios and rates.

The $\pm 55°$ fibreglass/epoxy tubes are tested with five stress ratios and three rates of loading. These tests revealed that the material properties of the tubular specimens are different with varying directions of loading. The failure stress envelopes summarize these differences with respect to loading rates and ratios of axial stress to hoop stress, σ_A/σ_{11}. In the case of the $\pm 55°$ tubes the strongest ratio was determined to be 2H:1A, the pressure vessel loading condition. It can be concluded that with the application of hoop stress the axial tensile strength of these tubes increases and the axial compressive strength decreases. The linear elastic behaviour is successfully described by modifying Hooke's law with respect to cylindrical anisotropy.

The failure modes and damage accumulation observed in the $\pm 55°$ tubes demonstrated the complex behaviour of filament wound tubes under biaxial loading conditions. It was determined that the failure modes and damage accumulation are dependent on stress ratio, σ_A/σ_{11}, stress rate and strain behaviour.

The rate effect was also investigated on the $\pm 55°$ tubular specimens and it can be concluded that there are time dependent properties for most stress ratios. It was determined that there is a drop in failure strength by as much as 25% with a change in

151

loading rate of about two orders of magnitude.

The multidirectional tubes, tested with six stress ratios at one stress rate, also exhibited different material properties with different stress ratios applied. There is little change in axial strength with increasing internal pressure until high hoop stresses are reached. The axial strength then drops dramatically. The same trend as the $\pm 55°$ tubes exists for the axial compression. Because of the complex lay-up in this tube, the linear elastic behaviour could not be described adequately by the modified Hooke's law.

Failure modes and damage accumulation observed in the multidirectional tubes also demonstrated the complexity of their behaviour. In addition to dependence on stress ratio, the failure modes and damage accumulation indicated that different ply orientations within the tube have different behaviours. Multiple forms of damage were observed under some loading conditions which indicates further study is needed to understand the failure process.

In general the results of the experimental, analytical and computational investigations reported here lead to the following conclusions. The strength and stiffness of glass fibre reinforced epoxy is affected by fibre orientation, stacking sequence, loading rate and loading direction.

7.2   Summary of Conclusions

I.   Lay-Up Sequence Effects in Laminates

i.   Strength and stiffness are affected by lay-up sequence, and edge effect.

ii.   Low stress level fatigue tests indicate ply constraint effects.

iii.   There is no apparent frequency effect.

iv.   Finite element analysis can be used to predict lay-up sequence effects, and interlaminar stresses.

II.   Biaxial Loading of ±55° Filament Wound Tubes

i.   Strength and stiffness are a function of stress ratio.

ii.   Linear elastic behaviour of the tubes can be described by a simplified Hooke's law.

iii.   Time dependent properties are present in the linear and nonlinear stress-strain behaviour.

iv.   Failure mode depends on stress ratio and stress rate.

v.   Damage accumulation depends on stress ratio, stress rate and strain behaviour.

153

III.   Uniaxial Loading of Multidirectional Tubes

i.   Strength and stiffness are a function of stress ratio.

ii.   Linear elastic behaviour of the multidirectional tubes can not be described

by a simplified Hooke's law.

iii.   Failure mode depends on stress ratio.

7.3   Future Work

Future work should be directed towards the evaluation of the time dependent properties of the multidirectional tubes. In addition, the stress distribution through the tube wall is to be analyzed and a criteria for defining the global behaviour needs to be developed. Both tube lay-ups should be tested under biaxial cyclic loading in order to define the S-N curve of the fatigue life. A generalized criteria for predicting the service life of these tubes has to be defined.

REFERENCES

Al-Salehi, F.A.R., Al-Hassani, S.T.S. and Hinton, M.J. (1989), "An Experimental Investigation Into the Strength of Angle Ply GRP Tubes Under High Rate of Loading", J. Composite Materials, Vol. 23, p. 288-303.

Bakis, C.E. and Stinchcomb W.W. (1986), "Response of Thick Notched Laminates Subjected to Tension-Compression Cyclic Loading", Composite Materials: Fatigue and Fracture, ASTM STP 907, H.T. Hahn, Ed., American Society for Testing and Materials, Philedelphia, p. 314-334.

Bax, J. (1970), "Deformation Behaviour and Failure of Glassfibre-Reinforced Resin Materials", Plastics and Polymers, p. 27-30.

Dew-Hignes, D. and Way, J.L. (1973), "Fatigue of Fibre-Reinforced Plastics: A Review", Composites, Vol. 4, No. 4, p. 167-173.

Daniel, I.M. and Charewicz, A. (1986), "Fatigue Damage Mechanisms and Residual Properties of Graphite/Epoxy Laminates", Engineering Fracture Mechanics, Vol. 25, p. 793-808.

Daniel, I.M., Rowlands, R.E. and Whiteside, J.B. (1974), "Effects of Material and Stacking Sequence on Behaviour of Composite Plates with Holes", Experimental Mechanics, January, p. 1-9.

Daniel, I.M. (1985), "Methods of Testing Composite Materials", Handbook of Composites: Failure Mechanics of Composites, p. 277-374.

Dillard, D.A. (1991), "Viscoelastic Behaviour of Laminated Composite Materials", Fatigue of Composite Materials, Composite Materials Series, Vol. 4, Ken L. Reifsnider, Ed., Elsevier.

Ellyin, F., Kujawski, D. and Chiu, A.S. (1993), "Cyclic Behaviour of Fibreglass/Epoxy Composite Laminates", Composites Behaviour, Proceedings of the Ninth International Conference on Composite Materials, ICCM/9, p. 700-706.

Fawaz, Z. (1992), "Étude Analytique, Numérique et Expérimentale Portant Sur La Rupture Et La Fatigue Biaxiale Des Lamelles Renforcées De Fibres", Ph.D. Thesis, Université de Sherbrooke, Sherbrooke, Quebec.

Foye, R.L. and Baker, D.J. (1970), "Design of Orthotropic Laminates", Presentation of the 11th Annual AIAA Structures, Structural Dynamics, and Materials Conference, Denver, Colorado.

155

Givens. P. (1994). Personal Communications.

Goetchius, G.M. (1987). "Fatigue of Composite Materials", Advanced Composites III: Expanding and Technology. Proc. of the 3rd Annual Conference on Advanced Composites, Detroit, Michigan, U.S.A.

Hahn, H.T. (1979). "Fatigue Behaviour and Life Prediction of Composite Laminates". Composite Materials: Testing and Design (Fifth Conference) ASTM STP 674, S.W. Tsai, Ed., American Society for Testing and Materials, p. 383-417.

Halpin, J.C. and Wu, E.M. (1971). "The Influence of Lamination Geometry on the Strength of Composites", presented at the Second ASTM Conference, Composite Materials: Testing and Design, Anaheim, California.

Higdon, A, Ohlsen, E.H., Stiles, W.B., Weese, J.A., and Riley, W.F. (1985), " Mechanics of Materials", Fourth Edition, John Wiley & Sons.

Highsmith, A.L. and Reifsnider, K.L. (1982), "Stiffness-Reduction Mechanisms in Composite Laminates", Damage in Composite Materials, ASTM STP 775, K.L. Reifsnider, Ed., American Society for Testing and Materials, p. 103-117.

Hull, D., Legg, M.J. and Spencer, B. (1978), "Failure of Glass/Polyester Filament Wound Pipe". Composites, Vol. 9, No. 1, p. 17-24.

Jones, M.L.C. and Hull, D. (1979), "Microscopy of Failure Mechanisms in Filament-Wound Pipe", J. of Materials Science, Vol. 14, p. 165-174.

Kassapoglu, C. and Lagace, P.A. (1986), "An Efficient Method for the Calculation of Interlaminar Stresses in Composite Materials", J. of Applied Mechanics, Vol. 53, p. 744-750.

Krokosky, E. (1967), "Behaviour of Time-Dependent Composite Materials", Modern Composite Materials, Ed. Lawrence J. Broutman, Addison-Wesley, p 120-145.

Labossière, P. (1987), "Failure Criterion for Composite Materials", Ph.D. Thesis, University of Alberta, Edmonton, Alberta.

Labossière, P. and Neale, K.W. (1987), "Macroscopic Failure Criteria for Fibre-Reinforced Composite Materials", Solid Mechanics Archives, Vol. 12, No. 2, p. 65-95.

Lagace, P.A. (1986), "Notch Sensitivity and Stacking Sequence of Laminated Composites", Composite Materials: Testing and Design (Seventh Conference), ASTM STP 893, J.M. Whitney, Ed., American Society for Testing and Materials, Philadelphia, p. 161-176.

Lee, J., Soden, P.D., Kitching, R. and Tse, P.C. (1989), "Strength of Filament Wound GRP Tubes with Axisymmetric Steps", Composites, Vol. 20, No. 3, p. 234-243.

Lekhnitskii, S.G. (1963), "Theory of Elasticity of an Anisotropic Elastic Body", Holden-Day Inc., SanFransisco.

Macek, R.W. and Hackett, R.M. (1992), "Viscoelastic Analysis of Filament-Wound Composite Material Systems", J. of Reinforced Plastics and Composites, Vol. 2, p. 567-581.

Mieras, H.J.M.A. (1973), "Irreversible Creep of Filament-Wound Glass-Reinforced Resin Pipes," Plastics and Polymers, Vol. 41, p. 82-89.

O'Brein, T.K. (1985), "Analysis of Local Delaminations and Their Influence on Composite Laminate Behaviour", Delamination and Debonding of Materials, ASTM STP 876, W.S. Johnson, Ed., American Society for Testing and Materials, Philedelphia, p. 282-297.

Pagano, N.J. and Pipes. R.B. (1971), "The Influence of Stacking Sequence on Laminate Strength", J. Composite Materials, Vol. 5, p. 50-57.

Peters, P.W.M. (1986). "Constrained 90-deg Ply Cracking in 0/90/0 and ±45/90/±45 CFRP Laminates", Composite Materials: Fatigue and Fracture, ASTM STP 907, H.T. Hayhn, Ed., American Society for Testing and Materials, p. 84-99.

Pipes, R.B. and Pagano, N.J. (1970), "Interlaminar Stresses in Composite Laminates Under Uniform Axial Extension", J. Composite Materials, Vol. 4, p. 538-548.

Puck A. and Schneider W. (1969), "On Failure Mechanisms and Failure Criteria of Filament-Wound Glass-Fibre/Resin Composites", Plastics and Polymers, p. 33-44.

Ramani, S.V. and Williams, D.P. (1977), "Notched and Unnotched Fatigue Behaviour of Angle-Ply Graphite/Epoxy Composites", Fatigue of Filamentary Composite Materials, ASTM STO 636, K.L. Reifsnider and K.N. Lauraitus, Eds., American Society for Testing and Materials, p. 27-46.

Ratwani, M.M. and Kan, H.P. (1982), "Effect of Stacking Sequence on Damage Propagation and Failure Modes in Composite Laminates", Damage in Composite Materials, ASTM STP 775, K.L. Reifsnider, Ed., American Society for Testing And Materials, p. 211-228.

Rosenow, M.W.K., (1984) "Wind Angle Effects in Glass Fibre-Reinforced Polyester Filament Wound Pipes", Composites, Vol. 15, No. 2.

157

Schapery, R.A. (1974). "Viscoelastic Behaviour and Analysis of Composite Materials", Composite Materials, Vol 2, Mechanics of Composite Materials, Ed. G.P. Sendeckye, Academic Press, p. 85-165.

Skudra, A.M. (1985), "Micromechanics of Failure of Reinforced Plastics", Failure Mechanics of Composites, Handbook of Composites, Vol. 3, G.C. Sih and A.M. Skudra Ed., p. 1-70.

Spain, R.G. (1967), "Graphite Fibre-Reinforced Composites", AFML-TR-66-384, Air Force Materials Laboratory, Wright-Patterson AFB, Ohio.

Soden, P.D., Highton, J. and Adeoye, A.B. (1985), "Fracture Stresses for ±75° Filament Wound GRP Tubes Under Biaxial Loads", J. Strain Analysis, Vol. 20, No.3, p. 139-49.

Soden, P.D., Kitching, R., Tse, P.C., Tsavalas, Y. and Hinton, M.J. (1993), "Influence of Winding Angle on the Strength and Deformation of Filament-Wound Composite Tubes Subjected to Uniaxial and Biaxial Loads", Composites Science and Technology, Vol. 46, p. 363-378.

Soden, P.D., Kitching, R. & Tse, P.C. (1989), "Experimental Failure Stresses for ±55° Filament Wound Glass Fibre Reinforced Plastic Tubes Under Biaxial Loads", Composites, Vol. 20, No. 2, p. 125-135.

Soden, P.D., Leadbetter, D., Griggs, P.R., and Eckold, G. C. (1978), "The Strength of a Filament Wound Composite Under Biaxial Loading", Composites, Vol. 9, p. 263-271.

Soni, S.R. and Pagano, N.J. (1982), "Elastic Response of Composite Laminates", Mechanics of Composite Materials: Recent Advances, Pergamon Press, p. 227-242.

Spencer, B. and Hull, D. (1978), "Effect of Winding Angle on the Failure of Filament Wound Pipe", Composites, Vol. 9, p. 263-271.

Stinchcomb, W.W. and Reifsnider, K.L. (1979), "Fatigue Damage Mechanisms in Composite Materials: A Review", Fatigue Mechanisms, Proc. of an ASTM-NBS-DSF Symposium, Kansas City, Mo, May 1978, J.J. Fong Ed., ASTM STP 675, American Society for Testing and Materials, p. 762-787.

Stinchcomb, W.W., Reifsnider, K.L., Yeung, P. and Masters, J. (1981), "Effect of Ply Constraint on Fatigue Damage Development in Composite Material Laminates", Fatigue of Fibrous Composite Materials, ASTM STP 723, p. 64-84.

Sun, C.T. and Zhou, S.G. (1988), "Failure of Quasi-Isotropic Composite Laminates with Free Edges", J. Reinforced Plastics and Composites, Vol. 7, p. 515-557.

Suvorova, J.V. (1985), "The influence of Time and Temperature on the Reinforced Plastic Strength", Failure Mechanics of Composite, Handbook of Composite Materials, Vol. 3, G.C. Sih and A.M. Skudra , Ed., p. 177-214.

Tsia, S.W. and Wu, E.M. (1971), "A General Theory of Strength for Anisotropic Materials", J. Composite Materials, Vol. 5, p. 58-80.

Tsai, S.W. and Roy, A.K. (1987), "Pressure Vessels", Composite Materials: Fourth Edition, Think Composites.

Tsai, S.W. (1987), "Failure Criteria", Composite Materials: Fourth Edition, Think Composites.

Wang, A.S. and Crossman, F.W. (1977), "Some New Results on Edge Effect in Symmetric Composite Laminates", J. Composite Materials, Vol. 11, p. 92-106.

Wang, S.S. and Choi, I. (1982), "Boundary-Layer Effect in Composite Laminates Part I Free Edge Stress Singularities", J. Applied Mechanics, Vol. 49, p. 541-548.

Wang, S.S. and Choi, I. (1982), "Boundary-Layer Effect in Composite Laminates Part II Free Edge Stress Singularities", J. Applied Mechanics, Vol. 49, p. 549-557.

Whitney, J.M. and Browning, C.E. (1972), "Free-Edge Delamination of Tensile Coupons", J. Composite Materials, Vol. 6, p. 300-303.

APPENDIX A

	[$0_2,45_2,-45_2$]$_s$			[$45_2,-45_2,0_2$]$_s$		
#	Stress MPa.	Nf	Speed	Stress MPa.	Nf	Speed
1	201	325034	F	201	284973	F
2	201	294551	F	201	136352	F
3	235	53597	F	235	31004	F
4	235	64903	F	235	16890	F
5	268	19685	F	268	4209	F
6	268	12627	F	268	2883	F
7	268	10120	F	302	1786	F
8	285	262	F	302	752	F
9	285	948	F	201	105194	S
10	302	402	F	268	2897	S
11	302	487	F	268	2795	S
12	201	247259	S	302	551	S
13	235	35737	S	302	231	S
14	268	2983	S			
15	268	961	S			
16	268	1522	S			
17	285	544	S			

APPENDIX B

$\pm 55°$ Tubes

	Stress Ratio	Stress Rate	σ_A(MPa)	σ_{11}(MPa)	Failure Mode
		kPa/s			
1	0H:1A	270	101	26	Complete Matrix Failure
2	1H:1A	553	199	199	Complete Matrix Failure
3	2H:1A	482	244	488	Burst
4	1H:0A	465	0	405	Burst
5	0H:-1A	194	-146	6.9	Shear
6	0H:1A	23	83	14	Complete Matrix Failure
7	1H:1A	46	199	201	Weepage
8	2H:1A	47	244	483	Burst
9	1H:0A	53	0	362	Burst
10	0H:-1A	15	-131	14	Shear
11	0H:1A	1.4	76	6.9	Weepage
12	1H:1A	2.6	165	168	Weepage
13	2H:1A	4.7	244	488	Burst
14	1H:0A	4.7	0	350	Burst
15	0H:-1A	1.6	124	6.9	Shear

161

Axial Stress	Hoop Stress	Axial Strain	Hoop Strain
	OH:1A		
	270 kPa/sec		
0.1	0.3	-0.005	-0.007
2.0	1.7	0.020	-0.010
5.9	2.8	0.042	-0.012
8.6	3.8	0.063	-0.017
12.4	4.5	0.090	-0.027
16.3	5.5	0.110	-0.032
18.9	6.2	0.137	-0.037
21.6	7.1	0.164	-0.037
25.5	8.3	0.186	-0.046
28.4	9.5	0.208	-0.056
32.0	9.9	0.237	-0.063
35.0	11.3	0.264	-0.071
38.8	12.3	0.293	-0.078
41.4	13.0	0.320	-0.090
45.3	14.0	0.352	-0.095
48.1	15.0	0.383	-0.110
52.0	16.1	0.417	-0.122
55.7	16.8	0.452	-0.137
58.5	17.8	0.491	-0.154
61.4	19.2	0.535	-0.166
65.3	20.2	0.576	-0.186
69.0	20.9	0.625	-0.205
71.8	21.8	0.676	-0.229
74.4	22.5	0.740	-0.251
78.2	23.5	0.811	-0.283
82.2	24.6	0.894	-0.325
84.9	25.6	0.991	-0.369
87.9	27.0	1.116	-0.420
91.6	27.7	1.282	-0.500
94.3	28.7	1.514	-0.598
97.9	29.1	1.973	-0.774
99.3	29.7	2.250	-0.900
	OH:1A		
	23 kPa/sec		
7.0	14.0	0.005	0.002
9.3	14.0	0.022	-0.012
11.7	14.4	0.042	-0.017
14.0	14.4	0.059	-0.022
17.1	14.0	0.076	-0.032

19.4	14.0	0.095	-0.044
21.9	14.4	0.117	-0.051
25.0	14.0	0.137	-0.059
27.3	14.0	0.159	-0.073
29.5	14.0	0.178	-0.081
31.8	14.0	0.203	-0.090
35.2	14.0	0.232	-0.105
37.8	14.7	0.256	-0.115
41.1	14.7	0.286	-0.129
43.4	14.7	0.313	-0.139
45.7	14.7	0.344	-0.159
47.9	14.7	0.374	-0.168
51.3	14.7	0.413	-0.144
53.5	14.7	0.449	-0.156
55.8	14.7	0.488	-0.173
59.2	14.7	0.527	-0.193
61.4	14.7	0.574	-0.215
64.8	14.7	0.627	-0.234
65.9	14.7	0.686	-0.264
69.3	14.7	0.754	-0.300
71.6	14.7	0.842	-0.332
75.0	14.7	0.945	-0.378
77.2	14.7	1.077	-0.437
79.1	14.0	1.262	-0.518
82.8	14.7	1.543	-0.627
81.7	14.7	2.034	-0.793
82.8	14.7	2.302	-0.945

OH:1A
1.4 kPa/sec

3.6	7.1	0.007	0.017
5.8	7.1	0.027	0.012
6.9	7.1	0.042	0.007
9.8	6.2	0.063	-0.002
12.8	7.6	0.078	-0.012
15.0	7.6	0.103	-0.017
17.3	7.6	0.122	-0.024
19.3	7.1	0.142	-0.034
21.2	6.4	0.166	-0.042
25.2	7.6	0.186	-0.049
26.9	6.4	0.215	-0.061
29.5	7.1	0.237	-0.071
31.9	7.6	0.264	-0.078
34.0	7.1	0.295	-0.090

36.5	7.6	0.322	-0.100
39.6	7.1	0.352	-0.112
40.4	6.4	0.386	-0.129
42.7	6.4	0.422	-0.139
46.4	7.1	0.457	-0.159
48.3	6.4	0.496	-0.171
50.9	7.1	0.540	-0.190
52.8	6.4	0.588	-0.210
55.0	6.4	0.640	-0.229
57.7	7.1	0.701	-0.254
61.0	7.1	0.769	-0.283
63.3	7.1	0.862	-0.315
65.7	7.6	0.962	-0.354
67.8	7.1	1.089	-0.398
70.0	7.1	1.260	-0.457
73.4	7.1	1.484	-0.540
75.7	7.1	1.863	-0.671
75.9	7.6	2.263	-0.740

1H:1A
553 kPa/sec

0.1	0.3	0.007	0.002
6.2	7.8	0.037	0.012
12.6	14.0	0.071	0.022
19.4	20.9	0.098	0.032
26.0	27.3	0.125	0.037
33.1	34.6	0.154	0.051
39.7	41.0	0.183	0.061
47.6	47.9	0.217	0.066
53.1	54.3	0.251	0.076
59.9	61.2	0.286	0.081
66.7	68.0	0.320	0.090
73.1	74.2	0.359	0.100
80.0	81.0	0.398	0.105
86.7	87.8	0.442	0.115
93.5	94.6	0.491	0.115
100.3	101.5	0.542	0.120
106.8	107.6	0.593	0.122
113.6	114.5	0.657	0.127
120.2	120.9	0.723	0.120
127.2	128.2	0.793	0.120
133.9	134.9	0.872	0.120
140.1	140.4	0.957	0.110
147.2	148.0	1.055	0.098

154.0	154.8	1.172	0.066
160.6	161.2	1.309	0.032
167.4	168.1	1.487	-0.020
178.4	178.7	1.880	-0.170
184.8	184.9	2.230	-0.360
192.0	192.5	2.980	-0.820
198.3	198.2	3.910	-1.465

1H:1A
46 kPa/sec

0.8	1.7	0.007	0.002
6.5	8.5	0.039	0.012
12.8	14.4	0.071	0.027
19.4	20.9	0.100	0.042
26.3	27.7	0.129	0.051
34.2	34.6	0.159	0.061
39.7	41.0	0.188	0.071
46.3	47.5	0.217	0.085
52.7	53.6	0.247	0.095
59.5	60.5	0.281	0.105
66.0	66.6	0.315	0.115
72.9	73.8	0.349	0.120
79.0	79.2	0.388	0.127
86.1	86.5	0.430	0.134
92.7	92.9	0.471	0.139
98.1	99.4	0.520	0.144
104.6	105.5	0.574	0.144
111.4	112.4	0.632	0.144
118.2	119.3	0.696	0.137
124.7	125.4	0.769	0.125
131.5	132.3	0.847	0.110
137.9	138.4	0.930	0.095
143.6	145.3	1.028	0.061
150.1	151.5	1.135	0.022
156.8	158.2	1.262	-0.032
163.3	164.3	1.418	-0.105
169.0	171.2	1.614	-0.217
175.8	178.0	1.873	-0.371
182.2	184.2	2.246	-0.596
191.2	193.0	2.970	-1.130
194.7	197.9	3.550	-1.680
199.0	202.0	4.370	-2.234

1H:1A
2.6 kPa/sec

0.8	1.7	0.002	0.002
5.8	7.1	0.039	0.012
11.0	13.0	0.061	0.022
17.1	18.5	0.085	0.032
23.4	24.2	0.110	0.042
28.6	30.1	0.134	0.054
34.5	35.1	0.161	0.061
40.8	41.0	0.188	0.071
44.6	46.5	0.217	0.076
50.4	51.2	0.242	0.085
55.7	57.4	0.276	0.090
62.1	63.3	0.313	0.100
67.0	68.7	0.352	0.100
73.1	74.2	0.388	0.110
78.3	79.9	0.432	0.115
84.2	85.1	0.481	0.115
90.3	90.6	0.535	0.110
95.7	96.7	0.593	0.115
100.7	102.2	0.662	0.110
105.6	107.6	0.735	0.105
112.0	113.5	0.818	0.098
117.0	119.0	0.911	0.081
123.1	124.4	1.023	0.061
128.2	130.2	1.152	0.029
133.2	135.6	1.311	-0.005
139.3	141.1	1.511	-0.056
144.5	147.0	1.760	-0.120
149.2	152.0	2.087	-0.222
155.6	157.9	2.542	-0.364
160.4	163.1	3.186	-0.574
165.7	169.1	3.740	-0.864

2H:1A
482 kPa/sec

0.8	1.7	0.015	-0.007
8.7	17.5	0.024	0.039
17.1	34.2	0.034	0.093
24.9	49.8	0.042	0.146
33.0	65.9	0.042	0.200
41.0	82.0	0.042	0.261
49.1	98.1	0.037	0.322
57.2	114.5	0.034	0.381

65.3	130.6	0.024	0.452
73.3	146.6	0.017	0.520
81.2	162.4	0.002	0.596
89.5	179.0	-0.012	0.669
97.6	195.1	-0.032	0.752
105.6	211.2	-0.051	0.833
113.7	227.3	-0.076	0.918
121.8	243.7	-0.103	1.003
129.7	259.4	-0.132	1.096
137.9	275.7	-0.164	1.187
145.8	291.6	-0.195	1.287
154.0	307.9	-0.229	1.377
161.9	323.9	-0.266	1.472
170.0	340.0	-0.300	1.570
178.0	356.1	-0.337	1.667
186.2	372.5	-0.376	1.770
194.3	388.6	-0.415	1.868
202.1	404.2	-0.452	1.975
210.3	420.6	-0.491	2.078
218.4	436.7	-0.530	2.183
226.4	452.8	-0.569	2.290
235.6	468.9	-0.608	2.395
243.4	484.9	-0.649	2.498
243.8	487.7	-0.654	2.520

2H:1A
47 kPa/sec

0.5	1.0	0.002	0.005
9.0	18.1	0.012	0.056
17.4	34.9	0.022	0.110
25.6	51.2	0.027	0.164
33.8	67.6	0.032	0.222
42.3	84.7	0.032	0.288
50.7	101.5	0.027	0.352
58.9	117.9	0.027	0.417
67.1	134.2	0.017	0.491
75.5	151.0	0.007	0.566
83.9	167.8	-0.005	0.647
92.2	184.5	-0.020	0.725
100.6	201.3	-0.037	0.808
108.7	217.4	-0.056	0.896
117.2	234.5	-0.081	0.984
125.4	250.8	-0.105	1.074
133.8	267.6	-0.129	1.169

142.1	284.3	-0.159	1.262
150.3	300.7	-0.183	1.360
158.7	317.5	-0.212	1.458
167.1	334.3	-0.242	1.555
175.5	350.9	-0.271	1.650
183.7	367.4	-0.305	1.753
192.3	384.5	-0.334	1.848
200.4	400.9	-0.364	1.946
208.8	417.5	-0.393	2.048
217.2	434.3	-0.422	2.146
225.6	451.1	-0.452	2.246
233.8	467.5	-0.486	2.341
242.1	484.2	-0.522	2.437
243.8	487.7	-0.557	2.473

2H:1A
4.7 kPa/sec

0.5	1.0	0.000	0.007
7.3	14.7	0.012	0.051
14.0	28.0	0.022	0.098
20.6	41.3	0.027	0.142
27.2	54.3	0.032	0.188
34.2	68.3	0.029	0.237
40.5	81.0	0.027	0.286
47.0	93.9	0.022	0.339
53.8	107.6	0.015	0.398
60.7	121.4	0.005	0.457
67.3	134.7	-0.002	0.520
74.0	148.0	-0.022	0.583
80.6	161.2	-0.039	0.652
87.3	174.7	-0.059	0.715
93.8	187.6	-0.078	0.789
99.9	199.9	-0.110	0.862
107.1	214.3	-0.129	0.938
113.8	227.6	-0.159	1.013
120.1	240.2	-0.190	1.091
127.3	254.6	-0.217	1.169
134.0	267.9	-0.247	1.243
140.6	281.2	-0.266	1.316
147.3	294.5	-0.293	1.389
153.8	307.5	-0.315	1.467
160.8	321.5	-0.352	1.545
167.3	334.5	-0.378	1.626
173.6	347.1	-0.408	1.707

168

180.3	360.6	-0.439	1.785
187.4	374.8	-0.469	1.868
193.9	387.9	-0.505	1.951
200.4	400.9	-0.535	2.034
241.5	483.0	-0.740	2.580

1H:0A
465 kPa/sec

0.5	1.0	0.002	0.005
0.2	11.6	-0.022	0.054
0.6	21.6	-0.051	0.105
0.1	31.8	-0.090	0.164
-0.4	42.0	-0.137	0.227
0.3	52.3	-0.188	0.293
0.9	62.6	-0.247	0.366
-1.2	72.1	-0.315	0.449
-0.2	83.0	-0.391	0.535
0.1	92.7	-0.481	0.637
1.1	103.6	-0.583	0.750
-0.9	113.1	-0.708	0.879
-0.3	123.3	-0.847	1.018
-0.8	133.7	-1.003	1.167
-0.2	143.9	-1.172	1.328
0.4	154.1	-1.370	1.506
-0.4	163.6	-1.580	1.694
-0.5	174.7	-1.809	1.892
-0.3	184.2	-2.053	2.102
-0.8	194.4	-2.312	2.317
-0.0	205.1	-2.588	2.537
-0.7	215.0	-2.874	2.766
-0.1	225.2	-3.174	2.998
-0.6	235.4	-3.489	3.240
0.0	245.7	-3.816	3.484
-0.8	255.3	-4.153	3.743
-0.0	265.8	-4.502	3.994
-0.5	276.2	-4.858	4.270
0.2	286.7	extrapolated	4.553
-0.6	296.3		4.851
-0.4	301.1		4.998
	405		extrapolated

1H:0A
53 kPa/sec

0.5	1.0	0.007	0.002

0.0	11.3	-0.027	0.046
0.4	21.1	-0.061	0.095
-0.2	31.1	-0.110	0.149
0.7	42.0	-0.159	0.210
-0.1	51.6	-0.215	0.273
0.5	61.9	-0.281	0.349
-0.0	72.1	-0.359	0.432
0.6	82.3	-0.449	0.525
-0.2	92.0	-0.554	0.632
0.4	102.2	-0.679	0.750
0.1	112.8	-0.823	0.886
0.7	123.0	-0.989	1.038
0.0	133.0	-1.174	1.204
-0.5	143.2	-1.387	1.382
-0.1	153.1	-1.619	1.567
0.4	163.1	-1.868	1.768
-0.1	173.3	-2.141	1.985
-0.6	183.5	-2.439	2.207
0.2	194.1	-2.751	2.439
-0.8	203.4	-3.079	2.673
0.1	214.3	-3.420	2.913
-0.8	223.8	-3.772	3.157
-0.2	234.0	-4.138	3.401
0.5	244.4	-4.514	3.650
-0.0	254.6	-4.910	3.899
-0.3	265.2	-5.410	4.153
0.1	272.4	-5.740	4.340
-0.8	278.8	-6.010	4.510
0.1	293.5	-6.630	4.890
-0.8	306.8	-7.370	extrapolated
-0.2	314.4	-7.730	
0.5	328.1	-8.440	
-0.0	341.4	-9.100	
-0.3	355.0	-9.750	
0.1	362.2	-10.260	

1H:0A
4.7 kPa/sec

0.3	0.7	0.000	-0.002
1.3	11.6	-0.042	0.046
0.6	21.6	-0.090	0.100
1.2	31.8	-0.139	0.154
0.4	41.3	-0.208	0.217
0.3	52.3	-0.281	0.286

0.7	62.1	-0.369	0.364
-0.0	72.1	-0.471	0.452
-0.5	82.3	-0.603	0.559
0.3	92.9	-0.752	0.679
0.7	102.9	-0.916	0.813
0.4	113.5	-1.111	0.962
0.8	123.3	-1.328	1.123
0.5	134.0	-1.575	1.301
-0.0	144.2	-1.838	1.487
0.4	154.1	-2.131	1.687
-0.1	164.3	-2.441	1.895
0.4	174.3	-2.781	2.109
0.1	184.9	-3.142	2.332
-0.3	195.4	-3.518	2.561
0.1	205.3	-3.923	2.795
-0.2	216.0	-4.348	3.040
0.4	225.9	-4.797	3.284
-0.1	241.6	-5.400	3.630
0.4	262.2	-6.240	4.050
0.1	283.3	-7.170	4.510
-0.3	296.6	-7.890	4.830
0.1	311.0	-8.680	extrapolated
-0.2	324.3	-9.490	
0.4	338.0	-10.360	
0.1	350.2	-11.060	

OH:-1A
194 kPa/sec

3.6	7.1	0.007	0.022
-2.1	7.1	-0.027	0.034
-6.6	7.1	-0.066	0.046
-11.1	7.1	-0.110	0.063
-16.7	7.1	-0.154	0.085
-21.2	7.1	-0.200	0.100
-26.9	7.1	-0.251	0.125
-31.4	7.1	-0.305	0.144
-37.0	7.1	-0.359	0.171
-41.5	7.1	-0.417	0.200
-46.0	7.1	-0.481	0.229
-51.6	7.1	-0.544	0.259
-57.3	7.1	-0.618	0.298
-61.8	7.1	-0.696	0.337
-67.4	7.1	-0.779	0.383
-71.9	7.1	-0.876	0.435

171

-76.4	7.1	-0.979	0.491
-82.1	7.1	-1.101	0.554
-86.6	7.1	-1.233	0.630
-92.2	7.1	-1.389	0.710
-96.7	7.1	-1.565	0.808
-102.3	7.1	-1.765	0.916
-106.8	7.1	-2.000	1.042
-111.4	7.1	-2.275	1.194
-117.0	7.1	-2.610	1.370
-121.5	7.1	-3.020	1.582
-127.1	7.1	-3.535	1.838
-131.6	7.1	-4.211	2.170
-136.1	7.1	-5.000	3.370
-140.6	7.1	-6.000	2.990
-142.9	7.1	-7.000	2.560
-146.3	7.1	-7.800	3.757

OH:-1A
15 kPa/sec

7.0	14.0	0.007	0.044
2.7	14.4	-0.032	0.059
-1.8	14.4	-0.066	0.076
-6.3	14.4	-0.105	0.093
-11.8	14.7	-0.149	0.110
-16.7	14.0	-0.193	0.137
-21.0	14.4	-0.247	0.156
-25.7	14.0	-0.295	0.183
-30.2	14.0	-0.349	0.212
-34.5	14.4	-0.408	0.242
-40.1	14.4	-0.471	0.276
-43.5	14.4	-0.535	0.315
-49.1	14.4	-0.608	0.354
-53.8	14.0	-0.686	0.398
-58.1	14.4	-0.776	0.452
-63.6	14.7	-0.876	0.515
-67.2	14.4	-0.994	0.583
-73.0	14.0	-1.121	0.664
-77.3	14.4	-1.270	0.754
-82.0	14.0	-1.440	0.852
-86.3	14.4	-1.643	0.974
-91.9	14.4	-1.875	1.113
-96.4	14.4	-2.156	1.277
-101.2	14.0	-2.498	1.472
-105.7	14.0	-2.927	1.702

-109.8	14.7	-3.479	2.000
-114.7	14.0	-4.192	2.390
-119.0	14.0	-5.000	2.890
-124.5	14.7	-5.880	3.350
-127.1	14.4	-6.850	4.040
-130.1	14.7	-7.850	4.500

OH:-1A
1.6 kPa/sec

3.6	7.1	0.007	0.017
0.4	7.6	-0.024	0.032
-4.1	7.6	-0.056	0.046
-9.2	6.4	-0.090	0.063
-13.1	7.6	-0.129	0.081
-17.6	7.6	-0.168	0.100
-21.0	7.6	-0.215	0.120
-26.6	7.6	-0.261	0.144
-30.7	6.2	-0.310	0.168
-34.5	7.6	-0.369	0.200
-39.0	7.6	-0.427	0.232
-43.5	7.6	-0.496	0.266
-48.3	7.1	-0.569	0.308
-52.8	7.1	-0.647	0.354
-57.6	6.4	-0.745	0.403
-62.1	6.4	-0.847	0.461
-65.2	7.1	-0.964	0.530
-69.7	7.1	-1.104	0.608
-74.2	7.1	-1.257	0.703
-78.7	7.1	-1.428	0.801
-83.2	7.1	-1.621	0.906
-87.7	7.1	-1.809	1.013
-91.9	7.8	-2.014	1.133
-96.5	7.6	-2.253	1.272
-99.9	7.6	-2.556	1.453
-104.4	7.6	-2.966	1.692
-108.9	7.6	-3.494	2.012
-113.3	7.8	-4.160	2.415
-117.3	6.4	-4.973	2.903
-121.3	7.6	-5.560	3.340
-124.7	7.6	-6.700	4.011

173

APPENDIX C

Multidirectional Tubes

	Stress Ratio	Stress Rate	σ_A(MPa)	σ_H(MPa)	Failure Mode
		kPa/s			
1	0H:1A	196	162	4.8	Structural Failure (0° fibres)
2	1H:1A	400	192	192	Weepage
3	2H:1A	335	124	248	Weepage
4	1H:0A	385	-1.4	277	Struct. Failure ($\pm$70° fibres)
5	1H:-1A	284	-131	131	Burst
6	0H:-1A	235	-266	4.8	Shear

Axial Stress	Hoop Stress	Axial Strain	Hoop Strain
	OH:1A		
	196 kPa/sec		
2.5	4.9	0.012	0.014
7.5	4.7	0.037	0.006
12.5	4.5	0.061	-0.013
18.5	4.7	0.085	-0.027
23.7	4.7	0.103	-0.031
29.4	4.5	0.137	-0.051
34.8	4.9	0.161	-0.059
40.7	4.9	0.190	-0.079
45.7	4.7	0.217	-0.092
51.7	4.9	0.247	-0.116
56.8	4.9	0.269	-0.133
62.5	4.5	0.305	-0.148
67.8	4.9	0.334	-0.173
73.6	4.7	0.364	-0.193
78.9	4.9	0.413	-0.222
84.7	4.9	0.457	-0.248
89.6	4.5	0.503	-0.278
95.6	4.7	0.562	-0.309
100.9	4.9	0.625	-0.352
106.0	4.9	0.686	-0.388
111.2	4.9	0.754	-0.433
116.8	4.5	0.825	-0.478
122.1	4.7	0.901	-0.519
127.3	4.9	0.989	-0.563
133.0	4.5	1.086	-0.614
138.3	4.9	1.174	-0.678
143.2	4.5	1.262	-0.742
149.4	4.9	1.348	-0.802
154.5	4.9	1.423	-0.861
159.6	4.9	1.506	-0.923
162.5	4.7	1.558	-0.956
	1H:1A		
	400 kPa/sec		
0.3	0.7	-0.002	0.004
6.5	7.1	0.015	0.017
12.6	13.5	0.037	0.027
18.6	19.7	0.054	0.037
24.8	26.1	0.063	0.049
31.5	32.2	0.078	0.061

36.8	38.4	0.093	0.075
43.5	44.5	0.110	0.087
49.7	50.9	0.120	0.100
55.7	57.0	0.137	0.116
62.4	63.2	0.149	0.128
68.6	69.6	0.168	0.137
74.7	76.0	0.186	0.151
81.4	82.1	0.198	0.169
87.6	88.5	0.210	0.177
93.7	94.8	0.232	0.195
99.6	100.8	0.247	0.209
106.5	107.2	0.266	0.232
112.4	113.3	0.291	0.243
118.6	119.6	0.320	0.258
125.5	126.0	0.356	0.278
131.6	132.4	0.388	0.299
137.5	138.3	0.422	0.322
143.6	144.7	0.452	0.340
150.4	150.9	0.486	0.352
156.5	157.3	0.508	0.377
162.5	163.4	0.532	0.401
169.2	169.5	0.562	0.413
175.5	176.2	0.588	0.439
181.4	182.1	0.618	0.453
188.3	188.5	0.637	0.470
191.7	192.5	0.647	0.476

2H:1A
335 kPa/sec

0.1	0.2	0.002	-0.002
4.4	8.7	0.007	0.023
8.4	16.8	0.005	0.051
12.4	24.8	0.010	0.071
16.4	32.8	0.007	0.100
20.6	41.2	0.007	0.120
24.6	49.2	0.007	0.151
28.6	57.3	0.005	0.177
32.7	65.5	0.002	0.206
36.8	73.5	0.002	0.244
40.9	81.9	-0.005	0.273
44.8	89.6	-0.002	0.312
48.8	97.7	-0.005	0.338
53.0	106.0	-0.012	0.377
56.9	113.7	-0.007	0.421

60.9	121.8	-0.020	0.453
65.1	130.1	-0.024	0.498
69.1	138.2	-0.027	0.543
73.2	146.4	-0.034	0.588
77.2	154.4	-0.042	0.635
81.2	162.5	-0.046	0.690
85.3	170.5	-0.054	0.742
89.3	⁻8.6	-0.061	0.788
93.4	.͵6.9	-0.066	0.840
97.6	195.1	-0.081	0.898
101.6	2ͷ3.2	-0.085	0.948
105.4	210.7	-0.093	1.005
109.6	219.2	-0.098	1.060
113.6	2ͷ7.3	-0.095	1.125
117.7	235.3	-0.105	1.186
121.8	243.7	-0.112	1.255
124.3	248.6	-0.112	1.292

1H:0A

385 kPa/sec

-0.6	0.2	0.012	-0.006
-0.3	9.7	-0.020	0.033
-0.1	18.9	-0.039	0.082
-0.5	28.4	-0.071	0.114
-0.5	37.1	-0.105	0.157
-0.2	46.6	-0.137	0.212
-0.6	56.1	-0.178	0.254
-0.5	65.0	-0.222	0.309
-0.3	74.3	-0.276	0.366
-0.1	83.5	-0.325	0.443
-0.6	92.9	-0.383	0.515
-0.3	102.2	-0.452	0.586
-0.1	1ͷ1.4	-0.515	0.668
-0.7	120.4	-0.598	0.755
-0.5	129.8	-0.671	0.843
-0.2	139.1	-0.750	0.937
-0.8	148.3	-0.842	1.038
-0.7	157.3	-0.925	1.148
-1.1	166.7	-1.023	1.259
-0.8	176.2	-1.125	1.365
-0.6	185.4	-1.211	1.471
-1.1	194.6	-1.316	1.581
-1.0	203.6	-1.414	1.707
-0.9	212.7	-1.531	1.817

-0.6	222.1	-1.631	1.939
-0.3	231.5	-1.738	2.053
-0.9	240.6	-1.846	2.175
-0.7	249.8	-1.960	2.297
-1.1	259.3	-2.070	2.419
-1.2	268.0	-2.195	2.539
-1.1	277.0	-2.363	2.655

1H:-1A
284 kPa/sec

0.1	0.2	0.007	0.006
-4.1	4.9	-0.024	0.028
-7.9	9.2	-0.051	0.063
-12.4	13.5	-0.085	0.083
-16.8	17.7	0.122	0.124
-21.3	22.0	-0.154	0.153
-25.7	26.4	-0.190	0.193
-30.3	30.5	-0.229	0.230
-34.0	34.4	-0.269	0.275
-38.3	38.3	-0.317	0.332
-42.7	43.8	-0.374	0.373
-47.2	48.1	-0.444	0.429
-51.7	52.3	0.505	0.484
-56.1	56.8	-0.586	0.548
-60.7	60.7	-0.664	0.617
-65.2	65.0	-0.754	0.683
-68.8	69.6	-0.857	0.767
-73.2	74.0	-0.957	0.836
-77.6	78.3	-1.069	0.917
-82.1	82.5	-1.152	1.009
-86.6	86.8	-1.235	1.080
-91.1	91.1	-1.272	1.182
-94.8	95.3	-1.348	1.263
-99.5	99.1	-1.460	1.353
-103.8	103.9	-1.633	1.448
-108.3	108.1	-1.792	1.540
-112.5	112.9	-1.924	1.646
-116.3	117.0	-2.046	1.739
-120.8	121.3	-2.195	1.858
-125.2	125.6	-2.366	2.008
-130.0	129.3	-2.617	2.232
-130.7	130.8	-2.666	2.289

OH:-1A
235 kPa sec

2.2	4.5	0.000	0.006
-4.1	4.9	-0.027	0.023
-10.8	4.7	-0.063	0.033
-16.9	4.5	-0.098	0.049
-23.3	4.7	-0.134	0.059
-29.9	4.7	-0.168	0.073
-36.5	4.9	-0.205	0.100
-43.3	4.5	-0.247	0.118
-49.9	4.5	-0.286	0.137
-56.5	4.5	-0.325	0.157
-62.4	4.5	-0.366	0.177
-68.8	4.9	-0.410	0.209
-75.4	4.9	-0.459	0.232
-82.0	4.9	-0.515	0.275
-88.1	4.5	-0.579	0.299
-95.2	4.9	-0.637	0.336
-101.1	4.9	-0.696	0.368
-107.7	4.9	-0.779	0.409
-114.3	4.9	-0.847	0.453
-120.9	4.9	-0.933	0.507
-127.8	4.5	-1.008	0.548
-133.4	4.9	-1.091	0.604
-140.1	4.7	-1.179	0.647
-146.7	4.7	-1.292	0.710
-152.5	4.9	-1.384	0.767
-159.0	5.2	-1.487	0.833
-166.5	4.9	-1.565	0.889
-172.3	4.9	-1.672	0.948
-178.9	4.9	-1.782	1.015
-193.6	4.9	-1.931	1.097
-217.9	4.9	-2.332	1.423
-225.9	4.9	-2.827	1.784

APPENDIX D

```
'*****************************************************************
'*
'*              MTS Biaxial Testing
'*                  Mal Carroll
'*                  May 7 1993
'*
'*****************************************************************

DECLARE SUB DAS8SET (a%())
DECLARE SUB DAS8RUN (a%(). spl. spp. sta. stp. filename$)
DECLARE SUB DAS8INIT (TIME!)
DECLARE SUB das8 (mode%, BYVAL dummy%, flag%)
DIM d%(6)               'Data transfer array variable
COMMON SHARED d%()
DIM a%(10000)

5 CLS

'*****************************************************************
PRINT "
******************************************************************"
PRINT "      *
PRINT "      *
PRINT "      *     FIBRE REINFORCED PLASTIC DOWNHOLE TUBING
PRINT "      *               BIAXIAL TESTING
PRINT "      *               Data Acquisition
PRINT "      *               Load - Pressure
PRINT "      *     Axial Strain - Extensometer. Gage. Stroke
PRINT "      *       Transverse Strain - Extensometer. Gage
PRINT "      *
P  NT "      *               Metrabyte DAS-8
PRINT "      *
PRINT "      *               May 7 1993
PRINT "      *       Last Modified - Jan. 14 1994
PRINT "      *
PRINT "
******************************************************************"
PRINT

'Data input

VIEW PRINT 17 TO 22
LOCATE 17
```

180

```
INPUT "Data filename ", filename$
INPUT "Pipe type - (red.black.white) ", type$
INPUT "Pipe inside diameter ", ID
INPUT "Pipe outside diameter ", od
INPUT "Stress ratio [Hoop:Axial] ", h, a
PRINT
'***************************************************************
'Initial calculations

TH = (od - ID) / 2
LSR = (3.14159 * (od ^ 2 - ID ^ 2) * (od   TH)) / (8 * TH)
IF h < > 0 THEN
   SR = (a - h / 2) / h
   lpr = LSR * SR
   LR = (R * 3.14159 * (od ^ 2 - ID ^ 2)) / 4
   PR = LR
END IF
IF a = 0 THEN
   LR = 0
   PR = R * TH * 2 / (od - TH)
END IF
IF h = 0 THEN
   P = 1000
   PR = 0
   LR = (R * 3.14159 * (od ^ 2 - ID ^ 2)) / 4
END IF
sta = 3.14159 * (od ^ 2 - ID ^ 2) / 4
stp = (od - TH) / (2 * TH)

spl = 84000                          'load span
spp = 15000                          'pressure span

PRINT USING "Load to pressure ratio- ##.### "; lpr
PRINT
PRINT "Max load = 84000 lbs.";
PRINT "      Max pressure = 12000 psi."
INPUT "Load span (lbs) ", splv
IF lpr = 0 THEN
   INPUT "Pressure span (psi.) ", sppv
   GOTO 7
END IF
sppv = splv / lpr
PRINT USING "Pressure span (psi.) = #####.#"; sppv
7 slv = (splv / spl) * 10
```

```basic
spv = (sppv / spp) * 10
PRINT USING "Load Span = ##.### V."; slv:
PRINT USING "    Pressure Span = ##.### V."; spv
PRINT
INPUT "Function generator rate "; fr
PRINT
```

```
'*************************************************************************
```

```basic
'Setup the das-8 card and the time for each data record
PRINT "Do not exceed 1000 data points."
INPUT "Time interval between data records (sec.)", PERIOD
TIME = 100 * PERIOD
```

```
'*************************************************************************
```

```basic
' graph set up

SCREEN 9
VIEW (20, 80)-(400, 300), , 1
WINDOW (-5, -5)-(5, 5)

COLOR 13
LOCATE 23, 21
PRINT "Axial Strain"
y1$ = "Axial Stress"
FOR i = 1 TO 12
    LOCATE 7 + i, 1
    PRINT MID$(y1$, i, 1);
NEXT i

COLOR 14
LOCATE 5, 21
PRINT "Diametral Strain"
y2$ = "Hoop Stress"
FOR i = 1 TO 11
    LOCATE 8 + i, 52
    PRINT MID$(y2$, i, 1)
NEXT i

COLOR 7

LOCATE 1, 1
PRINT "Filename- "; filename$:
```

182

```
PRINT "  Pipe type- ": type$:
PRINT "  I.D.- ": ID:
PRINT "Th.- ": TH

LOCATE 2, 1
PRINT "Stress ratio |Axial:Hoop]- ": a: ":": h

LOCATE 3, 1
PRINT USING "Load to pressure ratio- ##.##": lpr:

' set up for results

LOCATE 8, 55
PRINT "Sample #     - "

LOCATE 6, 55
PRINT "Oil Volume    -"

LOCATE 11, 55
PRINT "Axial Load   -"
LOCATE 12, 55
PRINT "Axial Stress -"

LOCATE 15, 55
PRINT "Axial Strain -"

LOCATE 18, 55
PRINT "Pressure      -"
LOCATE 19, 55
PRINT "Hoop Stress   -"

LOCATE 22, 55
PRINT "Trans. Strain-"

COLOR 15
LOCATE 1, 62
PRINT "(s) TO STOP"

COLOR 1
LOCATE 23, 1
PRINT "(-1,-1)"


' *****************************************************************
'Create a data file and open it
```

183

```
OPEN filename$ FOR OUTPUT AS #1

PRINT #1, USING "Filename- &    Tube type- &"; filename$; type$
PRINT #1, USING "I.D. ##.## O.D. ##.## Th. ##.##"; ID; od; TH
PRINT #1, USING "Stress ratio- #.#H : #.#A"; h; a
PRINT #1, USING "Load to pressure ratio- ###.#"; lpr
PRINT #1,
PRINT #1, USING "Sample every ##.## seconds"; PERIOD
PRINT #1,
PRINT #1, USING "Function generator rate = #######"; fr
PRINT #1,
PRINT #1, USING "Load Span ##.###    Pressure Span ##.###"; slv; spv
PRINT #1,
PRINT #1, "--------Output Conversions-------"
PRINT #1,
PRINT #1, "Load- 16800"
PRINT #1, USING "Axial Stress- #####.#"; 16800 / sta
PRINT #1, "Axial Strain- 1"
PRINT #1, "Pressure- 3000"
PRINT #1, USING "Hoop Stress- #####.#"; 3000 * stp
PRINT #1, "Diametral Strain- 1"
PRINT #1, "Axial Strain Gage- 1"
PRINT #1, "Transverse Strain Gage- 1"
PRINT #1, "Stroke---"
PRINT #1, "Oil Volume ---"
PRINT #1,
PRINT #1, "--------------------------------"
PRINT #1,
PRINT #1, "Sample    Load    Strain    Pres.    Strain    Gage A    Gage T    Stroke
Piston"
PRINT #1,
CLOSE #1

'*****************************************************************************
*

'Set up data aquisition and start taking data

LOCATE 13, 15
COLOR 15
PRINT "Press any key to start."
begin$ = INPUT$(1)
LOCATE 13, 15
PRINT "                        "
```

```
CALL DAS8INIT(TIME)

CALL DAS8SET(a%())

'*********************************************************************
*

'Check to see if new data has been taken and write to file when neccessary

CALL DAS8RUN(a%(), spl, spp, sta, stp, filename$)

SCREEN 0
GOTO 5

END

SUB DAS8INIT (TIME)

'Initialize das-8 board

md% = 0
BASADR% = &H308
flag% = 0
CALL das8(md%, VARPTR(BASADR%), flag%)
IF flag% THEN PRINT "ERROR MODE 0 ": STOP

'Configure timer

md% = 10
d%(0) = 2
d%(1) = 3
flag% = 0
CALL das8(md%, VARPTR(d%(0)), flag%)

'Load timer

md% = 11
d%(0) = 2
d%(1) = 23860   'FREQ=2.3864 Mhz./(D%(1))
CALL das8(md%, VARPTR(d%(0)), flag%)

'Cascade timer

md% = 10
```

```
d%(0) = 0
d%(1) = 3
flag% = 0
CALL das8(md%, VARPTR(d%(0)), flag%)

'Load timer

md% = 11
d%(0) = 0
d%(1) = TIME 'FREQ=2.3864 Mhz./D%(1)
CALL das8(md%, VARPTR(d%(0)), flag%)

'Initialize the digital outputs for the function generator

md% = 14
op% = 2
CALL das8(md%, VARPTR(op%), flag%)

END SUB

SUB DAS8RUN (a%(), spl, spp, sta, stp, filename$)

'If new data has been taken then write results to file and plot

i% = 1
ii% = 0
sn% = 0
COLOR 12
DO
    DO                'check to see if new data has been written
        md% = 21
        d%(0) = 2
        d%(1) = 0
        GOTO 999
        d%(2) = 0
        CALL das8(md%, VARPTR(d%(0)), flag%)
        IF flag% THEN PRINT "ERROR"; flag%: STOP
    LOOP UNTIL d%(3) > sn% OR d%(3) > 8000      'Continue if new data

    sn% = d%(3)
    a1 = (a%(sn% - 8)) * 10 / 4096
    a2 = -(a%(sn% - 7)) * 10 / 4096
    a3 = (a%(sn% - 6)) * 10 / 4096
    a4 = (a%(sn% - 5)) * 10 / 4096
```

186

```
a5 = (a%(sn% - 4)) * 10 / 4096
a6 = (a%(sn% - 3)) * 10 / 4096
a7 = (a%(sn% - 2)) * 10 / 4096
a8 = (a%(sn% - 1)) * 10 / 4096


'Write results to screen

   COLOR 12
   LOCATE 8, 69
   PRINT sn% / 8

   LOCATE 11, 69
   PRINT USING "#####.#lbs."; (84000 * a1 / 5)          'load
   LOCATE 12, 69
   PRINT USING "#####.#psi."; ((84000 * a1 / 5) / sta + (15000 * a3 * stp /
10))'axial stress
   LOCATE 15, 69
   PRINT USING "##.### %"; a2                           'axial strain
   LOCATE 18, 69
   PRINT USING "#####.#psi."; 15000 * a3 / 5            'pressure
   LOCATE 19, 69
   PRINT USING "#####.#psi."; 15000 * stp * a3 / 5      'hoop stress
   LOCATE 22, 69
   PRINT USING "##.### %"; a4 * 1.2                      'diametral strain

'Plot results

   COLOR 13
   PSET (a2, ((84000 * a1 / 5) / sta + (15000 * a3 * stp / 10)) / 4000)
   COLOR 14
   PSET (a4 * 1.2, a3)
   COLOR 12

'Intensifier piston position

   LOCATE 6, 69
   PRINT USING "#### %"; (a8 - .496) * 24.85


   IF sn% > 8000 THEN GOSUB SAVE

'If "s" is pressed then stop taking data and end

   IF INKEY$ = "s" THEN
```

```
        GOSUB OFFRESET
        GOSUB SAVE
        GOSUB ENDSTART
        sn% = 8001
    END IF


'If there is an error signal then stop the test (digital signal pin 27)

    md% = 13
    CALL das8(md%, VARPTR(od%), flag%)
    IF od% AND 4 THEN
        COLOR 15
        LOCATE 5, 47
        PRINT "------INTERLOCK ERROR------"
        IF ii% = 0 THEN
            inter% = sn% / 8
        END IF
        ii% = 1
    END IF


LOOP UNTIL sn% > 8000


GOTO 2


'Turn off interupt and reset function generator


OFFRESET:

    md% = 21
    d%(0) = 2
    d%(1) = 1
    d%(2) = 0
    CALL das8(md%, VARPTR(d%(0)), flag%)
    md% = 14                              'reset ramp
    op% = 0
    CALL das8(md%, VARPTR(op%), flag%)


RETURN


'Save the remaining data


SAVE:

999  OPEN filename$ FOR APPEND AS #1
```

```
FOR j = 8 TO sn% STEP 8

    a1 = (a%(j - 8)) * 10 / 4096
    a2 = -(a%(j - 7)) * 10 / 4096
    a3 = (a%(j - 6)) * 10 / 4096
    a4 = .8333 * ((a%(j - 5)) * 10 / 4096)
    a5 = (a%(j - 4)) * 10 / 4096
    a6 = (a%(j - 3)) * 10 / 4096
    a7 = (a%(j - 2)) * 10 / 4096
    a8 = (a%(j - 1)) * 10 / 4096

    PRINT #1, USING "#### : ##.###   ##.###   ##.###   ##.###   ##.###
##.###   ##.###   ##.###   ##.###"; j / 8; a1; a2; a3; a4; a5; a6; a7; a8
    NEXT j
    PRINT #1, USING "Interlock error at sample ####"; inter%
    CLOSE #1

RETURN

'Restart or end

ENDSTART:

    COLOR 15
    LOCATE 1, 62
    PRINT "Any key to end."
    LOCATE 2, 62
    PRINT "(a) to start again."
    begin$ = INPUT$(1)

RETURN

2 IF begin$ < > "a" THEN END

END SUB

SUB DAS8SET (a%())

'Write digital output to signal function generator to start ramp (pin 7)

md% = 14
op% = 3
CALL das8(md%, VARPTR(op%), flag%)
```

189

```
'Set up # of channels to be converted (pin 37,36,35,34,33,32,31,30)
' 37 - load
' 36 - axial strain (extensometer)
' 35 - pressure
' 34 - diametral strain (extensometer)
' 33 - axial strain (gage)
' 32 - transverse strain (gage)
' 31 - stroke
' 30 - intensifier piston position

md% = 1
d%(0) = 0
d%(1) = 7
flag% = 0
CALL das8(md%, VARPTR(d%(0)), flag%)
IF flag% THEN PRINT "ERROR"; flag%: STOP

'Set up data aquisition using interupt generated by the das-8 card

md% = 21
d%(0) = 0
d%(2) = 8000
d%(3) = 2
d%(1) = -1
d%(4) = VARPTR(a%(0))
d%(5) = VARSEG(a%(0))
CALL das8(md%, VARPTR(d%(0)), flag%)
IF flag% THEN PRINT "ERROR"; flag%: STOP

md% = 21
d%(0) = 1
d%(1) = 0
d%(2) = 0
d%(3) = 0
d%(4) = 0
d%(5) = 0
CALL das8(md%, VARPTR(d%(0)), flag%)
IF flag% THEN PRINT "ERROR"; flag%: STOP


END SUB
```